Politecnico di Milano

Department of Aerospace Science and Technology DAER

# Multidisciplinary Approach of Small Air Launched Rocket Preliminary Design

Master Degree in Space Engineering

Academic year: 2019-2020

**Candidate:**
Daniele Pilori
ID: 898460

**Supervisor:**
Prof. Michèle Lavagna

October 2, 2020

# Abstract

Air Launch to orbit is an interesting launch strategy nevertheless rarely used. It has advantages from the flexibility point of view and the overall efficiency, however interfaces with the carrier aircraft restrict the size of the launcher dramatically. This opens the possibility of designing a small air launched rocket designed to timely inject one nanosatellite at a time, nanosatellites whose market is expected to increase in the incoming years. This concept can broaden Europe and Italy launch capabilities to a new payload range, and can open the opportunity of launching directly from Europe, opportunity nowadays unfeasible.

Multidisciplinary approach is a kind of design method specifically thought for complex architectures where the subsystems are highly coupled among each others. This approach has been widely used in the space and launcher industry showing good results and faster design time.

Such a method is used to the preliminary design phase of a small air launched rocket thought to take service in a few years, this rocket would have the capability of launching specifically and individually one nanosatellite.

Some innovative tools are developed to enhance the design process of launchers and propose solutions for future upgrades. An novel multiconfiguration staging design is sized and used to create multiple configurations of the rocket in order to extend its market without increasing the costs. Another solution regards the usage of an innovative hybrid rocket engine configuration for improving the upper stage performances.

Finally a novel guidance control strategy is proposed for the rocket ascent trajectory, this solution is based on a Model Predictive Control law.

# Prefazione

Il metodo dell'aviolancio è una delle strategie di lancio più interessanti e promettenti, tuttavia poco utilizzata. Possiede vantaggi dal punto di vista della flessibilità di lancio e dell'efficienza complessiva del lanciatore, tuttavia l'interfaccia con l'aereo che lo trasporta riduce considerevolmente la taglia massima. Questa strategia apre alla possibilità di progettare un piccolo lanciatore aviolanciato pensato per lanciare un nanosatellite alla volta, nanosatelliti il cui mercato è previsto espandersi nei prossimi anni. Questa idea può ampliare le capacità di lancio Europee ed Italiane ad una nuova classe di satellite, e inoltre apre alla possibilità di lanciare direttamente da territorio Europeo, possibilità ad oggi irrealizzabile.

L'approccio Multidisciplinare è un tipo di progettazione pensato specificatamente per architetture complesse i cui sottosistemi sono intrinsicamente interconnessi tra loro. Questo tipo di approccio è stato ampiamente utlizzato nell'industria aerospaziale e dei lanciatori, fornendo ottimi risultati anche dal punto di vista del tempo di progettazione.

Questo metodo è usato per una progettazione preliminare di un piccolo lanciatore aviolanciato pensato per prendere servizio in pochi anni, tale lanciatore avrà la capacità di lanciare specificatamente e individualmente un nanosatellite alla volta.

Infine, alcune soluzioni innovative sono sviluppate per migliorare la progettazione dei lanciatori e alcune idee proposte per un futuro aggiornamento del progetto. Una nuova stadiazione multi-configurazione è stata ideata per creare una seconda configurazione del lanciatore al fine di allargare il potenziale mercato senza aumentare i costi. Un'altra soluzione riguarda l'uso di un motore ibrido per l'ultimo stadio al fine di aumentarne le prestazioni, e infine una strategia di controllo innovativa per la traiettoria di ascesa usando un metodo di controllo adattivo (Model Predictive Control).

*"Look again at that dot. That's here. That's home. That's us.*
*On it everyone you love, everyone you know, everyone you ever heard of, every human being who ever was, lived out their lives. The aggregate of our joy and suffering, thousands of confident religions, ideologies, and economic doctrines, every hunter and forager, every hero and coward, every creator and destroyer of civilization, every king and peasant, every young couple in love, every mother and father, hopeful child, inventor and explorer, every teacher of morals, every corrupt politician, every "superstar," every "supreme leader," every saint and sinner in the history of our species lived there–on a mote of dust suspended in a sunbeam."*

*Carl Sagan*

*To my family, my friends and everyone else who helped my during this period.*

# Contents

# List of Figures

# List of Tables

# List of Acronyms

**2BP** 2 Body Problem

**Al** Aluminum

**AP** Ammonium Perchlorate

**CEA** Chemical Equilibrium with Applications

**CFD** Computational Fluid Dynamics

**DCM** Direction Cosine Matrix

**DOF** Degrees Of Freedom

**EA** Euler Angles

**ESA** European Space Agency

**GA** Genetic Algorithm

**GOX** Gaseous OXygen

**HRE** Hybrid Rocket Engine

**HTPB** Hydroxyl-Terminated PolyButadiene

**LEO** Low Earth Orbit

**LOX** Liquid OXygen

**LRE** Liquid Rocket Engine

**MDO** Multidisciplinary Design Optimization

**MOO** MultiObjective Optimization

**MOPSO** MultiObjective Particle Swarm Optimization

**MPC** Model Predictive Control

**O/F** Oxidizer over Fuel Ratio

**ODE** Ordinary Differential Equations

**PD** Proportional Derivative

**PID** Proportional Integral Derivative

**RAAN** Right Ascension of the Ascending Node

**RCS** Reaction Control System

**SSO** Sun Synchronous Orbit

**SRM** Solid Rocket Motor

**T/W** Thrust over Weight Ratio

**TRL** Technology Readiness Level

**TVC** Thrust Vector Control

**VCLS** Venture Class Launch Services

**VFP** Vortex Flow Pancake

**VSVO** Variable Step Variable Order

# Chapter 1

# Introduction

”Rockets are cool!”

*Elon Musk*

Air Launched Rocket is a kind of launch vehicle that it is deployed by an aircraft instead of lifting off vertically from a launch pad like every other classical rockets. Maybe the most important advantage of this strategy regards the flexibility than can be achieved. Air to orbit launch vehicles do not need a launch pad, therefore they can reach orbit in a more wide variety of ways and different launch locations; this strength is given by the high maneuverability of the aircraft.

Another aspect regards the efficiency of such a launch strategy: sometimes the aircraft itself is considered to be the first stage of this kind of launcher which is more efficient than a rocket in terms of specific impulse (around an order of magnitude higher), and furthermore it is fully reusable. The rocket nozzle of the first stage also operates at low ambient pressure, increasing its efficiency.

The altitude at which the rocket is released plays an important role as well, being above 10 Km avoid the launcher flying inside the most dense layers of the atmosphere, this reduces significantly the drag losses as well as the gravity losses since the trajectory is not required to be as vertical as the one of a classical launcher.

The drawbacks are mainly represented by the presence of an aircraft, the launcher must respect the limits in terms of dimensions, weight and interfaces. Thus, the micro-launcher is the most interesting class of launch vehicle for this kind of solution. Furthermore, payload integration and propellant loading are performed before the aircraft takes off, this can introduce problems from the propellant boil off point of view.

On the other hand, small satellite's market is currently growing very fast, in particular satellites below 10 Kg, also called nanosatellites, are expected to increase more and more in the upcoming years as can be noticed in figure 1.1. Improvements in electronics and miniaturization techniques, have lead to the possibility of achieving good scientific and Earth observation results from satellites with a fraction of its original mass. In a few decades the standard satellite mass has decreased by order of magnitudes, making the nanosatellite class one of the most interesting from both the

scientific and the economic point of view.
Nowadays, those kind of small satellites are usually launched as secondary payloads of a primary spacecraft, thus they must share the same launch date and orbit. Currently operational small launch vehicles do not have an high launch frequency, therefore a small satellite with an highly time-dependent mission would probably be injected in a not optimal orbit for its purpose. Furthermore, as can be seen in figure 1.2, small launchers currently have the highest specific launch price among every other rockets, in particular the Pegasus-XL, which is the only air launched vehicle present in that figure, is far above the fitting curve.

Nowadays small satellites are usually launched in clusters mainly due to cost reduction, this is the case of Starlink satellites that are being launched by SpaceX, and the European SSMS (Small Spacecraft Mission Service). The aim of this works goes in the opposite direction, an Air launched rocket has the advantage of a short time-to-orbit which has a key importance for particular Earth observation missions.

A small air launched rocket would surely be a Europe-first, and moreover due to its very narrow capability would be the world first launch vehicle to put into orbit specifically and individually one nanosatellite at a time. If the cost per kilogram of the rocket would be lower than the fitting curve shown in 1.2 together with a simple and reliable design, this launch solution would surely see a lot of markets.

The aim of this master thesis is to perform a preliminary design of a small air launched rocket, capable of inserting a nanosatellite into Low Earth Orbit (LEO), this work is based on a multidisciplinary approach as required by the topic itself. The models used in this thesis are not particularly complex, this must be intended as a preliminary analysis to prove the feasibility of such a concept and provide rough budgets of mass, trajectory, launch location and ascent control. Tools are developed for each sector and interconnected by the others through a hierarchic multidisciplinary design, then some topics are deepened more proposing innovative solutions to improve the design not only on air to orbit launch vehicles but launchers in general.

The thesis is structured as follows:

- **Chapter 1: Introduction**
  Here a brief overview of the work is pointed out. At first the research motivation is expressed and explained in details, focusing in particular on the meaning of the air to orbit solution and the choice of the payload class. After that some preliminary analysis are performed regarding the carrier aircraft, the multidisciplinary workflow and the deployment conditions.
- **Chapter 2: Staging**
  In this chapter the selection of the stages configuration is performed, first using available theories and then showing a multi-configuration solution developed by the candidate.
- **Chapter 3: Propulsion System Design**
  Here the propulsion system is chosen and designed, focusing on the overall configuration of the launcher and proposing some innovative solutions as well. Budgets of mass and dimension are the outcomes.

- **Chapter 4: Trajectory and Launch Location**
  In this chapter using the data coming from the previous sections, the rocket dynamic is integrated using a simplified model to ensure the feasibility of the choices done so far and computing a reference trajectory for the next parts. Then some consideration are presented on the stages re-entry and the definition on the launch location.

- **Chapter 5: 6DOF Rocket Model**
  A full 6 degrees of freedom rocket model is implemented to simulate the ascent trajectory from the deployment to the payload orbit insertion. This is another important benchmark of the design.

- **Chapter 6: Ascent Control Law**
  The control law used to follow the desired trajectory is shown in this chapter, first a simple PD controller is used and then compared with another solution based on an MPC controller.

- **Chapter 7: Conclusions**
  This chapter summarizes the most relevant points rosen from the development research and addresses the work in terms of future steps to follow.

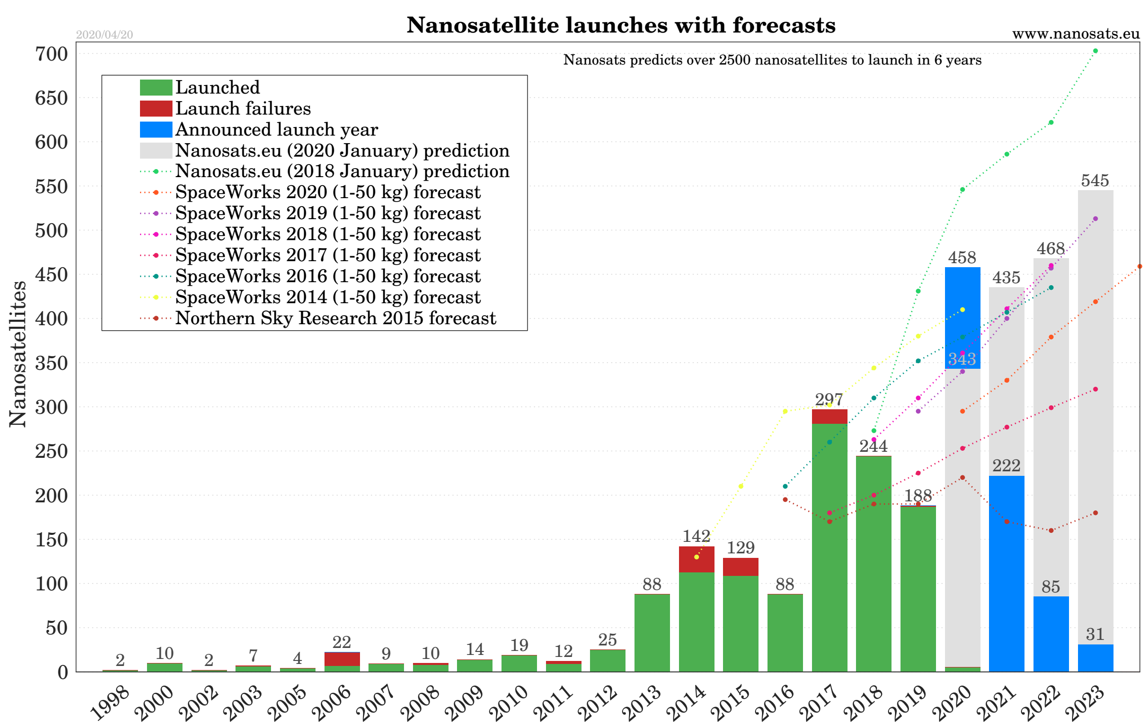


Figure 1.1: Nanosatellite Forecast [1]

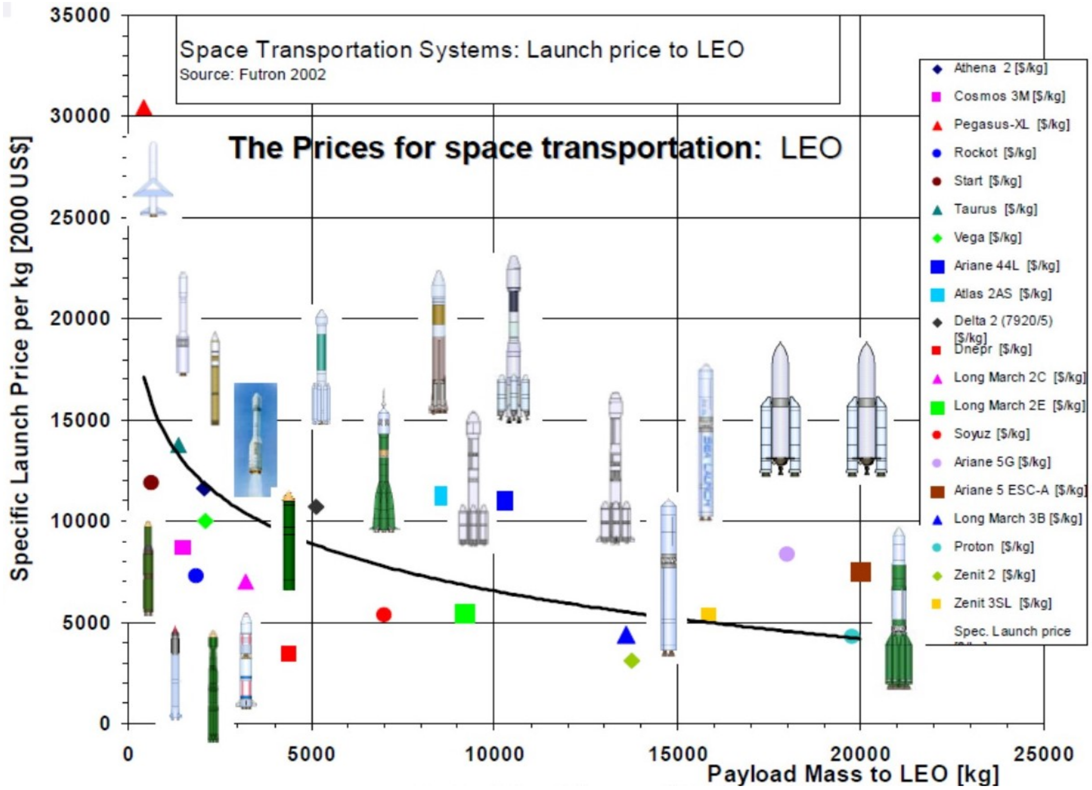


Figure 1.2: Launch Cost LEO [2]

## 1.1 Air Launch to Orbit State of the Art

In this section the state of the art regarding air launched rockets, and small launchers is presented. The state of the art regarding each subsystem is addressed at the beginning of the respective chapter.

Air launch to orbit has an history that is present since the dawn of the space era, in fact 1958 was the year of the NOTSNIK rocket, this was a US project part of the Pilot program developed to be a small air-launcher and anti-satellite weapon. It's a very simple launcher made of 5 stages solid rocket motors with a payload of 1 Kg to LEO, during the 1958 it performed 10 flight resulting in 10 failures therefore the project was abandoned. Nowadays only one air-launched rocket is operational, the Pegasus from Northrup Grumman; it's a 3 stages solid rocket motors launcher capable of inserting 250 Kg into LEO in its XL configuration [7]. It becomes operational in 1990 and since then it accomplished 39 successful launches many of them in the XL configuration, making it one of the most used launchers in the history despite an high specific cost per kilogram. Pegasus has also the possibility of using a fourth stage powered by hydrazine based monopropellant in order to increase the orbit insertion accuracy.

There's another launcher that will be operational in a few months, the LauncherOne from Virgin Orbit that performed its maiden flight on May 2020 but resulted in a failure after few seconds from its deployment [10]. Its architecture is quite different from the Pegasus, it is a 2 stages vehicle powered by NewtonThree and NewtonFour engines both working using RP-1 and LOX, it's capable of inserting 300 Kg into LEO [11].


Figure 1.3: From left to right: Pegasus XL, LauncherOne, NOTSNIK

For what concerns the small launch vehicles market, as reported previously, there are no launchers capable of inserting a single 1 nanosatellites into LEO, but the research in this field is growing fast. For this purpose NASA launched in 2015 the so-called VCLS (Venture Class Launch Services), a contract to finance space companies in order to develop small launch vehicles dedicated specifically for nanosatellites [12]. The 3 companies awarded are:

- Virgin Galactic with its LauncheOne rocket
- Firefly Space System with its Firefly Alpha rocket
- RocketLab with its Electron rocket

The LauncherOne has just been discussed, Firefly Alpha is a 2 stages rocket powered by the Raver and Lightning engines both using RP-1 and liquid oxygen, the LEO payload capability is around 600 kg but the maiden launch has not yet happened. The Electron instead flew many times in this years, it uses the Rutherford engine for both first and second stage which again works on RP-1 and LOX and can bring 150 Kg into LEO [13] [14]. However all those rockets are used not to launch just a single nanosatellite, but a bunch of those; this implies that some of them may not have the perfect launch date, or target orbit, therefore they would work in a slightly off-nominal condition. It is worth spending a few words regarding this 3 rockets; it can be noticed that the propulsion system is basically the same, 2 stages working with RP-1 and LOX as propellant couple. The choice is not surprising because RP-1 is a very reliable fuel used since the dawn of the space era, it allows to build simple engines and more importantly it has the highest density with respect to other classical liquid fuels, thus making the rocket smaller.

## 1.2 Motivation

The absence of any sort of air launched vehicle in national and European territory motivates the work here presented, the availability of such kind of vehicles to access space would increase European independence from American small launchers and moreover it would introduce a class of launch vehicles (extra-small) that is a world-first. Another important aspect that is worth mentioning is that currently operational European launchers (e.g. VEGA, Ariane) have their launch pad in Kurou French Guyana, so each satellites must be shipped oversea before launch, an air to orbit launch vehicle like the one considered in this master thesis would avoid such a transportation since it can be launched above the European territory.
The possibility of launching specifically and individually one nanosatellite at a time is something unique up to now, and as already said it would be key for satellites with highly time-dependent mission that do not want to share the same launch with a bunch of other satellites.
Looking at the current trend of the launch market, it can be noticed a spread in the capability. If in the past a launcher in the medium class (payload $\approx$ 5-20 tons to LEO) was able to accomplish the vast majority of the missions, nowadays the trend is moving towards dedicated launches for each class of payload.
Heavy and super-heavy rockets are being developed for Moon and Mars missions (e.g. SLS, Starship, New Glenn) and big space telescopes, while on the other hand, small launchers already cited are being designed for LEO applications of nano and micro satellites. Therefore, there is a very high meaning of developing micro launchers with high flexibility in this particular period.

## 1.3 Multidisciplinary Approach

A launch vehicle is a very complex and highly coupled system, it is composed by many subsystems implying different subjects such as structural mechanics/dynamics, propulsion, fluid-dynamics, control laws.
Usually such design is addressed using a Multidisciplinary Design Optimization (MDO), this method takes advantage of those coupling effects to find out the global optimal design of a launch vehicle, moreover it results in faster design time. Many different methods can be used in a MDO process, the most used are certainly CO (Cooperative Optimization) and MDF (Multi Discipline Feasible) [15] [16] [17].

The design strategy used in this master thesis, is not properly a full MDO, since it is not the aim of this work. Nevertheless is possible to get some property of the MDO adopting a multidisciplinary approach.

Particularly important is the work done by Francesco Castellini with his PhD thesis [18], where he designed a Multidisciplinary Design Optimization for an expendable launch vehicle; here many different Multidisciplinary approaches are shown including the one adopted in this master thesis.

The choice here is mainly driven by simplicity and the presence of a well defined direction of proceeding in the design. Therefore is possible to create a design path from requirements to outcomes that passes through different subsystems. This is something currently done by in tactical

missile design as can be seen in figure 1.4. The workflow of this master thesis follows a similar path, but the order of the subsystem and the back iterations are different.
The decomposition in this case is called "hierarchic", meaning that some is worth designing some subsystems before others using its outputs as inputs of the followings.

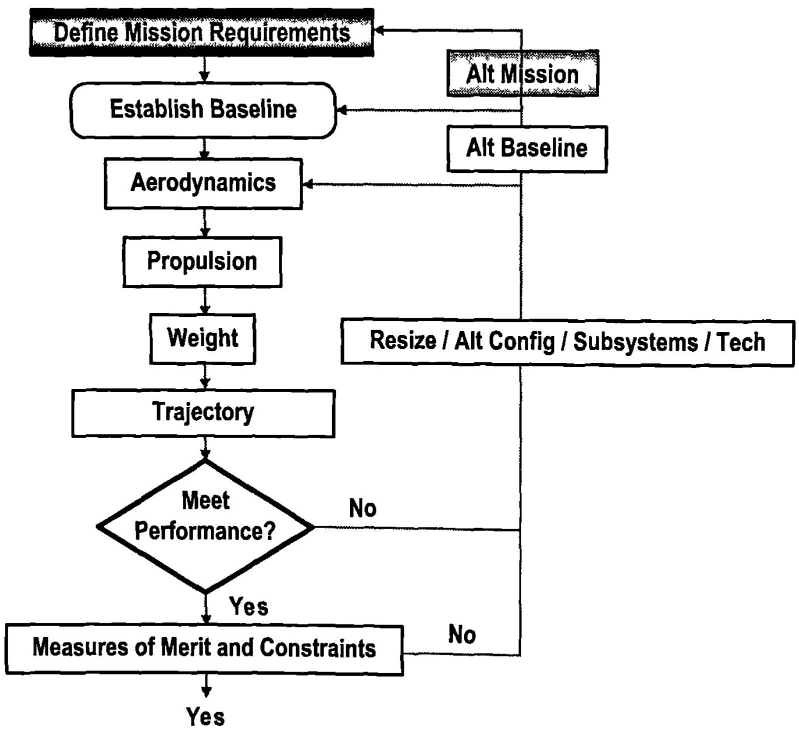


Figure 1.4: Tactical Missile Design Process [3]

In figure 1.5 the hierarchic design workflow selected for this master thesis can be seen.
The first block is the **High Level Requirements** which introduces basically requirements of Payload kind, orbit required, total cost of the launch etc; all those requirements come from customer surveys and market analysis. Another critical input comes from the **Carrier Aircraft Specification**, as already said an air launched rocket must be compliant with its carrier aircraft that is way more restrictive than a common launch pad; those specification are the mechanical/electrical interfaces as well as the initial conditions which should be optimal for the launcher but must be compliant with the aircraft capabilities.
The outcome of the design process is a set of mass and dimension budgets of the air launched vehicle, validated using a complete rocket model.

The first design block is the **Propulsion System Choice**, where a first selection of the propulsion system is performed based upon the high level requirement and already existing solutions. The output is a set of typical values of specific impulses ($I_{sp}$) and structural mass indexes ($\xi$) coming from literature.

The next step is the **Staging Design** that computes the staging configuration using the values found in the previous block; the results are the propellant $M_{p_i}$ and structural masses $M_{s_i}$ for each stage.
Then, one of the most important block in this diagram is the **Propulsion System Design**, in this block a more refined propulsion analysis is done using the propellant masses just computed. Here the dimensions of each stage are computed $L, D$, as well as the thrust profile $T$, the grain configuration (in the case of solid rocket motors), the propulsion performances like specific impulse $I_{sp}$, characteristic velocity $C^*$ and burning time $t_b$.

Connected to this last subsystem is the **3DOF Trajectory Design**, here a simple point mass 3 degrees of freedom is implemented in order to test what has been done so far. The ascent trajectory is integrated and a back iteration to the propulsion system design block is performed in case the rocket is not able to reach the desired orbit; often the problem is identified in the thrust profile which is very difficult to model.

When the trajectory is compliant with all the requirements, another back iteration is done to re-compute the staging using this time specific impulses and structural mass indexes not from literature but computed in the propulsion system design block, this passage gives better values of the staging and therefore a more optimal solution at the end. When the difference between those values is near zero the procedure can go on; the overall output is the final configuration of the launcher and a reference trajectory computed using the simplified model.

The final step is to integrate the launch trajectory using a more refined **6DOF Rocket Model**, this model takes into account also the attitude of the vehicle and therefore a **Control Law** is required to follow the reference trajectory. The final results of this Multidisciplinary workflow are the masses breakdown of each stage, the launch location, propulsion performances, and finally the trajectory simulation done in order to prove the feasibility of all the design done so far.

## 1.4 Scenario Definition

Before starting with the first block of the multidisciplinary approach, is worth discussing some preliminary considerations about which kind of payload is considered, what are the initial conditions and why, and finally which carrier aircraft has been selected for launcher.

### 1.4.1 Payload and Orbit Definition

As said in the introduction, the mass of the payload target is around few kilos, satellites in that range are often called *CubeSats*. Cubesat is a small satellite made by multiple units of 10cmx10cmx10xcm each as dimensions. Regarding the mass, each unit has a mean mass of 1.33 kg, however not every satellite has the exact same structure, so a variation is made between 1 and 1.5 kg for each unit.

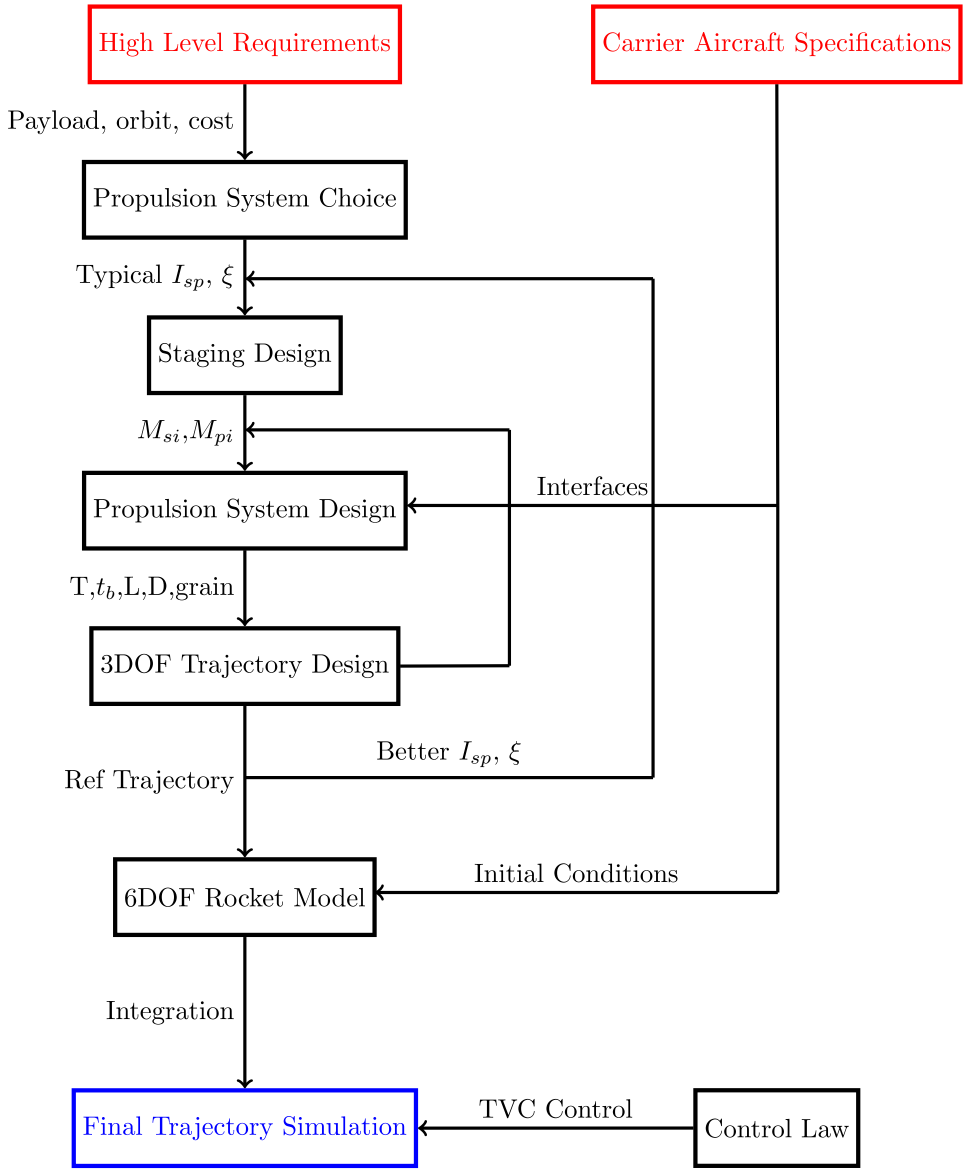


Figure 1.5: Multidisciplinary Workflow Scheme

The nominal mass for each unit has been selected as the higher limit (1.5 Kg), to account for lighter CubeSats, the launcher can be deployed at lower velocity or lower altitude. This fact stresses again the importance of the flexibility that an air launched rocket can exploit. The mass distribution for each CubeSat is shown in figure 1.6.

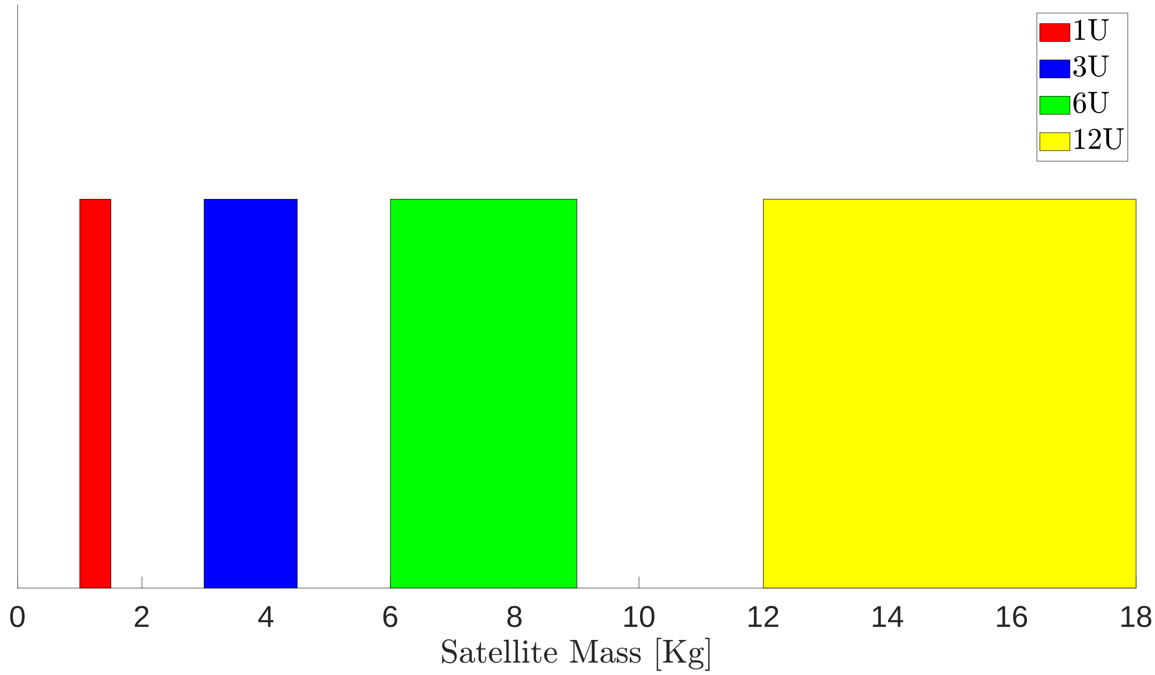


Figure 1.6: Satellite Mass

The overall payload mass that is be considered from here on is not simply the satellite mass, but it includes also deployer, fairing and the margins.

The way to compute it is the following:

$$M_{pay} = ((M_{sat} + M_{deployer})\,1.1 + M_{fair})\,1.2 \tag{1.1}$$

Regarding the orbit, as said CubeSats are usually placed into LEO, in particular in an altitude between 400 and 600 Km. Since many of those satellites are thought for Earth observation, the most used orbit for this purpose is the Sun Synchronous Orbit (SSO), this particular orbit exploit the $J_2$ perturbation of the Earth to make observation with the same Sun aspect angle along its whole mission. [19]

The variation of the Right Ascension of the Ascending Node (RAAN) due to keplerian parameters is given by the following equation:

$$\frac{d\Omega}{dt} = -\frac{3}{2}J_2\left(\frac{R_e}{a(1-e^2)}\right)^2\sqrt{\frac{\mu_e}{a^3}}\cos i \tag{1.2}$$

Fixing the semi-major axis to 500 Km, the eccentricity to 0 and the RAAN rate to 360 degrees per year, the resulting orbit inclination is: $i = 97.4°$.

The orbital velocity is immediately computed using the 2BP equations.

$$V_{orbit} = \sqrt{\frac{\mu_e}{a}} \tag{1.3}$$

Considering a launch location at 45 degrees latitude (Italy), the Earth's rotational velocity to be considered is 329 m/s in east direction. So the required launch velocity is 7666 m/s at an inclination of 99 degrees from east.

### 1.4.2 Fairing and Deployer

As said in the previous section, both fairing and deployer concur to the overall payload mass, a simple way to estimate them is by means of regression lines from existing hardware.

Satellites deployer is a mechanism that separate the satellite from the rocket upper stage by means of a spring; it also provides mechanical interfaces between satellite and launcher, so it acts as a common payload adapter. Adapters are usually designed based on the launcher's specifications and customer requirements, CubeSats deployers instead can be used on every launcher since they have standardized dimension like CubeSats are. The regression line is made considering the CubeSats adapter from ISIS Space [20].

$$M_{deployer} = 0.6967 M_{sat} + 0.2868 \tag{1.4}$$

Fairings instead are very complex structures, there are no available hardware off-the-shelf but it is designed for each launcher specifically. A full design of the fairing is useless at this current point, but a simple way to estimate its mass can be implemented. Looking at some existing fairings like the one developed by RUAG Space (for Ariane, VEGA, Atlas) [21] is possible to estimate the thickness of the fairing shells. Two major assumptions must be done, the first is assuming a constant density throughout the whole structure while the second assumes a shape made up by a semi-spherical shell above an hollow cylinder with the same thickness overall. With those assumptions is possible to compute the thickness of the existing fairings, and then use it to compute the mass of the fairing in this case based on the dimension of the launcher and the satellite. This procedure follows a simplified approach, since the fairing is made up by many materials and elements and the shape is not described by the shape discussed previously; however, the major role of this piece of hardware, is to protect the payload from environmental stresses and since an aero-launcher usually feels lower dynamic pressure with respect to traditional rockets, this procedure somehow overestimates the thickness of the fairing therefore introducing more margins.
Without reporting all the computations, this rough estimation leads to the following relation.

$$M_{fair} = \frac{4}{15}\left(M_{sat} + M_{dep}\right) \tag{1.5}$$

Despite being considered as part of payload mass, the fairing is deployed after the first stage burn, when the launcher is basically outside the atmosphere.

| **Masses**<br>Units | $\mathbf{M_{sat}}$<br>Kg | $\mathbf{M_{dep}}$<br>Kg | $\mathbf{M_{fair}}$<br>Kg | $\mathbf{M_{pay}}$<br>Kg |
|---|---|---|---|---|
| 1U | 1.5 | 1.13 | 0.70 | 4.31 |
| 3U | 4.5 | 1.99 | 1.73 | 10.64 |
| 6U | 9 | 3.28 | 3.27 | 20.14 |
| 12U | 18 | 5.86 | 6.36 | 39.13 |

Table 1.1: CubeSats masses breakdown

### 1.4.3 Carrier Aircraft

The selection of the carrier aircraft is a critical point in the design of an air launched rocket, this choice inevitably influences the design because it introduce limits in the deployment conditions as well as the maximum mass of the rocket. The carrier aircraft for the Pegasus rocket is a Lockheed L-1011 TriStar, which is an airplane commonly used for commercial lines, the launcher is placed below the fuselage. The LauncherOne is deployed by a Boeing 747-400 aircraft named Cosmic Girl, like the L-1011 is usually used in commercial flights and the rocket is placed below one wing, since the airplane was thought to have 2 more engines that it now has.
The carrier aircraft selected for this rocket is the Eurofighter Typhoon, a military fighter used by many European air forces.

The Eurofighter Typhoon is a military aircraft which is operational since 2003 in many European airforces, it has two turbojet EJ200 engines that provides 180 kN thrust in total and around 2000 s of specific impulse [4]. Looking at its armament it can bring the rocket both under the fuselage and below the wing like a missile, the choice of where put the launcher, the electro-mechanical interfaces between the aircraft and the rocket are all topics for a further development. In Italy there are only two military bases where the Eurofighter can be prepared for flight, one in Sardinia and the other in Puglia qua serve una reference, this can restrict the launch locations to a few around Italy and this topic is pointed out in more details in chapter 4.

### 1.4.4 Deployment Conditions

Looking again at existing air launched vehicles, is possible to infer some insights about typical velocity, altitude and pitch of the carrier aircraft at the deployment of the rocket. PegasusXL is deployed at an altitude of almost 12 Km, a velocity of Mach 0.82 and a pitch not defined in its manual but looking at some videos it can be fixed at no more than 20 degrees [7]. The LauncherOne

Figure 1.7: EuroFighter Typhoon [4]

is released at an altitude of around 11 Km, the velocity is not specified but should be around Mach 0.8 like the Pegasus, the pitch angle in this case is 27.5 degrees.

Up to this point is impossible to fix precise values of deployment conditions, but some typical values can be get from literature and existing technologies like the one just pointed out above. Since the carrier aircraft is a military based technology there are no very stringent boundaries to respect, but at this point is better taking standard values and if a later design find out how much is feasible to push those limit, is possible to get more optimal deployment conditions for the rocket trajectory.

The deployment altitude is fixed to 11 Km and the velocity of Mach 0.8, that, using the standard atmospheric model explained later on and the perfect gas hypothesis, corresponds to a speed of 236.1 m/s.

For what concerns the initial pitch angle, a work done by Sarigul-Klijn [22] shows how much is important the initial angle for the $\Delta V$ gain of an air launched rocket with respect to a classical one. Increasing the initial angle provides a better performance up to 30 degrees, and after that the gain remains almost constant for higher angles. However that model only takes into account the energetic gain but not other factors like the tvc required, analysis has been done on this topic in chapter 4 and it turns out that a good initial pitch is around 50 degrees.

# Chapter 2

# Staging Design

The stage configuration is one of the most important feature in a launcher design, a good staging can lead to efficient orbit insertion while minimizing the overall initial mass. The aim of this chapter is to find the best solution for this purpose and study new tools for designing the configuration of small launch vehicles.
The preliminary propulsion selection, according to what said in section 1.3, leads to a solid choice for every stage. The values of $I_{sp}$ and $\xi$ (defined as inert mass over propellant mass) considered for the staging design can be seen in table 2.1.

| **Parameters** | $\mathbf{I_{sp}}$ | $\xi$ |
|---|---|---|
| Units | s | - |
| 1st Stage | 279 | 0.09 |
| 2nd Stage | 290 | 0.1 |
| 3rd Stage | 293 | 0.16 |

Table 2.1: Propulsion Hypothesis for Staging Design

A detailed analysis on the propulsion system is done in chapter 3, where those values are validated and discussed.

## 2.1 Preliminary Hypothesis

Before beginning, it is worth spending a few words about the hypothesis involved in this chapter. First of all, the following theories are based upon the Tsiolkovsky Equation.

$$\Delta V_i = I_{sp_i} g_0 \log(N_i) \tag{2.1}$$

Where $N_i$ is the mass ratio of the i-th stage.
This equation defines the $\Delta V$ value given the specific impulse of the stage, a parameter which

defines the efficiency of the engine, and the mass ratio which gives information about how much of the stage mass is propellant.

The Tsiolkovsky equation is based on two major assumptions, the former is constant specific impulse and the latter is the absence of gravity and drag losses. Constant specific impulse is not a big issue, its variations are due mainly to changes in ambient pressure or in engine parameters (O/F, Pc ...). Drag and gravity losses have instead a more important contribution and must be taken into account, the former is higher for classical launchers while an air-deployed rocket feels lower drag losses being released at high altitude.

To take those contributions into account the required orbital $\Delta V$ has been margined by a factor of 1.22, in the following chapters models that takes into consideration those losses are explained, and the losses are estimated in more details.
In this section the mass of each stage is considered as made by two contributions:

$$M_{0_i} = M_{p_i} + M_{s_i} \tag{2.2}$$

Where $M_{p_i}$ represent the whole propellant mass of the i-th stage, and $M_{s_i}$ the inert mass, so: engines, tvc, structures...
So the Tsiolkovsky equation for each stage can be re-written as:

$$\Delta V_i = I_{sp_i} g_0 \log \left( \frac{M_{0_i}}{M_{0_i} - M_{p_i}} \right) \tag{2.3}$$

## 2.2 Optimal Staging Theory

A first guess can be done according to the Optimal staging theory, this method makes use of the Lagrangian multipliers to minimize the initial mass given the payload mass and the total $\Delta V$ as constraint.
The mass ratio of the i-th stage can be written in the following way.

$$N_i = \frac{M_{s_i} + M_{p_i} + M_{s_{i+1}} + M_{p_{i+1}} + ...M_{pay}}{M_{s_i} + M_{s_{i+1}} + M_{p_{i+1}} + ...M_{pay}} = \frac{M_{0_i} + M_{0_{i+1}} + ...M_{pay}}{M_{0_i}\epsilon_{s_i} + M_{0_{i+1}} + ...M_{pay}} \tag{2.4}$$

The constraint is imposed by the required $\Delta V$.

$$\Delta V = \sum_{i=1}^{n} C_i \ln N_i \tag{2.5}$$

Where $n$ is the number of stages and $C$ is the equivalent exhaust velocity.
The function to minimize is the overall launcher wet mass, but for demonstration reasons it is normalized by the payload mass. $M_R$ represents the initial mass not including the payload.

$$M_R = \sum_{i=1}^{n} M_{0_i} \tag{2.6}$$

$$\frac{M_R + M_{pay}}{M_{pay}} = \frac{M_{0_1} + M_{0_2} + ...M_{pay}}{M_2 + ...M_{pay}} \frac{M_{0_2} + ...M_{pay}}{M_{0_3} + ...M_{pay}} ... \frac{M_{0_n} + M_{pay}}{M_{pay}} \tag{2.7}$$

Re-arranging the terms, the cost function can be written as:

$$\frac{M_R + M_{pay}}{M_{pay}} = \prod_{i=1}^{n} \frac{(1 - \epsilon_{s_i})N_i}{1 - N_i \epsilon_{s_i}} \tag{2.8}$$

Considering that:

$$\epsilon_{si} = \frac{M_{s_i}}{M_{s_i} + M_{p_i}} \tag{2.9}$$

Now, taking the logarithm of the cost function and exploiting the logarithm properties.

$$\ln\left(\frac{M_R + M_{pay}}{M_{pay}}\right) = \sum_{i=1}^{n} \left[\ln(N_i) + \ln(1 - \epsilon_{s_i}) - \ln(1 - N_i \epsilon_{s_i})\right] \tag{2.10}$$

Taking the partial derivatives according to Lagrange multipliers optimization method, the procedure ends up with a system of equations to be solved numerically. An analytical solution can be found under the hypothesis of constant parameters $C_i$, $\epsilon_{s_i}$, but this is not the purpose of this analysis.

$$\begin{cases} \frac{1}{N_i} + \frac{\epsilon_{s_i}}{1 + N_i \epsilon_{s_i}} - \lambda \frac{C_i}{N_i} = 0 \qquad i = 1...n \\ \Delta V - \sum_{i=1}^{n} C_i \ln N_i = 0 \end{cases} \tag{2.11}$$

The result of this system is a set of mass ratios $N_i$ for each stage from which it is possible to compute the initial rocket mass as well as the breakdown of each stage.

$$M_0 = M_{pay} \prod_{i=1}^{n} \frac{1 - \epsilon_{si} N_i}{1 - N_i \epsilon_{si}} \tag{2.12}$$

$$M_{p_i} = M_{0_i}(N_i - 1)/N_i \qquad i = 1...n \tag{2.13}$$

$$M_{s_i} = M_{p_i}(\epsilon_{s_i} - 1)/\epsilon_{s_i} \qquad i = 1...n \tag{2.14}$$

$$M_{0_{i+1}} = M_{0_i} - M_{p_i} - M_{s_i} \qquad i = 1...n-1 \tag{2.15}$$

An important aspect that this theory does not account for, and is worth spending a few words about, is the interstage mass. Usually rockets have 2 to 4 stages and, of course, the presence of more stages allows the launcher to be more mass efficient and each engine nozzle can be optimized at the right altitude. However, there are some inevitable mass additions due to interstages, separation mechanisms, and moreover, the structural mass indexes become higher for smaller stages. For those reasons, the maximum number of stages considered for this preliminary design has been fixed to 3.

## 2.3 Multi-Configuration Design

From the optimal staging theory is quite easy to get the stage subdivision and then proceed with the design of the launcher, but as can be seen in equation (2.12) the initial mass depends a lot on the payload mass; this opens the question on which kind of CubeSat should be selected as target payload and why. One solution could be to look at CubeSats already launched and planned, and then infer which may get the largest market in the future.

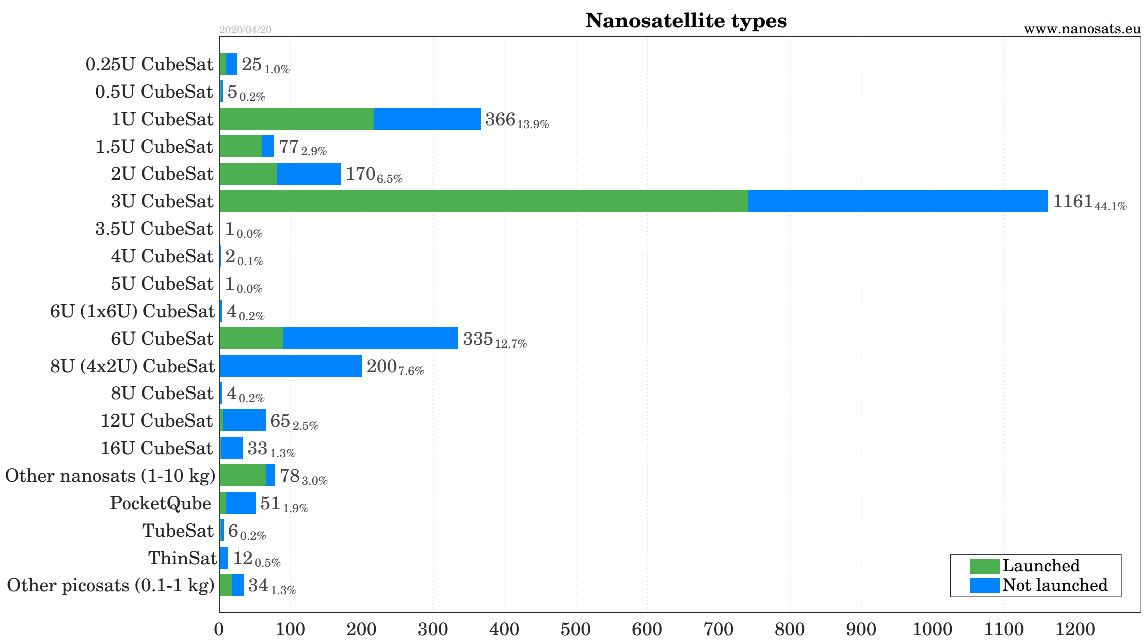


Figure 2.1: Nanosatellite Type [1]

Looking at figure 2.1, it's easy to notice that 3U CubeSat will be a perfect candidate as target payload, however 6U is still very important due to its possibility of using heavier instruments while being quite small at the same time. So, designing the rocket for the 3U makes impossible launching a 6U, while designing for the 6U constrains the rocket to launch two 3U at a time, therefore loosing the capability of dedicated launches.
One interesting alternative is to make different configurations of the same rocket for different classes of payloads, this is currently being done by launchers such as Ariane6 with its 2/4 SRB configurations and Atlas V that could use 0 to 5 strap-on boosters. This solution leads to the possibility of increasing the payload mass range designing only few more rocket motors, thus keeping the costs lower.

For this purpose a novel approach is proposed. A first staging design is made for the lighter payload ($M_{pay}^{I}$), then one of the stages is enhanced or one more is added to make the rocket capable of launching the heavier one ($M_{pay}^{\text{II}}$). This approach can be applied to any couple of payloads and any orbit, the value considered in this chapter are taken from section 1.4. Several solutions are possible, and are shown in the list below.

**1** 2 Stage Rocket with an Enhanced First Stage

**2** 2 Stage Rocket with an Enhanced Second Stage

**3** 2 Stage Rocket with the addition of a Third Stage

**4** 3 Stage Rocket with an Enhanced First Stage

**5** 3 Stage Rocket with an Enhanced Third Stage

**6** 2 Different 2-Stage Rockets both Optimal

**7** 2 Different 3-Stage Rockets both Optimal

Solution **1** means a 2 stage rocket capable of launching $M_{pay}^{I}$, then a second configuration of the first stage is created, such that using the same second stage as before, the rocket can launch $M_{pay}^{\text{II}}$ into orbit. This creates two configurations of the rocket.

Solution **2** does basically the same procedure, but in this case the first stage is kept constant and a second configuration of the second stage is created.

Starting from the same 2 stage rocket for $M_{pay}^{I}$, solution **3** does not change those two stages, but instead adds a third one on top such that this 3 stage rocket is able to launch $M_{pay}^{\text{II}}$ into orbit.

Solution **4** is basically the same as **1** but in this case the rocket has 3 stages, and again only the first stage is enhanced keeping the same second e third stage.

Similar to this latter, solution **5** starts with a 3 stage rocket for $M_{pay}^{I}$ and a second configuration of the third stage this time is created for $M_{pay}^{\text{II}}$.

Finally, solution **6** is composed by a two stage rocket fully optimized for $M_{pay}^{I}$ using the just derived optimal staging theory, and by another two stage rocket optimized this time for $M_{pay}^{\mathrm{II}}$.

Solution **7** does basically the same procedure like this latter, but in this case both rockets have 3 stage each.

Those 7 different solutions basically create two configurations of the rocket changing one or more stages doing so. Figure 2.2 helps understanding better all those solutions.
Now is worth asking which of them provides the best solution, and to do so a cost function to discriminate better and worse solutions must be found.
Like the optimal staging theory, a good cost function could be the initial wet mass of the rocket. But two launchers are present here, the rocket in the first and in the second configuration. If the initial wet mass of the first configuration is chosen as cost function, the final result would be optimal for $M_{pay}^{I}$ and sub-optimal for $M_{pay}^{\mathrm{II}}$ and vice versa.

Since at this stage is not meaningful benefiting one payload class more than the other, a result as wide as possible should be left for a further development. Detailed market analysis and customer surveys can address this question in a future work.
A MultiObjective Optimization (MOO) is suitable for this kind of problem, since it optimize both the initial wet masses of the two configurations at the same time. And a Pareto-Front result can provide a set of dominant solutions including the optimal values for the two payload classes.
Moreover, another important parameter is the total number of different stages (or better, motors) to be developed. This value is strictly linked to the overall cost and complexity of the project, therefore this must be added to the cost vector.

To compute those initial wet masses, a procedure must be implemented.
Table 2.2 shows which variables are needed by each solution process, and also the $n_{Motors}$ value.

| **Solution** | **Independent Variables** | $\mathbf{n_{Motors}}$ |
|---|---|---|
| 1 | $M_{s_2}$ | 3 |
| 2 | $M_{s_1}$ | 3 |
| 3 | $M_{s_2}$ | 3 |
| 4 | $M_{s_2}$,$M_{s_3}$ | 4 |
| 5 | $M_{s_1}$,$M_{s_2}$ | 4 |
| 6 | - | 4 |
| 7 | - | 6 |

Table 2.2: Staging Solutions

Therefore, the independent variables vector is chosen to be made by the inert masses of the 3 stages, also the propellant masses can be used since are linked through the structural mass indexes $\xi_i$ already assumed. However the 3 inert masses have values closer one to each other with respect to the propellant ones, this gives meaning for such a choice.

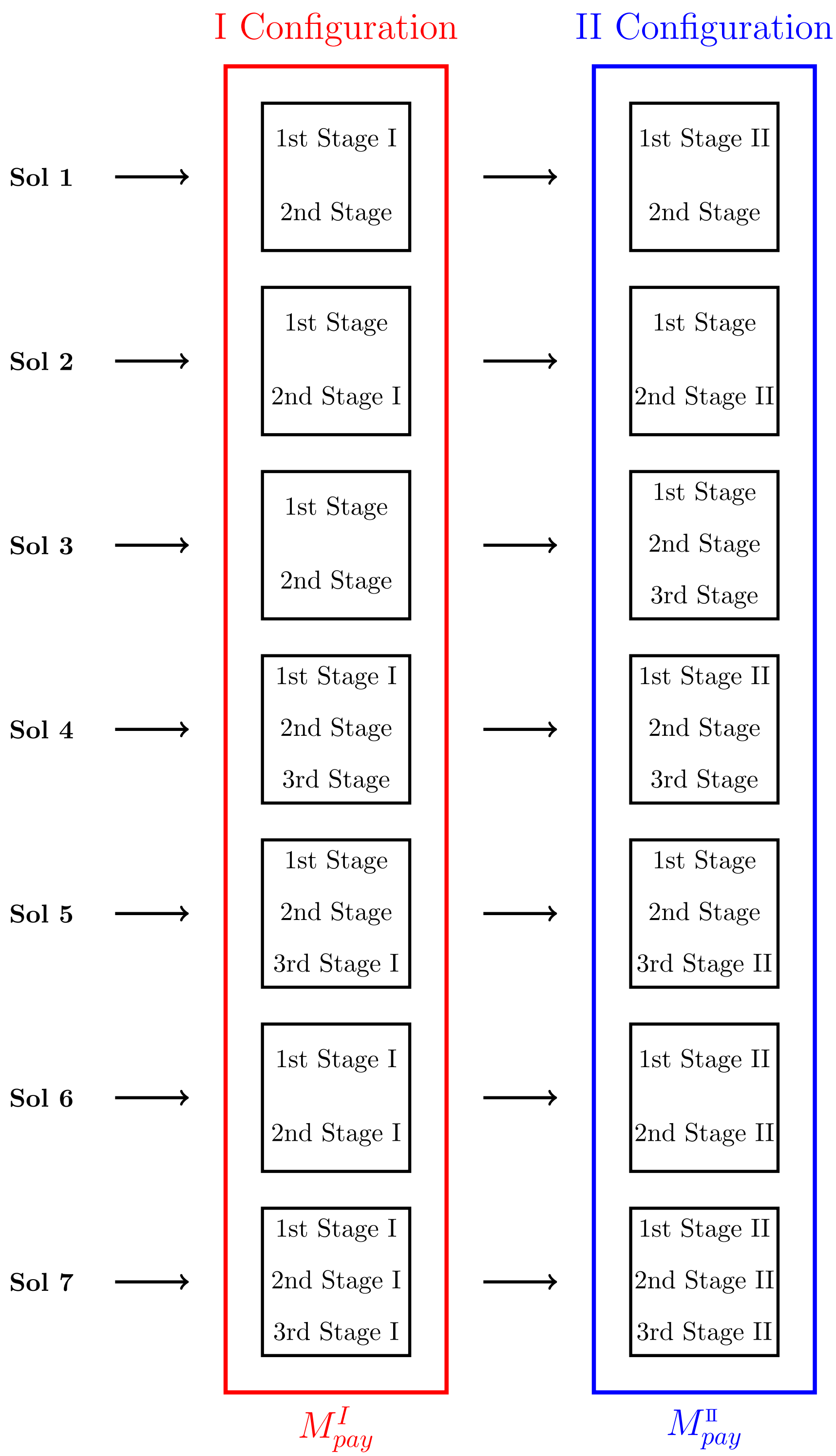


Figure 2.2: Multi-configuration Solutions Breakdown

Figure 2.3 gives another point of view of the 7 solutions, dividing the ones implying a 2 stage design rocket to a 3 stage one. Moreover it also introduces the problem on how to compute the cost functions $M_0^I$ and $M_0^{\mathrm{II}}$. Some of them require a numerical solution while others can be solved analytically. The solutions that express an enhancement of the first stage, can be computed analytically since only the first mass ratio depends on the first stage elements. While the replacement or the addition of an upper stage must be solved numerically, because every mass ratio is function of the upper stage values.
The following list summarizes the solving procedure.

- Solutions **6** and **7** are computed using the optimal staging theory, expressed by system of equation (2.12).
- Solutions **1** and **4** can be computed using an analytical approach.
- Solutions **2**, **3** and **5** are found using a numerical process.

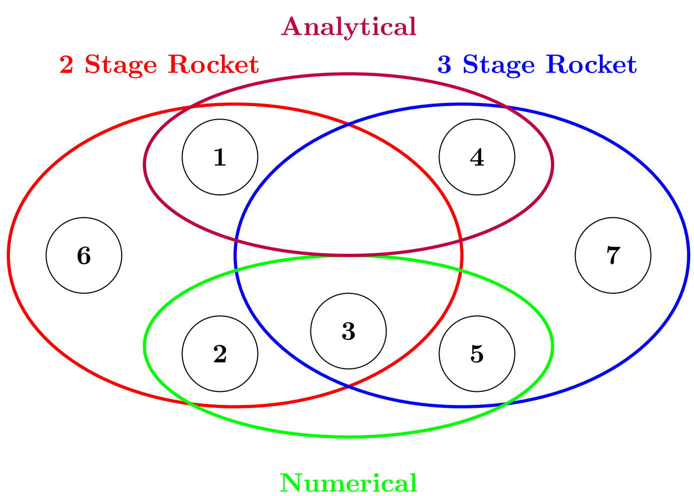


Figure 2.3: Multi-configuration staging, solution methods

### 2.3.1 Analytical Solution

As figure 2.3 shows, solutions **1** and **4** can be computed analytically since they are dealing with the enhancement of a first stage. Solution **4** is more general, therefore the passages to compute its wet masses are shown here, while solution **1** can be solved in the same way just neglecting the presence of a third stage.

Given $M_{s2}$ and $M_{s3}$ as independent variables, as first step the propellant masses $M_{p_2}, M_{p_3}$ are computed simply dividing respectively by the structural mass index $\xi$. Then, the second and the third stage mass ratios of the first configuration are computed.

$$M_{s_i} = M_{p_1}\xi_i \tag{2.16}$$

$$\begin{cases} N_2^I = \frac{M_{s_2}+M_{p_2}+M_{s_3}+M_{p_3}+M_{pay}^I}{M_{s_2}+M_{s_3}+M_{p_3}+M_{pay}^I} \\ N_3^I = \frac{M_{s_3}+M_{p_3}+M_{pay}^I}{M_{s_3}+M_{pay}^I} \end{cases} \tag{2.17}$$

The remaining mass ratio is immediately found from the $\Delta V$ constraint.

$$N_1^I = \exp\Big(\frac{\Delta V - C_2\log(N_2^I) - C_3\log(N_3^I)}{C_1}\Big) \tag{2.18}$$

And from it the propellant mass of the first stage, consequently its structural mass by means of $\xi_1$ is found as well.

$$M_{p_1}^I = \frac{M_{s_2} + M_{p_2} + M_{s_3} + M_{p_3} + M_{pay}^I}{1 + \xi_1 - N_1^I \xi_1}(N_1^I - 1) \tag{2.19}$$

The initial mass of the launcher in its first configuration is then computed:

$$M_0^I = M_{p_1}^I + M_{s_1}^I + M_{p_2} + M_{s_2} + M_{p_3} + M_{s_3} + M_{pay}^I \tag{2.20}$$

Regarding $M_0^{\mathrm{II}}$, the same procedure from (2.17) to (2.20) can be done using in this case $M_{pay}^{\mathrm{II}}$ as payload mass.

As already explained, solution **1** follows a very similar procedure but the only independent variable is $M_{s_2}$ and each variable referring to the third stage is not considered.

### 2.3.2 Numerical Solution

Solutions **2**, **3** and **5** must be solved numerically since they are dealing with the replacement or the addition of an upper stage.
In this subsection, is worth focusing on one solution in particular and showing the procedure to solve it. Then it can be proved that the other two solutions can be solved in a very similar way. The solution solved in this section is number **3**.

In case of this solution, the independent variable is $M_{s_2}$. The first step is to compute the masses of the first stage such as this 2 stage rocket is capable of launching $M_{pay}^I$. This is done in the same way of solution **1** already explained in the previous section.

Once the first and second stage are computed, the complex part is to calculate a third stage such

as, if placed on top of the existing two stages, the resulting 3 stage launcher is capable of launching $M_{pay}^{\text{II}}$.
This can be simply done by numerically solving equation (2.21) as a function of the propellant mass of the third stage (or the inert mass, is the same).

$$\Delta V = C_1 \ln(N_1^{\text{II}}) + C_2 \ln(N_2^{\text{II}}) + C_3 \ln(N_3^{\text{II}}) \tag{2.21}$$

A better way to do so, is to switch from a non-linear solving problem, to an optimization process. It is very important to point out that this optimization is **NOT** the MultiObjective optimization explained before, this is another way to numerically solve equation (2.21), everything in this subsection that treats about an optimization is referred to this one, and not the MOO.
The meaning of this switch comes after a few passages. The cost function in this case is $J$, that is clearly equal to 0 when equation (2.21) is solved.

$$J = \Big(\Delta V - C_1 \ln(N_1^{\text{II}}(M_{p3})) - C_2 \ln(N_2^{\text{II}}(M_{p3})) - C_3 \ln(N_3^{\text{II}}(M_{p3}))\Big)^2 \tag{2.22}$$

A question that is important to answer, is if any value of the independent variable $M_{s_2}$ can lead to a zero of $J$, and consequently to a feasible value of $M_{p_3}$.

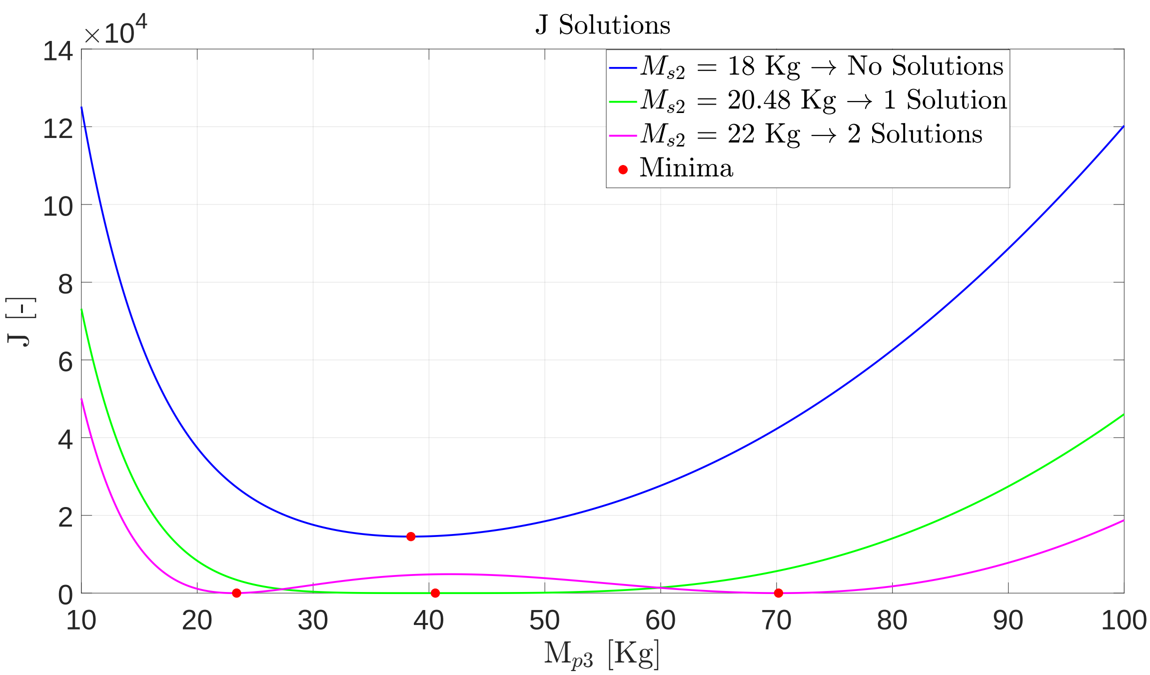


Figure 2.4: J Possible Solutions

Figure 2.4 can answer to this question, for $M_{s_2}$ lower than a certain threshold $J$ does not have a zero which means no solution. At that threshold there is only one solution of the equation, but for higher values two solutions appear and start spreading out for increasing value of $M_{s_2}$.

Now is worth asking which of those 2 solutions leads to a lower value of $M_0^{\text{II}}$, clearly $M_0^I$ does not depend on which of the two solutions is picked up, but instead only on $M_{s_2}$.
As can be seen in figure 2.5, the higher solution tends to increase almost linearly with $M_{s_2}$, the lower solution instead has a small decrease and then has a linear increment but with a less stiff slope.

An important aspect that can be inferred from 2.5 is that the lower solution provides always better results than the higher one, this fact has a key importance when defining the initial condition of the gradient based optimization without recurring to global one.
Regarding the values of $M_{s_2}$ smaller than the threshold, as said previously they do not provide any feasible solution, however for continuity purposes, $M_0^{\text{II}}$ has been penalized by the value of the minimum $J$ shown in equation (2.22). This explains the choice of using an optimization process instead of a non-linear solver. So, in case of available solutions, the penalty is simply 0.

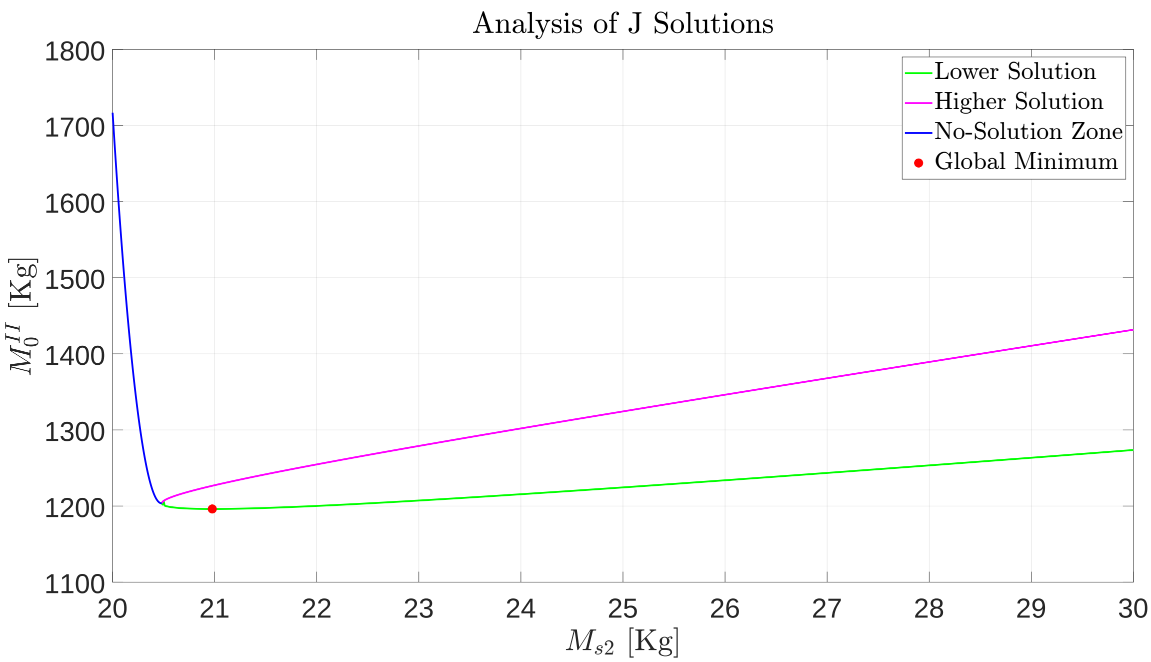


Figure 2.5: Analysis of the 2 J Solutions

Regarding the other solutions, number **2** is solved by doing the same optimization twice. In this case $M_{s_1}$ is the independent variable, and the optimization outcomes are $M_{p_2}^I$ and $M_{p_2}^{\text{II}}$ for the two classes of payloads respectively.
Finally, solution **5** is slightly more complex. The independent variables are $M_{s_1}$ and $M_{s_2}$ while the optimization outcomes are $M_{p_3}^I$ and $M_{p_3}^{\text{II}}$. Again the same optimization is done twice.

The optimization algorithm chosen for this numerical solution, is a gradient-based method that depends on the initial conditions. This gives further meaning to the analysis of the 2 $J$ solutions just done, because depending on the initial value of the optimization the algorithm can converge on the higher or lower solutions shown in figure 2.5.

### 2.3.3 MultiObjective Optimization

Finally is possible to set up the whole MultiObjective Optimization process. The independent variable vector is the following:

$$\underline{X}_{opt} = \begin{bmatrix} M_{s_1} & M_{s_2} & M_{s_3} & n_{sol} \end{bmatrix} \tag{2.23}$$

Where $n_{sol}$ is an integer number ranging from 1 to 7 that identifies the solutions proposed previously.
The multiobjective algorithm chosen is a heuristic MultiObjective Particle Swarm Optimization (MOPSO), this is chosen mainly for the availability of this algorithm in the coding environment where this process is implemented. The same optimization has been performed using this case a Genetic Algorithm (GA) multiobjective, however it results with a slightly worse outcome and a slower computational time.

## 2.4 Results

What can be seen from figure 2.6 is that the best solution for both $M_0^I$ and $M_0^{\mathrm{II}}$ is number **7**, this is not surprising because that solution is basically made of 2 different rockets both optimized for their respective payload class. Solutions **2**, **5** and **6** do not appear meaning that there are solution with the same number of engines which are more mass efficient.

Is worth discussing also of solutions **1** and **3**, with the same number of motors they lead to different design both optimal depending which payload class is worth benefiting. Up to this point there is not reason to favor one payload class with respect to the other, a wide choice is left to a further design only neglecting the sub-optimal solutions.
Finally, solution **4** is the most interesting one. Using 4 different motors it gets very close to the optimal solution given by **7** saving also 2 motors, then, among the Pareto-Front solutions, the closest to the origin has been selected as working point from now on.

What can also be noticed of that solution, is that the two outermost points of that front, correspond to the optimal value expressed by solution **7** in the two classes. For instance, the top point of that front, has the same $M_0^I$ as the optimal solution, while the other outermost point (to the right) has the same $M_0^{\mathrm{II}}$ of the optimum. A future work may find out which one of the two classes is worth optimizing the rocket for, and one of the solutions belonging to that front may be selected. Table 2.3 shows all the outcomes resulting from this optimization.

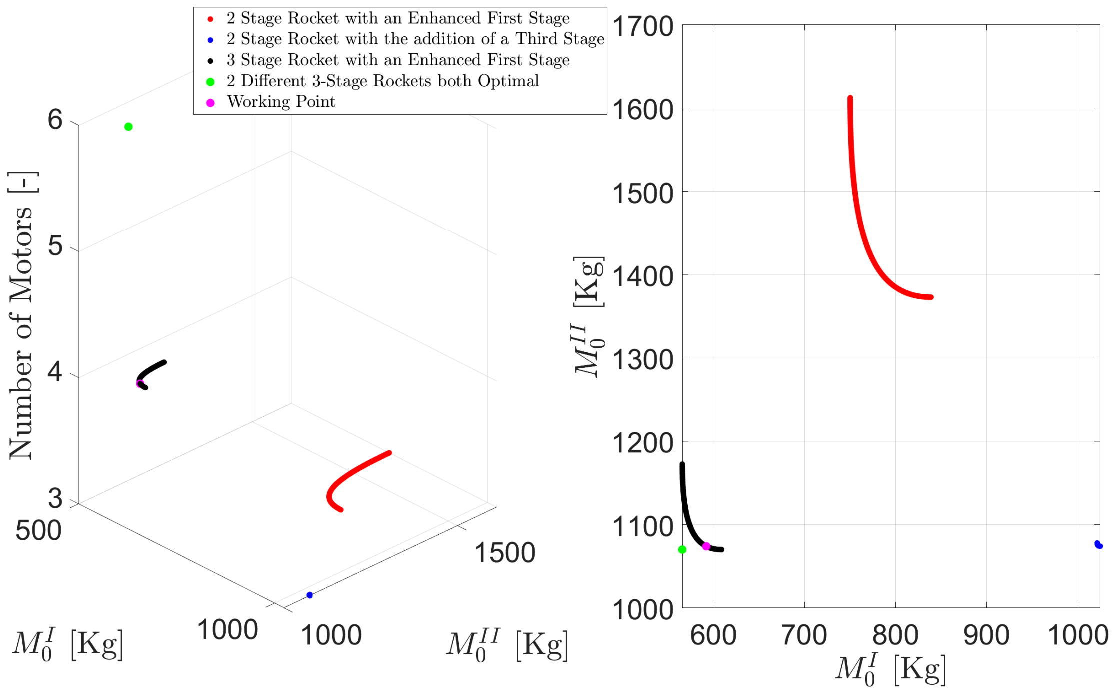


Figure 2.6: 3D Pareto-Front Solution

## 2.5 Validation

Even if the computations are quite clear and the results can be verified just looking at the resulting $\Delta V$, a very brief validation can be interesting also to understand better the results.
A very simple way to prove the optimal staging theory is by means of a so-called grid search analysis. As explained, if the payload mass and the total $\Delta V$ are fixed, a 3 stage rocket has 2 degrees of freedom that can be expressed in various different ways. The ones selected are the inert masses of the second and the third stage, having those values it is possible to compute the rest of the launcher and estimate its total wet mass. Again the choice over the inert masses with respect the propellant ones is due to the fact that those values are much closer one to the others, but exactly the same can be done with the propellants.
This has been done for varying values of those two independent elements, and a contour has been made to show the total initial mass of the launcher in both configurations.

Looking at figure 2.7, it is easy to notice that the results from the optimal staging theory (red dots) match perfectly the minima of both configurations, the green dot represent the optimal value in the other configuration and the blue one shows the solution selected for this work. The blue dot in fact is somewhere in between the two optimal results which is an expected outcome. It can be proved that the solutions of the Pareto front analysis shown in figure 2.6, identified by the black line, are part of an hypothetical curve joining the two minima.

| **Parameters** | $\mathbf{M_p}$ | $\mathbf{M_s}$ | $\mathbf{M_{tot}}$ |
|---|---|---|---|
| Units | Kg | Kg | Kg |
| 1st Stage I | 346.8 | 31.2 | 378 |
| 1st Stage II | 778.9 | 70.1 | 849 |
| 2nd Stage | 156.3 | 15.6 | 172 |
| 3rd Stage | 27.7 | 4.5 | 32 |
| Full Rocket I | 531 | 51.3 | 593 |
| Full Rocket II | 963 | 90.2 | 1073 |

Table 2.3: Staging Results

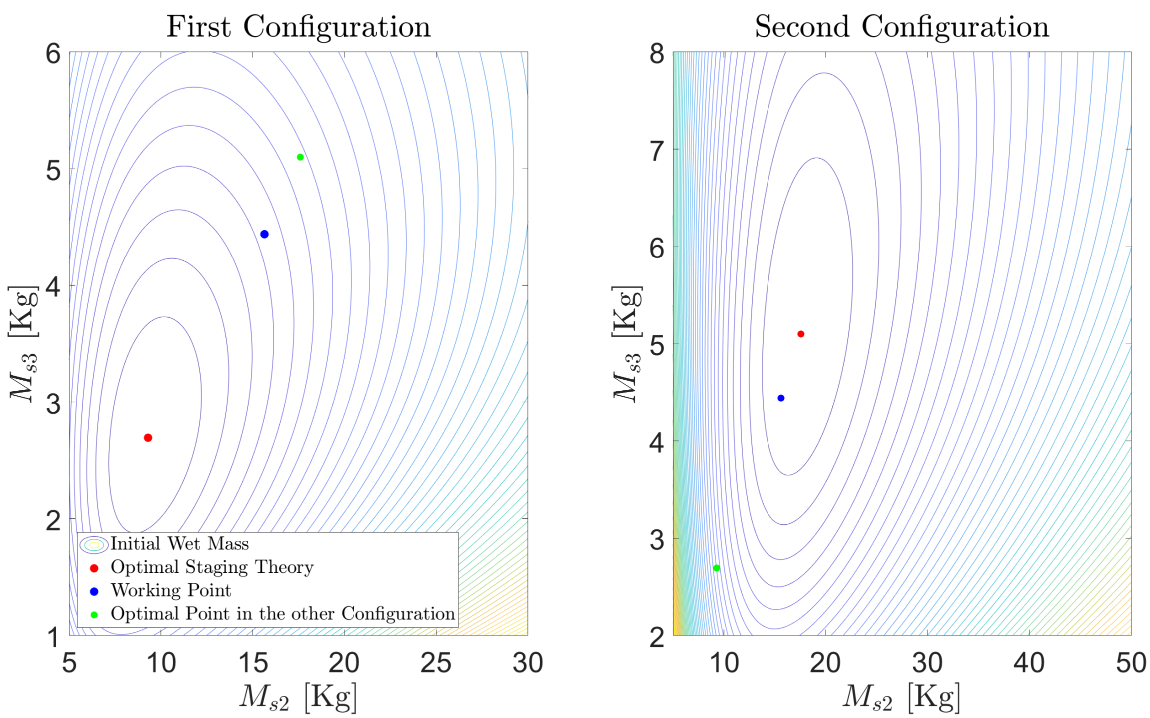


Figure 2.7: Staging Validation

# Chapter 3

# Propulsion System Design

The propulsion system is a key part in the design of a launch vehicle, maybe the most important one. A good propulsion selection can lead to high engine efficiency, that is strictly linked to the initial mass of the launcher. Many different propulsion choices are available, from liquid to solid passing from hybrid, each one has its own advantages and drawbacks. In this chapter the propulsion system is selected and designed, the guesses used in chapter 2 are checked and at the end, an innovative solution is proposed for further development.

## 3.1 Propulsion System Choice

As said in the introduction, the market of air launched rockets and small launchers usually adopts simple propulsion solutions like solid rocket motors or liquid rocket engines powered by RP-1 and LOX for their simplicity, reliability and energy density. Liquid rocket engines can provide higher specific impulse and more thrust control but they are more complex, have higher structural mass indexes, induce sloshing issues, and usually even thermal control problems.
On the other hand, solid propulsion is way simpler and cheaper but has lower engine performances and provides a less precise orbit insertion which has a key importance since usually CubeSats do not have primary propulsion therefore correcting a wrong orbit is harder.
Some liquid propellants can be storable not at cryogenic temperature, therefore avoiding thermal control issues, but a typical storable propellant couple like $UDMH + N_2O_4$, widely used in in-space applications and some rockets like the Proton, is highly toxic thus not desirable. Other classical liquid propellant couples (e.g. $CH_4 + LO_2$, $RP{-}1 + LO_2$, $LH_2 + LO_2$) require at least one cryogenic fluid, consequently inducing boil-off and thermal control issues. Moreover, it is important to point out that a classical launcher usually lift-off a few minutes after the fueling process, an air launched rocket instead must be fueled, integrated on the carrier aircraft and then launched after several minutes of flight depending on the launch location. Solid rocket motors also grant higher structural resistance with respect to liquid, thus the launcher can withstand higher accelerations improving its trajectory-related efficiency.
For the reasons just pointed out, the propulsion system of every stage is a solid architecture. Another motivation to this choice is the Pegasus rocket, which makes use of the same kind of architecture. More consideration are done regarding precision orbit insertion and possible future different archi-

tectures in section 3.4.

## 3.2 Propulsion Performances

As a first step in the design process there is the propellant composition choice, there are several solutions but many currently used solid rocket motors adopt a mixture of Ammonium Perchlorate (AP) as oxidizer, a binder and some energetic additives. In Italy there is a company which has cutting-edge technology in terms of solid rocket motors, AVIO, placed in Colleferro, designs and builds all the solid stages for the VEGA rocket as well as the booster for the Ariane5 and the incoming Ariane 6.
Therefore propellant composition selected for this study is based on AVIO technology, the mixture is named HTPB 1912. It uses AP as oxidizer, Hydroxyl-Terminated PolyButadiene (HTPB) as a binder and Aluminum (Al) as energetic additive, the mass percentage of such a mixture is the following:

$$\begin{cases} AP = 69\% \\ HTPB = 12\% \\ Al = 19\% \end{cases} \tag{3.1}$$

A first important parameter to fix is the combustion chamber pressure. It has a very important role in a solid rocket motor design, first of all it provides effects into chemical reactions inside the combustion chamber, but most importantly it drives the burning rate by means of the Vieille law [23].

Again more considerations are needed in terms of grain geometry and burning rate, for simplicity the combustion chamber pressure is taken as 50 bar as a reference value coming from typical operational solid rocket motors.

After the pressure another crucial parameter is the specific impulse. There are several ways to estimate that parameter, a first very simple way is to take the values from existing SRM like the ones developed by AVIO that forms the VEGA rocket for instance. Another solution is instead to estimate it using a chemical equilibrium software and after that correct the value using a propulsion efficiency taken from literature. In the case of this work both solution are followed and then compared in order also to validate this choice.

In table 3.1 are reported every motors currently being developed and built by AVIO with its corresponding performances like specific impulse and altitude of ignition.

So a good estimate of specific impulses based on that values can be the following:

| **Parameters** | **Thrust** | $\mathbf{I_{sp} - vac}$ | $\mathbf{t_b}$ | $\mathbf{H_{ign}}$ |
|---|---|---|---|---|
| Units | $kN$ | $s$ | $s$ | $Km$ |
| **P120 C** | 4500 | 278.5 | 132.8 | 0 |
| **P80** | 3015 | 280 | 110 | 0 |
| **Zefiro 23** | 1120 | 287.7 | 77.1 | 52 |
| **Zefiro 40** | 1304 | 293.5 | 92.9 | 52 |
| **Zefiro 9** | 317 | 295.9 | 119.6 | 127 |

Table 3.1: AVIO Solid Rocket Motors [8] [9]

$$\begin{cases} I_{sp1}^{avio} = 280s \\ I_{sp2}^{avio} = 293s \\ I_{sp3}^{avio} = 295s \end{cases} \tag{3.2}$$

The other solution starts with the usage of Chemical Equilibrium and Application (CEA) software developed by NASA [24], given a propellant composition, the combustion chamber pressure and the expansion ratio of the nozzle it provides all the thermochemical values and performances of the engine in the ideal case. The propellant composition and the chamber pressure are defined above, while the expansion ratios are discussed in a few lines. A shifting equilibrium is preferred with respect to a frozen model because the aim is to get the perfect ideal values, and only after they are adjusted with the corresponding efficiency.

$$\begin{cases} I_{sp1}^{id} = 301.2s \\ I_{sp2}^{id} = 313.3s \\ I_{sp3}^{id} = 317.4s \end{cases} \tag{3.3}$$

As expected those impulses are way greater than the estimated ones, in order to account for all the losses (two phase flow, divergence flow, chemical recombination, boundary layer, throat erosion etc...) one possibility is to model all the losses, but it is not so much meaningful at this stage of the development. The other possibility is to take the efficiency of classical solid rocket motors from literature; and in this case the work of Landsbaum, Salinas and Leary comes in handy [25]. They compared experimental values of specific impulses from different solid rocket motors with the ideal ones in order to check the validity of a losses model. The total efficiency resulting from their analysis ranges between 0.92 and 0.93, with this consideration is possible to adjust the specific impulses of the motors simulated before with CEA.

$$\begin{cases} I_{sp1}^{cea} = 279s \\ I_{sp2}^{cea} = 290s \\ I_{sp3}^{cea} = 293s \end{cases} \tag{3.4}$$

As can be noticed, the estimate is very precise with around 1% of error compared to the AVIO values.

The selection of the Thrust is another very important aspect in a propulsion design, an high trust-to weight (T/W) ratio reduces gravity and drag losses but the dynamic loads would be higher for the structure and the payload. Usual manned launchers have T/W around 1.2 [5], but an air launched rocket can afford higher values, taking as a reference the Pegasus XL, the thrust value for each stage is set in the following way:

$$\begin{cases} T_1^I = 2g_0 M_0^I \\ T_1^{\mathrm{II}} = 2g_0 M_0^{\mathrm{II}} \\ T_2 = 3g_0 \frac{M_{0_2}^I + M_{0_2}^{\mathrm{II}}}{2} \\ T_3 = 3g_0 \frac{M_{0_3}^I + M_{0_3}^{\mathrm{II}}}{2} \end{cases} \tag{3.5}$$

The T/W ratio is equal to 2 for the first stage, and 3 for the other stages. Since the second and third stages have different initial masses across the two configurations, a mean has been considered.

Then, some brief considerations on the nozzle must be done to complete the propulsion analysis. First of all the throat area $A_t$ is computed using the data previously assumed, in the following equation $C^*$ represent the characteristic velocity which is a parameter of merit of the combustion chamber performance; this has been computed along with the specific impulse using the CEA tool and it results 1578 m/s.

$$A_t = \frac{C^* T}{P_c I_{sp} g_0} \tag{3.6}$$

Is worth pointing out that the throat area, in particular in SRM, changes in time, regenerative or film cooling cannot be done like in LRE, so the only solution available not to melt the nozzle is to cover the throat with ablative materials like graphite; those however increase the throat area and change the motor performances during flight. For simplicity those effects are not considered in this work and the throat area is assumed constant throughout the whole burn.

Once defined the throat area, the next step is to select the expansion ratio of the nozzle. Usually it is optimized at the altitude of ignition, but that is true only in case of atmospheric flight; for vacuum stages it is usually fixed looking at existing motors.

The first stage ignites at 11 Km altitude, so from the external pressure and the specific heat ratio $\gamma$ coming again from CEA code is possible to compute the nozzle expansion ratio by means of the following isoentropic relation.

$$\frac{A_t}{A_e} = \frac{1}{\epsilon} = \left(\frac{\gamma+1}{2}\right)^{\frac{1}{\gamma-1}} \sqrt{\frac{\gamma+1}{\gamma-1}} \left(\frac{P_e}{P_c}\right)^{\frac{1}{\gamma}} \sqrt{1 - \left(\frac{P_e}{P_c}\right)^{\frac{\gamma-1}{\gamma}}} \tag{3.7}$$

The other two expansion ratios are instead selected from literature [23] because a nozzle is never optimized in vacuum. All the 3 expansion ratios are reported in the following part.

$$\begin{cases} \epsilon_1 = 44 \\ \epsilon_2 = 80 \\ \epsilon_3 = 100 \end{cases} \tag{3.8}$$

The last part of the nozzle regards its shape, assuming a double truncated cone shape which is by far the simplest choice, is possible to compute the length of the divergent part. The convergent one instead is considered to be inside the rocket case and in any case it does not give an high contribution to the overall length. Assuming a typical divergent angle $\theta_{dv}$ of about 20 degrees, the length is found as follows.

$$L_{nozz} = \frac{r_e - r_t}{\tan \theta_{dv}} \tag{3.9}$$

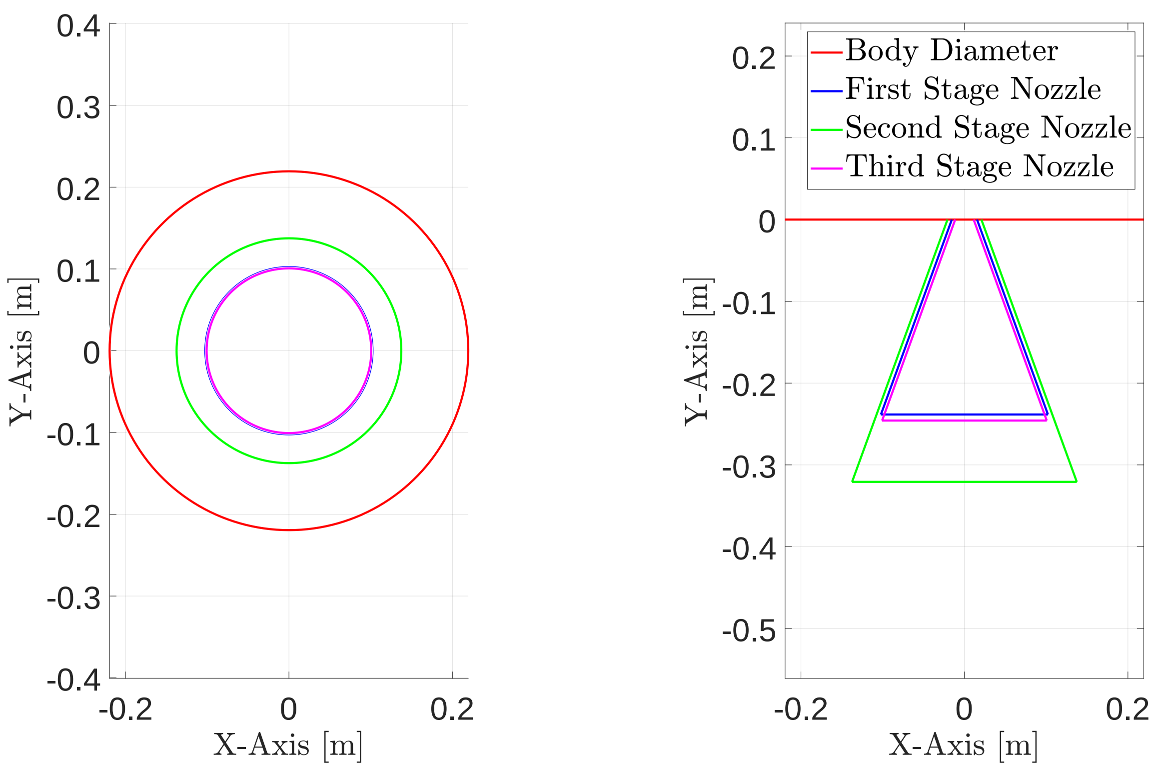


Figure 3.1: Nozzle Dimensions

Now the next step is to compute the rocket dimensions, given the overall propellant mass from the staging section, the volume of this latter is immediately found with its density imposed at $\rho_P = 1600\ Kg/m^3$.
$\eta_V$ is the ratio between the propellant volume and the case volume, a typical value from literature [26] is 0.9.

$$\eta_V = \frac{V_P}{V_{case}} \tag{3.10}$$

$$fineness = \frac{4V_{tot}}{\pi D^3} + \frac{L_{fair}}{D} + \frac{L_{nozz}}{D} \tag{3.11}$$

Standard fineness ratios for space launcher vary from 5 to 25 [3], having the overall rocket volume and imposing a fineness ratio allows to solve equation (3.2) and compute the diameter D. Constraints on the diameter and length are introduced by the carrier aircraft capability and the adapter dimensions.

The maximum length acceptable by the Eurofighter Typhoon is around 6 meters, so no problem from this point of view, while the payload deployer has dimensions a little bit greater than the CubeSat inside (assumed as 20% more), for instance a 6U CubeSat has a deployer of around 12x24x36 cm. Also the dynamic envelope of the fairing must be considered, so a rough estimation of the minimum diameter is 30 cm.

In table 3.2 are reported the propulsion performances of each stage as well as the whole rocket in both configurations.

| **Parameters** | **L** | **D** | $\epsilon$ | **T** | $\mathbf{I_{sp}}$ | $\mathbf{A_e}$ |
|---|---|---|---|---|---|---|
| Units | $m$ | $m$ | $-$ | $kN$ | $s$ | $cm^2$ |
| 1st Stage I | 1.61 | 0.44 | 44 | 11.6 | 279 | 328 |
| 1st Stage II | 3.40 | 0.44 | 44 | 21.1 | 279 | 594 |
| 2nd Stage | 0.86 | 0.44 | 80 | 6.5 | 290 | 319 |
| 3rd Stage | 0.24 | 0.44 | 100 | 1.4 | 293 | 85 |

Table 3.2: Propulsion Performances Overview

## 3.3 Masses Breakdown

As shown in the staging chapter 2, mass indexes are set as an initial guess for each stage, the aim of this part is to set a simple analytical procedure that computes the structural mass given the propellant mass and therefore check the validity of that guess.

This part is very important especially for the 3rd stage, because it has a propellant mass too low to make comparison with existing solid rocket motors, so estimating a structural mass index is very difficult and could results in outcomes very far from common values. Of course further work is required in this section in order to get a better estimation of the overall mass including avionics and other elements not included in this preliminary design.
The reference for the following models is the Humble book [26].

The inert mass of each stage can be divided into 6 main contributions:

$$M_s = M_{ign} + M_{ins} + M_{case} + M_{noz} + M_{tvc} + M_{misc} \tag{3.12}$$

Where, $M_{ign}$ is the mass of the igniter, $M_{ins}$ is the contribution of the thermal insulator, $M_{case}$ is simply the propellant case, $M_{noz}$ is the nozzle mass and finally $M_{tvc}$ is due to the presence of a thrust vector control system. $M_{misc}$ is made by every other element not considered in that list.

The main contribution is not surprisingly the case. The structure must withstand inertia loads as well as the high pressure inside the vessel. Looking at existing SRM, the italian company AVIO already mentioned makes use of filament winding with pre-impregnated carbon fiber in order to create more lightweight casings than common metal vessels. Taking advantage of this technique to make more efficient structures is crucial in the propulsion design, furthermore the mass indexes $\xi$ are lower than using classical metal casings. This facts give meaning to the choice of carbon composite casing in this work.

The case thickness is given by the thin walled formula where the main load is introduced by the combustion chamber pressure $P_c$.

$$t_{case} = f_s \frac{P_c R_{case}}{F_{tu}} \tag{3.13}$$

Where $f_s$ is the safety factor imposed at 1.25 and $F_{tu}$ is the ultimate tensile strength of carbon fiber, 600 MPa. Imposing a cylindrical shell with a planar bulkhead in front, the mass of the case can be immediately found.

The igniter is a device that starts the combustion process throughout the grain, solid rocket motors usually use a pyrogenic igniter, which is basically a small SRM that provides hot gases and pressure if triggered by an electrical current. A correlation to compute its mass is the following:

$$M_{ign} = 0.0138 V_{port}^{0.571} \tag{3.14}$$

Where $V_{port}$ is the volume of the central port computed again my means of a correlation.

$$V_{port} = V_p(\frac{1}{\eta_V} - 1) \tag{3.15}$$

Thermal insulation is critical in a solid rocket propulsion system, temperature inside the combustion chamber reaches around 3500 K that is too high to withstand for any casing, in particular if made by composite material. Standard insulation materials are rubber-based with low thermal conductivity and are around 1cm thick.
In order to compute the mass another correlation is used.

$$M_{ins} = 1.788 \times 10^{-9} M_p^{-1.33} t_b^{0.965} (L/D)^{0.144} L_{sub}^{0.058} A_w^{2.69} \tag{3.16}$$

Where $M_p$ is the propellant mass in Kg, $t_b$ the burning time in s, $L_{sub}$ is defined as the length of the submerged nozzle in cm divided by the overall stage length in meter, and finally $A_w$ is the wetted area in $cm^2$.
Despite being very good for standard SRMs, this correlation provides higher results than expected for the motors designed so far. Another solution still taken from Humble suggests half of the case mass, this latter has been therefore used.

The nozzle is very difficult piece of hardware to model, it is made by many different parts with different materials. A very rough correlation can be set up but further analysis are required to get more precise values.

$$M_{noz} = 2.56 \times 10^{-5} \left[ \frac{(M_p C^*)^{1.2} \epsilon^{0.3}}{P_c^{0.8} t_b^{0.6} \tan(\theta_{cn})^{0.4}} \right]^{0.917} \tag{3.17}$$

Where $\theta_{cn}$ is the angle of the converging nozzle, and $t_b$ is the burning time.

Like the nozzle, the thrust vector control is hard to model, as a first approximation it can be thought to scale like the nozzle itself. So as Humble's book suggest, half of the nozzle mass can be a good first estimation.

$$M_{tvc} = \frac{1}{2} M_{noz} \tag{3.18}$$

At last there are all the elements which are not included in the just mentioned contributions, like the interstages for instance, to take those into account this miscellaneous mass is considered to be 10% of the total mass computed so far.

$$M_{misc} = 0.1(M_{ign} + M_{ins} + M_{case} + M_{noz} + M_{tvc}) \tag{3.19}$$

Table 3.3 shows all the masses breakdown of each stage and the entire launcher in both configurations.

| **Parameters** | $\mathbf{M_p}$ | $\mathbf{M_{case}}$ | $\mathbf{M_{ins}}$ | $\mathbf{M_{ign}}$ | $\mathbf{M_{noz}}$ | $\mathbf{M_{tvc}}$ | $\mathbf{M_{misc}}$ | $\mathbf{M_s}$ |
|---|---|---|---|---|---|---|---|---|
| Units | Kg | Kg | Kg | Kg | Kg | Kg | Kg | Kg |
| 1st Stage I | 346.8 | 13.46 | 7.81 | 4.27 | 2.65 | 1.32 | 3.17 | 34.8 |
| 1st Stage II | 778.9 | 28.95 | 15.93 | 6.78 | 5.73 | 2.86 | 6.32 | 69.5 |
| 2nd Stage | 156.4 | 6.64 | 4.43 | 2.71 | 1.43 | 0.71 | 1.82 | 20 |
| 3rd Stage | 27.8 | 2.03 | 1.60 | 1.01 | 0.25 | 0.13 | 0.62 | 6.8 |
| Full Rocket I | 531 | 22.13 | 13.84 | 7.99 | 4.33 | 2.16 | 5.60 | 61.6 |
| Full Rocket II | 963 | 37.62 | 21.96 | 10.50 | 7.40 | 3.70 | 8.75 | 96.3 |

Table 3.3: Mass Breakdown Budget

In table 3.4, the mass indexes assumed in the staging design are compared with the ones just computed. First and second stage have a low error, meaning that the assumption was good enough.

| **Parameters** | **Assumed** $\xi$ | **Computed** $\xi$ |
|---|---|---|
| Units | - | - |
| 1st Stage I | 0.09 | 0.0902 |
| 1st Stage II | 0.09 | 0.0830 |
| 2nd Stage | 0.1 | 0.1042 |
| 3rd Stage | 0.16 | 0.1755 |

Table 3.4: Mass Indexes Comparison

What it turns out is that the structural mass index of the third stage after many iterations approaches the value of 0.21, which is even higher of the one belonging to the tactical missile world [3]. The meaning could be that the model used so far are based on existing rocket motors far bigger than the third stage, therefore those correlations are not perfectly suitable for that motor. A good compromise is imposing this value at 0.16, which is in the middle between the space launchers world ($\xi \sim 0.1$) and the tactical missile one ($\xi \sim 0.2$). Further work is certainly required, to compute the inert masses of the stages without adopting correlations of any kind.

### 3.3.1 Validation

To validate the masses breakdown just done, those results are compared to values of existing motors and find out if a visual correlation exists. The motors considered are: RSRM (Reusable Solid Rocket Motor), ASRM (Advanced Solid Rocket Motor) from the Space Shuttle, Titan IV, SRMU, Castor IVA, GEM, ORBUS 21, ORBUS 6E, Star 48B, Star 37XFP, Star 63D, Orion50SAL, Orion 50, Orion 38 [26].

In figure 3.2, the blue dot represent the reference motors while the red ones show the 4 motors developed in this chapter. As can be noticed, case, insulation, nozzle and overall ratio between propellant and structures are well in line with the references. Igniter and miscellaneous instead

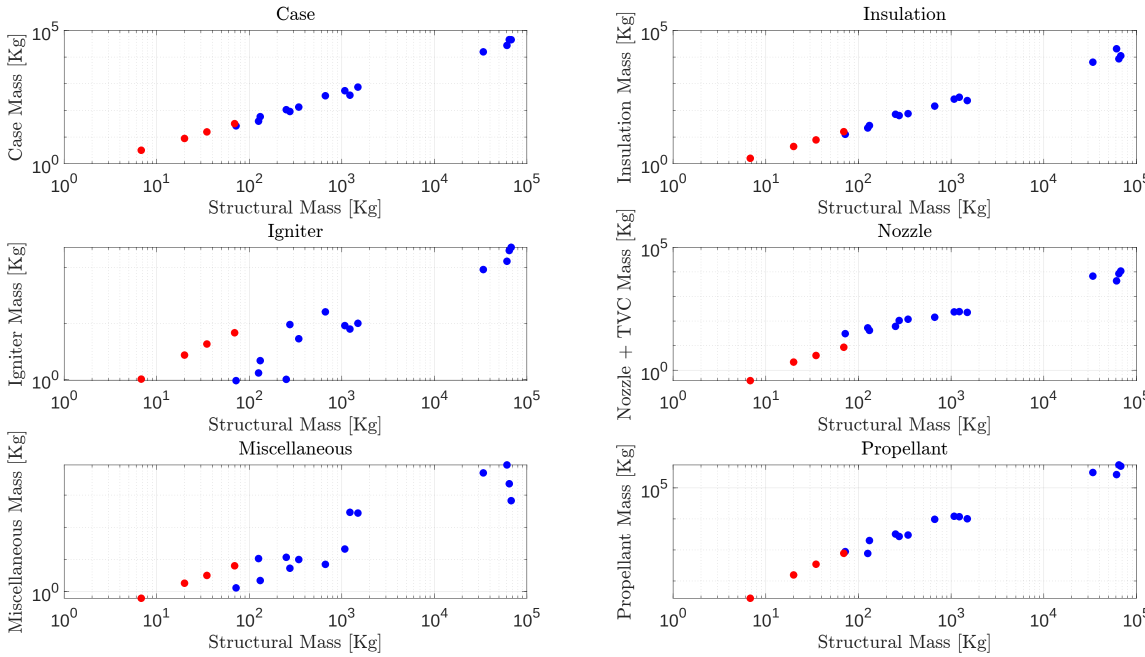


Figure 3.2: Breakdown Masses Validation

varies a little bit, but it must be said that even the reference motors are more sparse than the other contributions Therefore it is a fully acceptable result.

## 3.4 Hybrid Rocket Engine Alternative

Performing the orbit insertion with a solid upper stage can lead to a rough altitude precision, liquid rocket engines instead have the possibility of throttling the engine, and in case, shut it down when the velocity reaches the desired one with no particular issue. Looking at the two air launched rockets mentioned in the introduction, the Pegasus XL with its solid third stage has an accuracy of $\pm$ 45 $km$ altitude and $\pm$ 15 $km$ with the addition of its hydrazine fourth stage, while LauncherOne has a liquid second stage and its altitude accuracy is $\pm$ 15 $km$ [7] [6].
Again to stress the importance of a throttlable upper stage, the launcher VEGA which is made of 3 solid rocket motors, works with a 4th stage that uses a liquid engine powered by hydrazine-based storable propellant; this allows VEGA to get, again, an altitude accuracy of $\pm$ 15 $km$ [9].

This work does not want to deal with toxic propellant, so the choice of a liquid upper stage powered by hydrazine has been discarded, classic liquid rocket engines using liquid oxygen as oxidizer are way to complex and can lead by many issues already discussed in the introduction of this chapter. One alternative could be a liquid green monopropellant based on Ammonium DiNitramide (ADN), however there are no benefits from both the specific impulse point of view and the complexity that would derive from.

One very interesting solution could be using an hybrid rocket engine (HRE). This engine can throttle up and down allowing a better orbit insertion than a solid, it has higher specific impulse and it does not introduce too much complexity in the design. Numerous works regarding the application of an HRE to air launched vehicles has already been done, this stresses the feasibility of such a concept [27] [28] [29] [30]. Moreover, the only hybrid rocket engine nowadays operational, is being used by the Virgin Galactic SpaceShipTwo vehicle, which, by the way, is aero-deployed.

The choice on the propellant couple falls over a classic HTPB as fuel and hydrogen peroxide as oxidizer. HTPB is a very common choice in hybrid rocket propulsion, it is very reliable, well known, and can lead to high specific impulses even in the absence of metallic additives. Most of the studies uses liquid or gaseous oxygen as oxidizer, but this choice leads to the storability and boil-off problems addressed before. Hydrogen peroxide instead is storable, can gives specific impulses comparable to gaseous oxygen if used in high concentration and moreover it can be used as monopropellant for attitude control thruster as many studies proved it [31].

Standard architectures of HRE are mainly composed by a cylindrical shaped fuel grain with one or many ports where the oxidizer is injected in. This is done because one of the biggest issue of HRE is the low regression rate and therefore thrust. One interesting alternative could be a so-called Vortex Flow Pancake (VFP) configuration, where two fuel disks are placed on the top and bottom of the combustion chamber, and the oxidizer is injected in between forming a vortex flow. Another important feature of this exotic configuration, is the geometric ration between length and diameter which is below 1 very different from classical HRE solutions. Looking at the dimension of the third stage 3.2, those values gives further meaning to such an exotic solution.

As already said, this work is limited to near term feasible concept, therefore since the HRE propulsion has a Technology Readiness Level (TRL) below 6/7 this section has only the aim to show what could be achieved with such a technology and propose a future upgrade of the launcher. Therefore the following chapters use the third stage solid rocket motor designed in the previous sections.

First of all, a propulsion analysis is performed using again the CEA code. It turns out that at O/F of 6.5 (stoichiometric ratio) the specific impulse is around 330 s, literature suggests that using gaseous oxygen instead of hydrogen peroxide the specific impulse can get up to 350 seconds [32]. However, if the concentration of the hydrogen peroxide is high enough (>95%), it can be compared as a first approximation to the results of gaseous/liquid oxygen [33].

Together with this value, a structural mass index is assumed based on literature studies (despite being applied to classic hybrid configurations), a further analysis is required to estimate better that value for VFP configurations. This, in general, is higher than the solid equivalent. Hybrid rocket engines require, of course, case, insulation and nozzle that can be considered at a first approximation the same as SRMs; the usage of hydrogen peroxide allows to save the mass of the igniter since the propellant couple are hypergolic [33]. However HREs require the oxidizer tank as well as all the pressurizing gas and pipe lines that increase the overall inert mass. Preliminary analysis of HREs used in air to orbit applications, suggest a structural mass index $\xi$ ranging between 0.22 and 0.28 [28] [30], therefore, the value selected for this preliminary work is 0.25.
Using this index together with the computed specific impulse is possible to re-calculate the staging

design with the multiconfiguration strategy explained in chapter 2. The results can be seen in table 3.5, the initial masses of the two launchers are slightly lower than the standard rockets with solid upper stages.

| **Parameters** | $\mathbf{M_p}$ | $\mathbf{M_s}$ | $\mathbf{M_{tot}}$ |
|---|---|---|---|
| Units | Kg | Kg | Kg |
| 1st Stage I | 353.7 | 31.8 | 385.5 |
| 1st Stage II | 781.5 | 70.3 | 851.8 |
| 2nd Stage | 149 | 14.9 | 164.3 |
| 3rd Stage | 22.5 | 5.6 | 28.1 |
| Full Rocket I | 525.5 | 52.4 | 588.6 |
| Full Rocket II | 953.3 | 90.9 | 1064 |

Table 3.5: Staging Results with Hybrid Third Stage

One of the major aspect of an HRE that must be taken into account is the O/F shift during the burn, and, if the oxidizer mass flow rate is kept constant, also a thrust shift. A simple procedure can be done in order to estimate the importance of that shift get more insights about this particular solution.
The first, very important equation is the fuel regression rate as a function of the total mass flux. The coefficients and the definition of mass flux in a VFP engine are taken from C. Paravan's work [34]. Again those are referred to gaseous oxygen, but assuming an hydrogen peroxide concentration over 95% is possible to consider true those relations as a first approximation.

$$r_b = 1.08 \times 10^{-4} G_{tot}^{0.595} \tag{3.20}$$

Where $G_{tot}$ is the total mass flux composed by the fuel and the oxidizer. The cross section area is defined by the radius of the combustion chamber (assumed as 80% as the rocket radius) times the height which varies with time. The engine scheme can be seen in figure 3.3 to better understand this procedure.

$$G_{tot} = G_{ox} + G_f = \frac{\dot{m}_{ox}}{R_c H_c} + \frac{\dot{m}_f}{R_c H_c} \tag{3.21}$$

The fuel mass flow rate is a function of the regression rate and the burning area assumed as the surface of the two disks decreased by 10% to account for the nozzle aperture.

$$\dot{m}_f = \rho_f A_b r_b \tag{3.22}$$

Imposing an initial oxidizer mass flow rate and combustion chamber height is possible to simulate the burning process of the fuel disks and get out propulsion performances as well as undesired effects such as the O/F shift.

Assuming a specific impulse of 330 s, a thrust equal to the nominal value of the third stage SRM, is possible to compute the mass flow rate and with an O/F of 6.5 the mass flow rates of oxidizer and fuel.
An initial combustion chamber height is assumed, $H_0$ then the fuel mass flow rate can be computed solving numerically equation (3.23) and get $\dot{m}_f$.

$$\dot{m}_f = \rho_f A_b 1.08 \times 10^{-4} \left( \frac{\dot{m}_{ox}}{R_c H_k} + \frac{\dot{m}_f}{R_c H_k} \right)^{0.595} \tag{3.23}$$

Then, the regression rate can be computed and used to update the combustion chamber height with a discretized time step $\Delta t$.

$$H_{k+1} = H_k + 2 r_b \Delta t \tag{3.24}$$

Finally the performances can be found.

$$\begin{cases} T = I_{sp} g_0 \left( \dot{m}_f + \dot{m}_{ox} \right) \\ O/F = \dot{m}_{ox} / \dot{m}_f \end{cases} \tag{3.25}$$

The specific impulse is a function of the O/F ratio, the values are taken from CEA simulation.
If the initial height is chosen wisely, at the end of the simulation both the oxidizer and the fuel web thickness $t_{web}$ are over at the same time. Therefore the initial height $H_0$ is changed until that condition is completely satisfied.

The resulting performances are shown in figure 3.4. It can be seen that the O/F ratio changes a little during the burn, with a mean very close to the stoichiometric relation, therefore an high efficiency is expected throughout the whole burn. The thrust instead has not the mean close to the nominal value, however the variation is always below 2% of the nominal this means a good result overall.
Finally, the resulting L/D of the combustion chamber results of around 0.8-0.9. Standard VFP Hybrid rocket engines usually have those value even smaller than that. It can be proved that if the thrust is increased the L/D ratio can decrease down to 0.5 or even below.

To sum up, in the following list are reported the pros and cons of such a solution:

## PROS

- Higher $I_{sp}$ (up to 350 s)
- Possibility of using $H_2O_2$ as monopropellant for RCS thrusters
- Throttlability $\implies$ Precision Orbit Insertion
- Possibility of 3rd stage controlled de-orbit
- Cracks Resistance

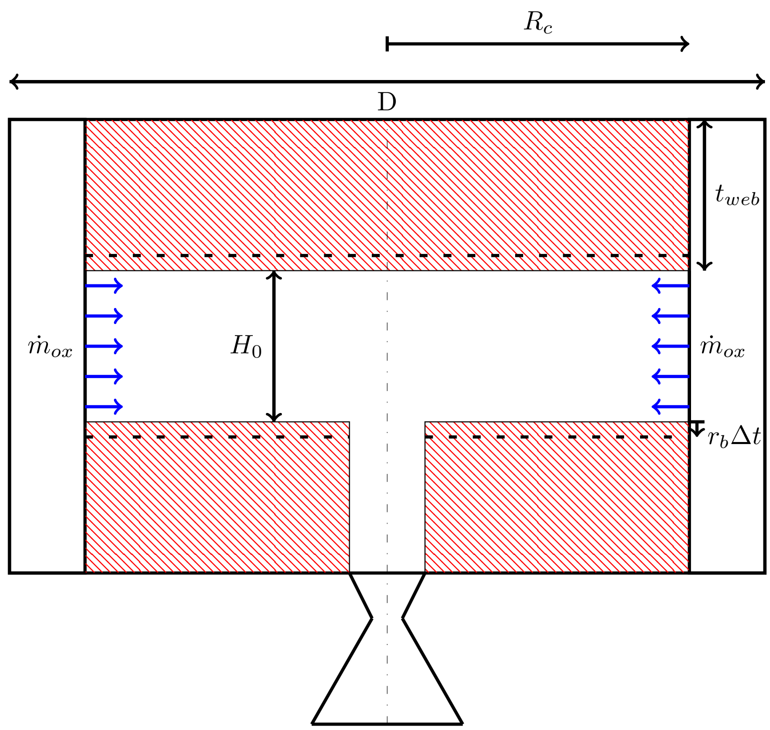


Figure 3.3: VFP Hybrid Rocket Engine Scheme

- Innovative Solution

# CONS

- Higher Complexity
- Higher $\xi$
- Low TRL
- O/F Shift

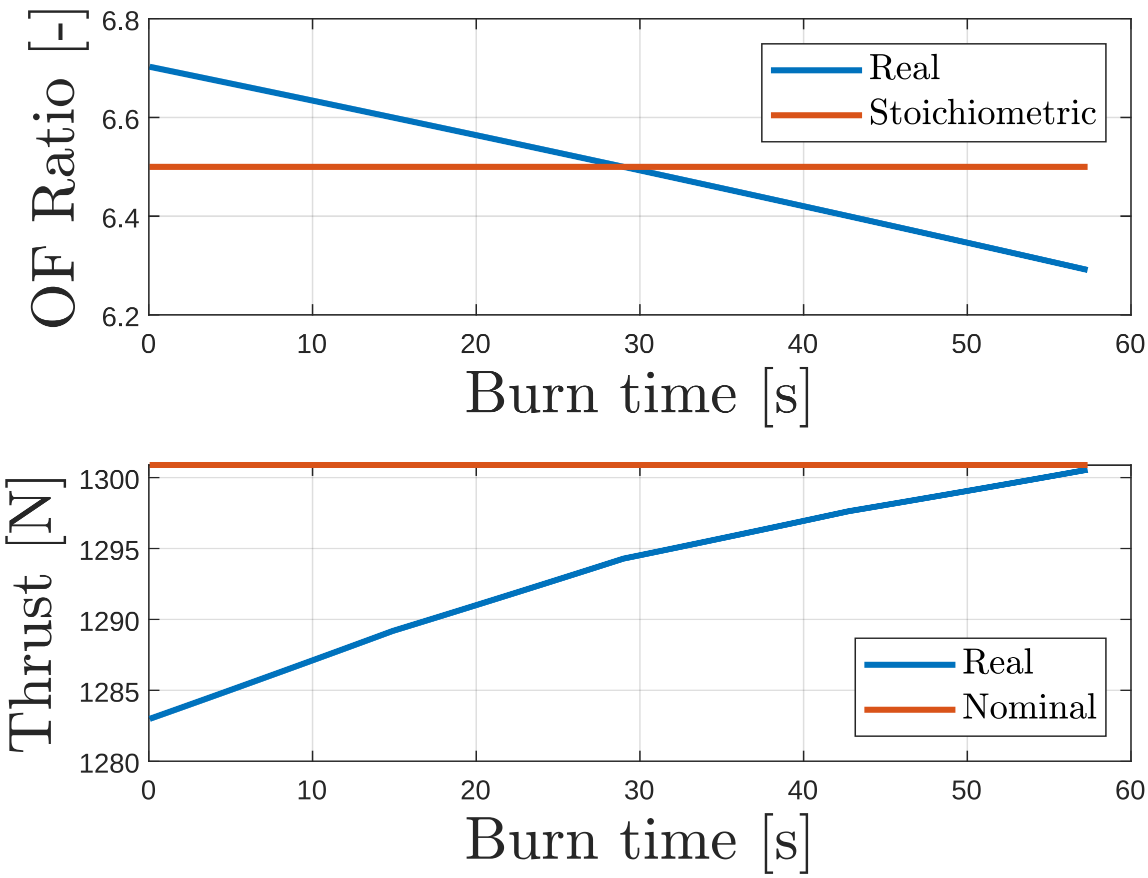


Figure 3.4: Hybrid Performances

# Chapter 4

# Trajectory and Launch Location

Once the staging and propulsion parameters are computed, the next step is to find out if those values allow reaching the desired orbit with a good trajectory. First of all a simple 3DOF model is implemented to simulate the rocket ascent trajectory, this could lead results such as a reference trajectory useful in the following 6DOF model, and considerations regarding the launch location and the possible threat given by the stages fall down. Furthermore, as explained in section 1.3, an iteration can be done to select the best propulsion parameters that achieve the best trajectory possible.

The trajectory selected for this launcher makes use of a free coasting phase between the second stage burnout and the third stage ignition, that exploit the gravity turn to decrease the flight path angle and to eliminate the vertical component of the velocity which is not desirable once in orbit. Pegasus XL does the same between its second and third stage burn, while LauncherOne does a small ballistic part between its two second stage ignitions.

## 4.1 3DOF Model

For the purposes just explained a very simple point mass 3 degrees of freedom model can be implemented, this is taken from Sforza's book [5].

The reference system is a round Earth centered non rotating model, the 3 degrees of freedom are: $V$ velocity, $\gamma$ flight path angle and $r$ distance from the center of the planet with the addition of the mass $m$.
The set of Ordinary Differential Equations (ODE) to be integrated is the following:

$$\begin{cases} \dot{V} = T/m \cos\chi - D/m - g\sin\gamma \\ V\dot{\gamma} = T/m \sin\chi - g\cos\gamma + \frac{V^2}{r}\cos\gamma \\ \dot{r} = V\sin\gamma \\ \dot{x} = \frac{V}{r} R_E \cos\gamma \\ \dot{m} = -\frac{T}{g_0 I_{sp}} \end{cases} \tag{4.1}$$

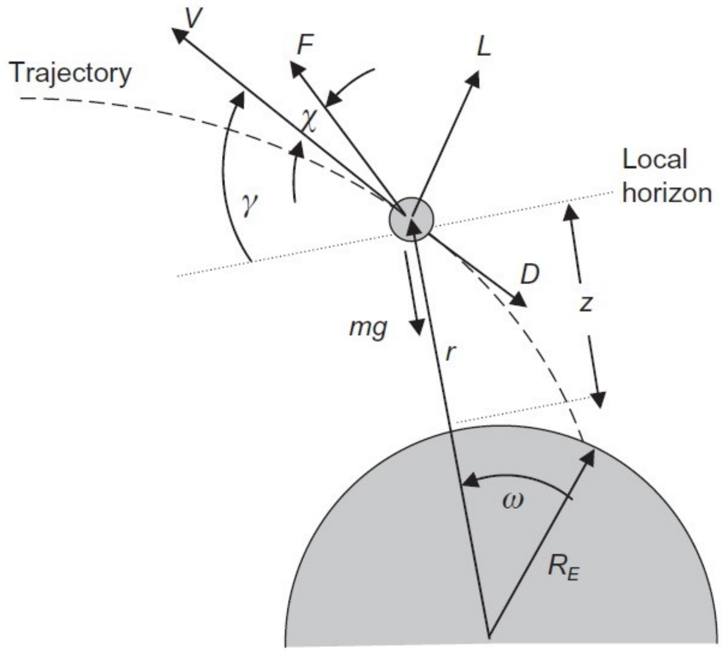


Figure 4.1: 3DOF Model Scheme [5]

Where $R_E$ is the radius of the Earth and $g$ the gravitational acceleration computed as:

$$g = \mu/r^2 \tag{4.2}$$

While $D$ represent the drag compute in the following way.

$$D = \frac{1}{2}\rho V^2 S C_D \tag{4.3}$$

$S$ is the cross section area of the rocket, $\rho$ is the atmosphere density which is function of the altitude and finally $C_D$ is the drag coefficient. As a first estimate this can be considered to be constant, however a more refined model is explained in the next chapter.

The integration algorithm is a variable-step, variable-order (VSVO) Adams-Bashforth-Moulton PECE solver, with both relative and absolute tolerances set as $10^{-9}$.
Since the burning time of each stage can be easily computed:

$$t_{b_i} = \frac{M_{p_i} I_{sp_i} g_0}{T_i} \qquad i = 1...3 \tag{4.4}$$

The only variables to be defined are the thrust deflection angles $\chi_i$ for each stage and the coasting time between stage 2 and 3. It is important to point out that this angle is considered from the velocity vector, therefore is not the real angle at which the nozzle is tilted. One simple way to optimize those variables is by means of an heuristic optimization. The $\chi$ angle of each stage is considered linear with the burning time, so 2 variables are required for each one.

$$\chi_i = \chi_i^c + \chi_i^l \,(t - t_{0i}) \tag{4.5}$$

Where the subscripts $c$ and $l$ represent respectively the constant contribution and the linear one. Therefore the optimization vector is made up by 7 elements in total.

$$X_{opt} = \begin{bmatrix}\chi_1^c & \chi_1^l & \chi_2^c & \chi_2^l & \chi_3^c & \chi_3^l & T_{coasting}\end{bmatrix} \tag{4.6}$$

The result trajectory must arrive at 500 km altitude at the end of the simulation having flight path angle equal to 0 and moreover the maximum altitude shall not exceed the orbit one to avoid overshoot problems.

Therefore the cost function to be minimized is the following:

$$Min\ J \qquad J = \mid r_{end} - r_{orbit} \mid /r_{orbit} + \mid \gamma_{end} \mid /\pi + \mid r_{max} - r_{orbit} \mid /r_{orbit} \tag{4.7}$$

It can be noticed that no final control is imposed to the velocity magnitude, the reason is that the aim of this trajectory design is to get to the desired orbit with the highest velocity possible. If then this velocity is higher than the orbital one, the $\Delta V$ margin used in the staging design would be decreased accordingly. Of course the opposite is done in case of lower final velocity. This fact stresses again the necessity of back iterations throughout the whole design process.

## 4.2 Re-entry Considerations

It's worth spending a few words on the re-entry phase of the stages. Usual rocket stages re-entry is done over the sea (like ESA or American does) or over inhabited land like Kazakhstan for RosCosmos to avoid any potential threat to people or buildings. Atmospheric re-entry of upper stages is a very complex subject that is not the topic of this work, however a very brief analysis can be done just to identify what happens to dead rocket bodies once detached in flight.

A nice and simple way of introducing the topic of aerothermodynamic is given by a NASA course [35], an orbital or sub-orbital body has a very high kinetic energy during flight, across the re-entry phase only a small fraction (1% - 5%) of that energy is transferred to the body in terms of heat while the rest is dispersed in the atmosphere. This fraction depends on many factors like the ballistic coefficient, re-entry corridor and many others effects too difficult to estimate correctly.

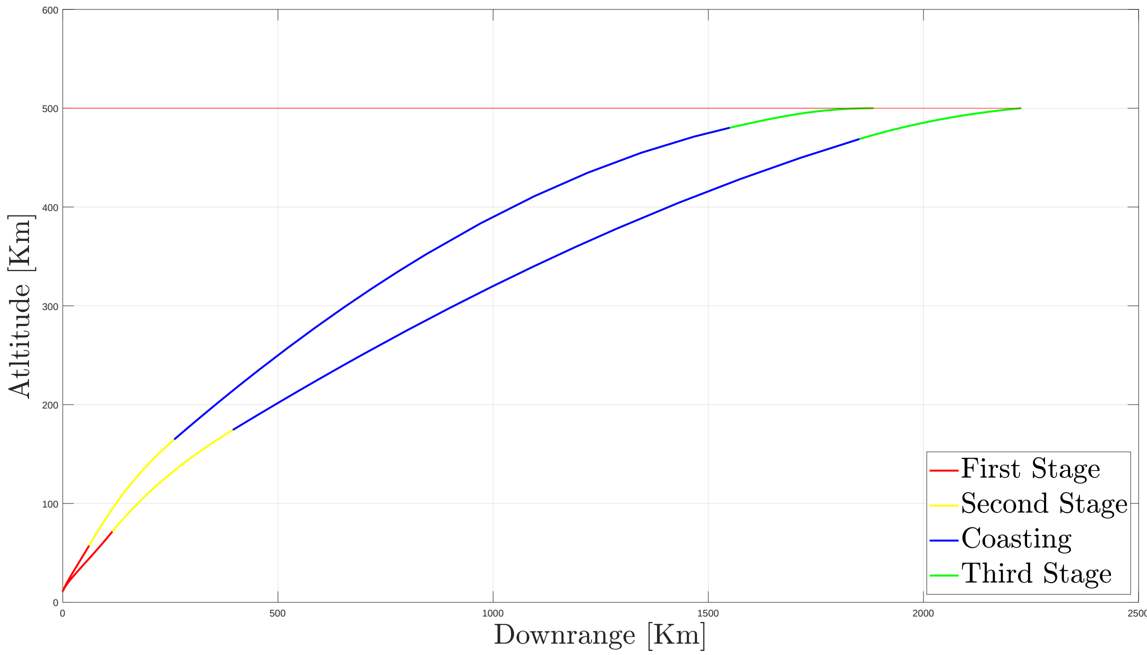


Figure 4.2: Rocket Ascent Trajectory

The energy per unit mass of a body can be easily computed as:

$$\frac{E}{m} = \frac{1}{2}V^2 + gh \tag{4.8}$$

In figure 4.4, the specific energy during fall can be seen. The energies involved are in the order of tens of MJ per Kg, and it can be noticed that the second stage feels roughly one order of magnitude more energy than the first. To give a sense of scale, water boils at 2.3 MJ/Kg, iron vaporizes at 6 MJ/Kg and carbon at 60 MJ/Kg.
Due to its higher mass and lower absorbed energy, it is reasonable to say that the first stage body must fall into the sea not to create any potential threat.
The second stage dead motor instead has low mass and high surface area, which means that the ballistic coefficient is considerably smaller than the one of a working rocket. Therefore the expected absorbed energy is higher.

$$BC = \frac{M}{C_d S} \tag{4.9}$$

Assuming an heat capacity of around 1000 J/Kg/K taken from carbon fiber composite [36], the temperature increment is roughly of 200-800 K depending of the percentage of that heat absorbed. This is clearly not enough to vaporize the carbon fiber composite which is the main component of the structure, neither any other metallic material. However it is enough to compromise its struc-

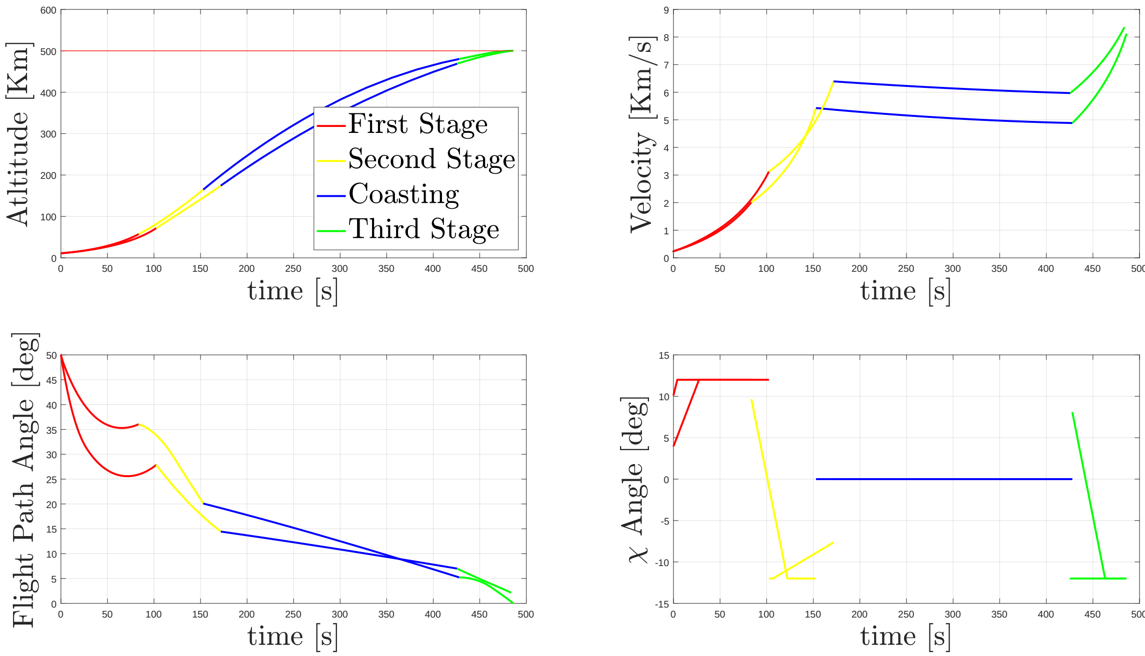


Figure 4.3: Altitude, Velocity, Pitch and $\chi$ During Ascent

tural integrity given by the epoxy resin, this together with the high mechanical stresses introduced by aerodynamic forces, leads to the conclusion that the chances to become a threat are significantly lower than the first stage. However there is the possibility that chunks of metallic material could arrive at ground, to ensure it a detailed aerothermodynamic analysis must be performed in future works.

The third stage releases the payload at orbital velocity so basically is injected in the same orbit as the CubeSat. Since the target orbit is a LEO, the dead rocket body re-enters into the atmosphere and get destroyed in a few years [37], however using an liquid/hybrid upper stage a controlled de-orbit can be done like the VEGA rocket does with its fourth stage AVUM [9]. Controlled and fast de-orbit is always desirable; space debris is a big issue and the possibility of not introducing dead rocket bodies, even if for few years, is always nice to have.

To sum up what just explained, the first stage rocket body can be a threat if it falls over living areas, the second stage has a significant lower possibility but further analysis are required to ensure it, and the third stage is unlikely to be dangerous especially if a controlled de-orbit strategy is adopted.

## 4.3 Launch Location

A very nice solution is to find out a launch location that allows the rocket to fly above the sea for the entirety of the launch, but this could lead to candidates very far from the coast therefore

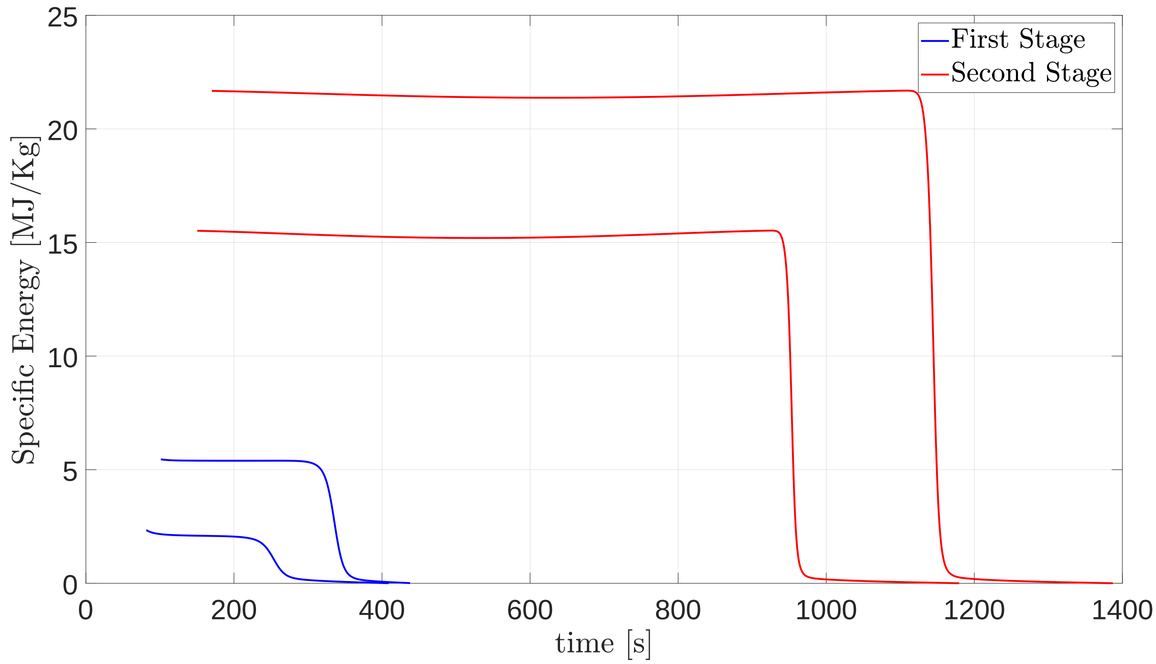


Figure 4.4: Energy per unit mass of falling dead stages

creating issues for the carrier aircraft. As said in the previous section, the first booster must absolutely fall into the ocean, while this requirement is not strictly true for the second stage (but of course, desirable), another important safety requirement is that the entirety of the first stage burn is performed above the sea. Therefore in case of a sudden engine shut-down, the flight termination system surely destroys the rocket but the falling debris do not create any threat to living areas. A good way to propose many different solutions is by means of some *Safety Levels*. A safety level is a number that goes from 1 to 5 that defines a certain requirement that the launch zone must fulfill in order to be taken into consideration. The expected result of this analysis is a set of launch zones where each one satisfies one or more those requirements.

**Safety Level:**

1. 1st booster falls into ocean
2. 1st booster falls into ocean and 1 stage flies above the sea
3. Both boosters fall into ocean
4. Both boosters fall into ocean and 1 stage flies above the sea
5. The whole launch happens above the sea

In order to identity the zones, a code takes the falling distances from the previous section and computes the location of the expected rocket touchdown in terms of latitude and longitude by means of spherical triangles rules. It is important to point out that for simplicity and computational time reasons, small island and the north pole are not considered as proper "land" over which the code triggers the falling effects.

Since the modeling of the re-entry is a very complicated subject, and since it is absolutely not the aim of this thesis, a MonteCarlo analysis has been performed in order to estimate the range in which is more likely to land the stages. The analysis uses the same 3dof model discussed so far to compute the falling trajectory of the dead body, the initial conditions are taken from the final ones of that particular stage, where the velocity is reduced due to the retro-rockets that help the stage separation. Furthermore, a normal distribution is imposed on each variable with as mean value the final conditions, and as standard deviation 1% of that mean.

The results of the MonteCarlo analysis can be seen in figures 4.5 and 4.6 for the first and second configuration respectively.

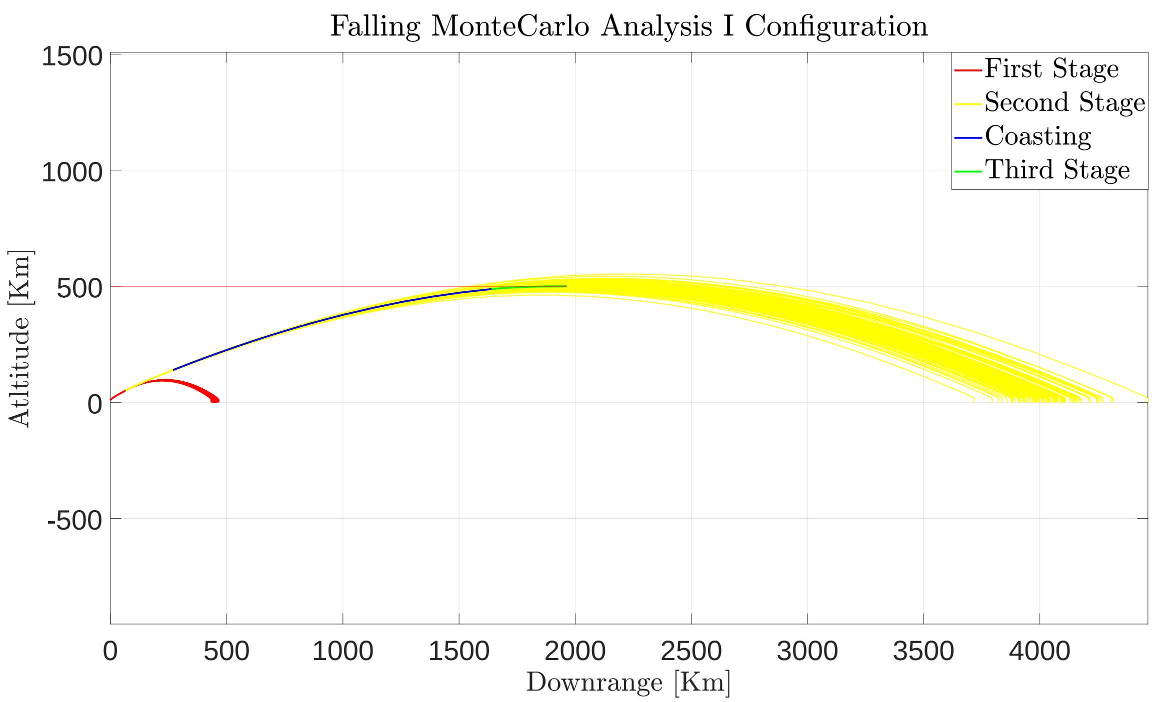


Figure 4.5: MonteCarlo Analysis of Stages Re-entry I Configuration

In figures 4.7, 4.8, 4.9, 4.10, 4.11 the possible launch locations for each safety level can be seen. The blue line represents the groundtrack of the falling first stage, the green line the second stage instead, and finally the red line represents the probable falling areas given by the MonteCarlo analysis.

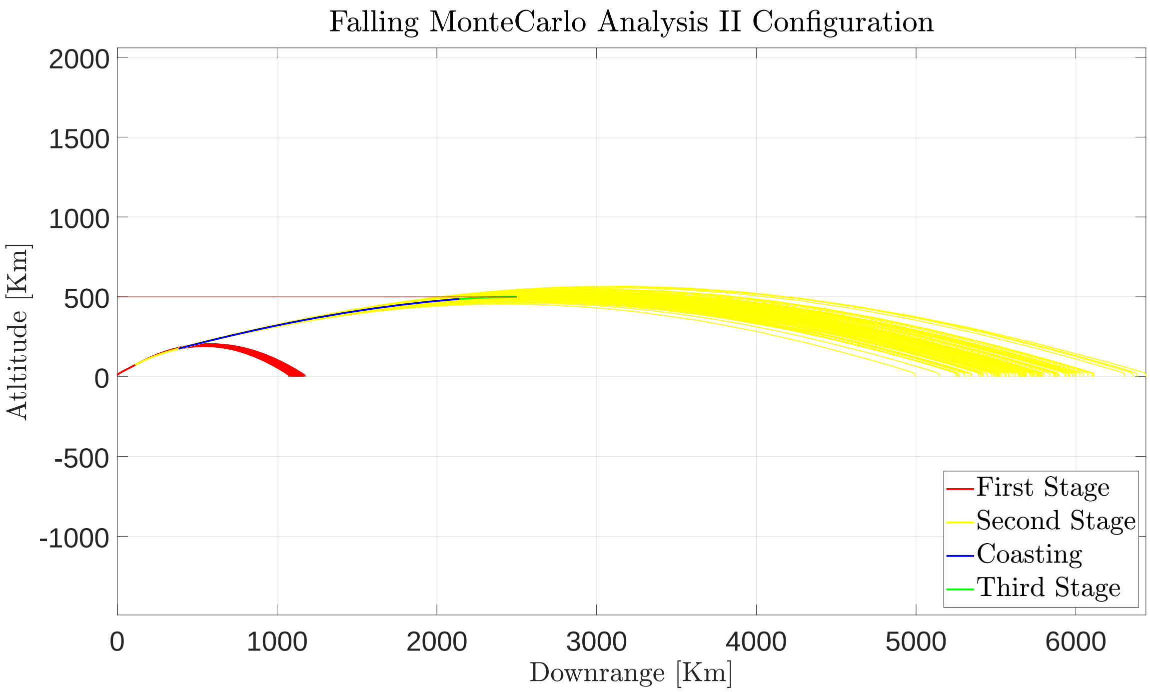


Figure 4.6: MonteCarlo Analysis of Stages Re-entry II Configuration

5 different zones can be identified by this analysis.
**Launch Locations:**

- **ESS** East Sardegna Sea
- **SIS** South Ionio Sea
- **WSA** West Spain Atlantic
- **WAA** West Africa Atlantic
- **NES** North European Sea

Of course **ESS** and **SIS** are the most desirable ones, in those zones the aircraft can lift off from italian territory but not every safety level is guaranteed. **NES** instead is far from Italy, thus the aircraft must lift off from north Europe, but in this zone the maximum safety is guaranteed. **WSA** and **WAA** provides good results from the first configuration point of view, and average from the second. Even the choice of those zones requires a foreign airport.

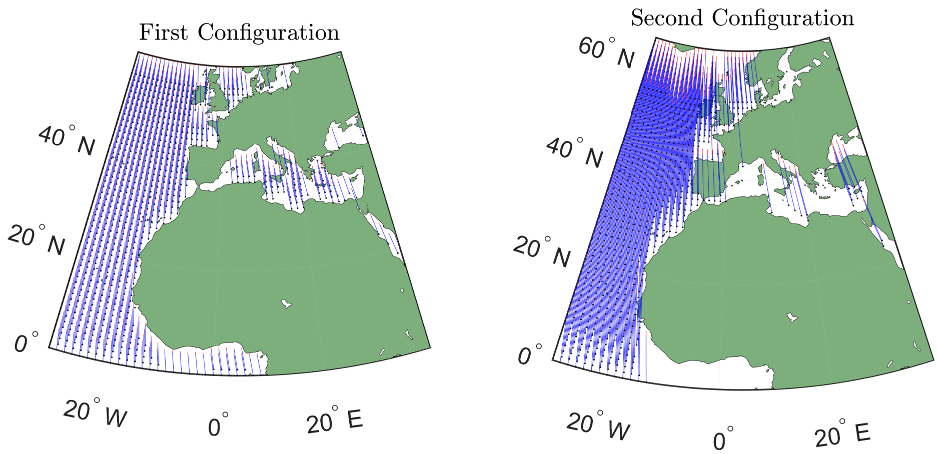


Figure 4.7: Safety Level 1 Zones

Table 4.1 shows what safety levels are respected by each zone in both configurations [1]
.
What turns out from this analysis is not a single feasible launch zone, but 5 different possibility with pros and cons each. At this level a decision is impossible, further work is required to get better trajectory results and most importantly, political agreements between countries regarding rocket flights over foreign territory or usage of military airports for payload integration and aircraft lift off.

[1]Green means feasible, red not feasible, yellow partially feasible

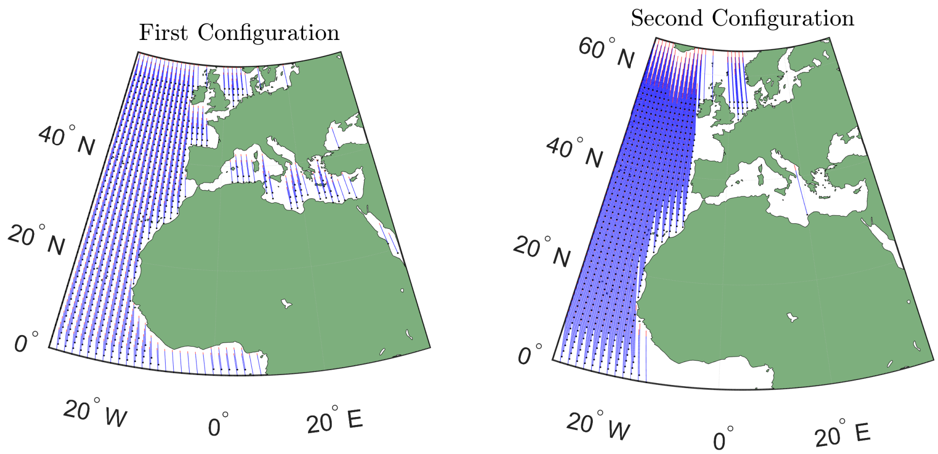


Figure 4.8: Safety Level 2 Zones

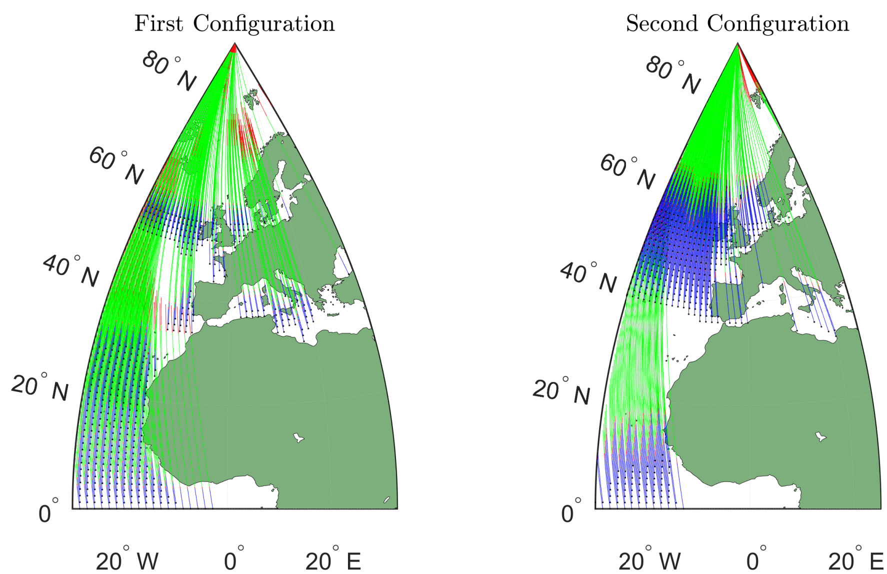


Figure 4.9: Safety Level 3 Zones

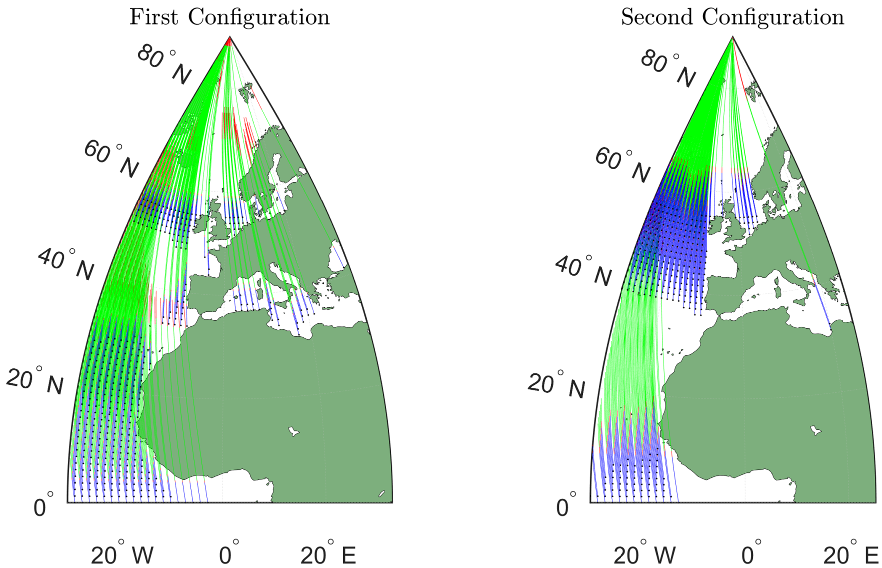


Figure 4.10: Safety Level 4 Zones

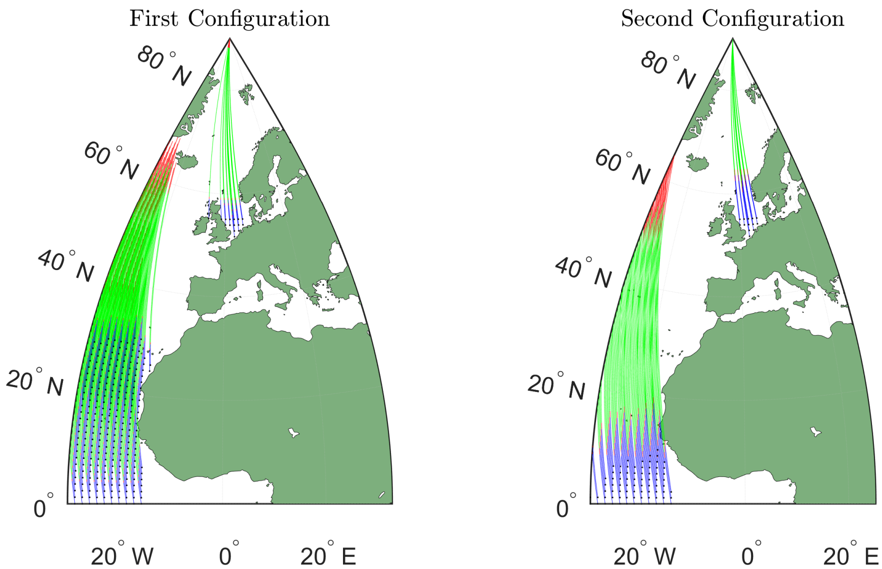


Figure 4.11: Safety Level 5 Zones

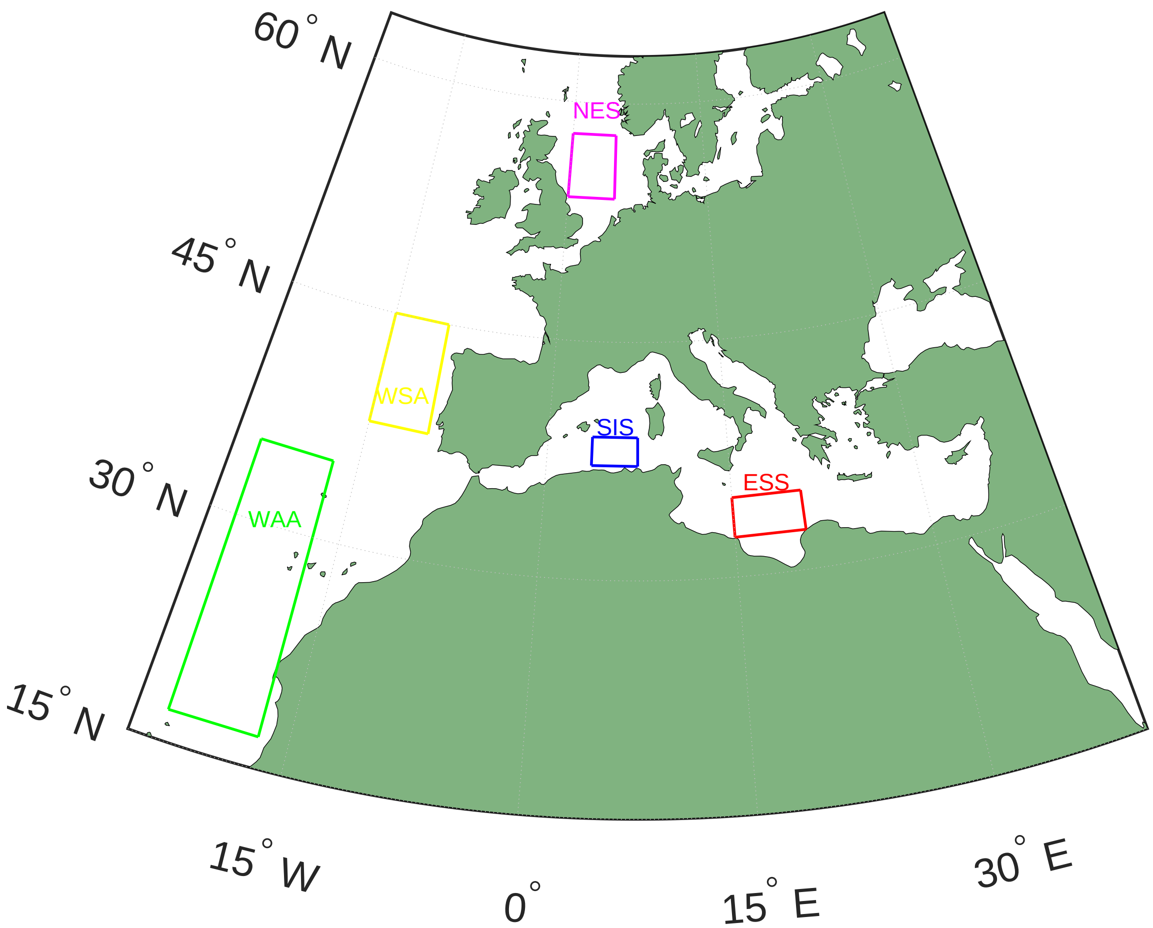

Figure 4.12: Launch Zones

| Safety Level | ESS | SIS | WSA | WAA | NES |
|---|---|---|---|---|---|
| **Configuration I** | | | | | |
| Safety Level 1 | | | | | |
| Safety Level 2 | | | | | |
| Safety Level 3 | | | | | |
| Safety Level 4 | | | | | |
| Safety Level 5 | | | | | |
| **Configuration II** | | | | | |
| Safety Level 1 | | | | | |
| Safety Level 2 | | | | | |
| Safety Level 3 | | | | | |
| Safety Level 4 | | | | | |
| Safety Level 5 | | | | | |

Table 4.1: Launch Zones Feasibility

# Chapter 5

# 6DOF Rocket Model

After having used a simplified model for testing the feasibility of the design done so far and computing the ideal trajectory, the next step is developing a more complete six degrees of freedom rocket model to simulate many more effects and used it to test various type of control. After that, the model is linearized making it useful for the upcoming MPC control law.

This model is not a point mass but a 3D body with a well-defined attitude, also the aerodynamic forces are augmented and some consideration are done about the presence or not of aerodynamic surfaces on the body.

The first step is to define two reference systems, an inertial one where the equations of motion are integrated and a body one where are defined aerodynamic and thrust forces.
The body reference system has the origin in the center of mass, the X axis is simply the longitudinal axis of the body, while Y and Z can be placed everywhere since up to this level of detail the rocket is assumed to have cylindrical symmetry, the scheme is represented in figure 5.1. The body is perfectly rigid however a few consideration of oscillations and natural frequencies can be done later on.

The inertial reference system is placed at the launch location, the Z axis is in the direction of the local zenith, while X and Y axis represent respectively the downrange and cross-range directions, the scheme is shown in figure 5.2. The Earth is round but non rotating, to account for this simplification a $\Delta V$ value is added for the Earth rotation as explained in section 1.4.1.

## 5.1 Atmosphere Model

The model used to represent the atmosphere in this work is the *1976 U.S. Standard Atmoshpere Model* which is taken from Sforza's book [5], this model is based on different layers where each has a linear variation of the temperature with respect to the altitude. Once the temperature profile is known $T = T(h)$ the pressure can be computed using the hydrostatic relation $P = P(h)$ and finally the density which if found thanks to the perfect gas assumption $\rho = \rho(h)$. The temperature at sea level is fixed to $15°C = 288.5K$. This model is quite simple because it does not account for

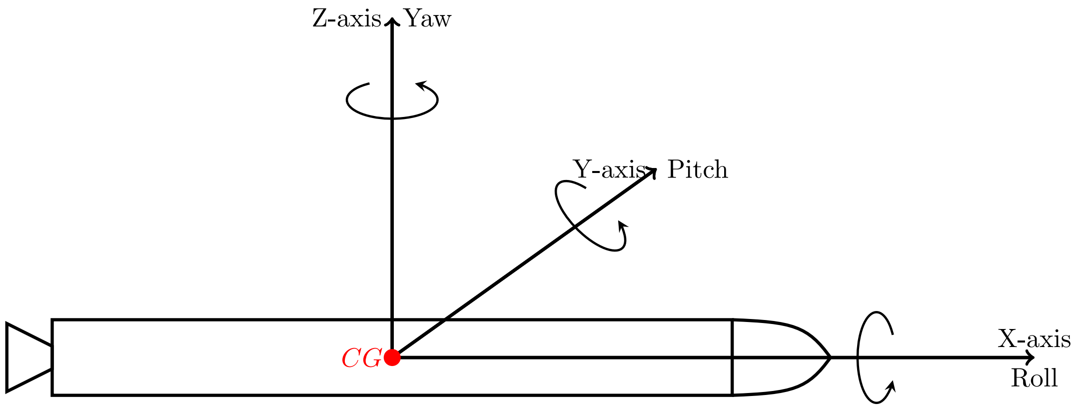


Figure 5.1: Rocket Body Reference System

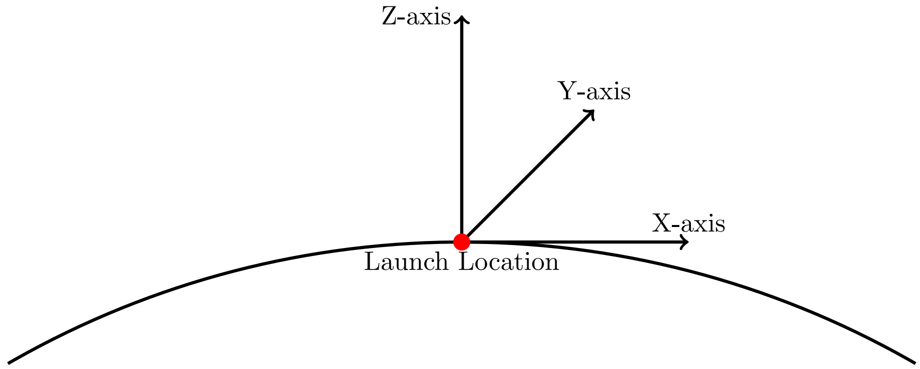


Figure 5.2: Inertia Reference System

any diurnal/nocturnal variation, as well as, solar cycles; the atmosphere composition is considered constant which is not too strong as an hypothesis below 100 Km. As said in the introduction aerodynamic effects have a minor contributions on air launched rocket than classical ones, so a simple model like this is more than enough to estimate the effects on the launch.

The temperature rates and the atmosphere layers up to 100 Km are set in table 5.1.

The procedure to compute pressure and density is straightforward and can be seen in Sforza's book [5].
Above 100 Km the temperature can be modeled as an exponential that tends to 1000 K just for Mach number purposes as can be seen in figure 5.3, pressure and density instead are too low to give significant contributions to the problem, for this reason over 100 Km are set to 0.

| Layer | Altitude [Km] | Temperature rate [K/Km] |
|---|---|---|
| 1 | 0 | -6.5 |
| 2 | 11.02 | 0 |
| 3 | 20.06 | 1 |
| 4 | 32.16 | 2.8 |
| 5 | 47.35 | 0 |
| 6 | 51.41 | -2.8 |
| 7 | 71.80 | -2 |
| 8 | 86 | 0 |
| 9 | 92 | 1.03 |

Table 5.1: Atmosphere Layers

## 5.2 Aerodynamic Model

In this section the passages and models to compute the aerodynamic forces acting on the launcher are shown. The models are taken from [3], the validity hypothesis are discussed at each contribution, however it is important to point out that those models have been chosen for their simplicity. For a complete rocket design, tools such as CFD (Computational Fluid Dynamics) must be used, but for a preliminary analysis analytical expression and correlations are a good compromise.

Aerodynamic forces have a major contribution in the first phases of a rocket launch, drag is responsible for $\Delta V$ losses, while lift provides an instability effect on the vehicle to be fixed using control actions. Despite an air launched rocket has a significantly lower contribution of those latter than a standard launcher, they can't be discarded.

Starting from the aerodynamic drag, the zero-lift drag coefficient can be seen as a sum of three different contributions.

$$C_{D0} = C_{D0_{Base}} + C_{D0_{Wave}} + C_{D0_{Friction}} \tag{5.1}$$

$C_{D0_{Base}}$ is due to the pressure difference between the nose and the engine section that feels a lower pressure given by the flow separation at the base. This contribution can be correlated with the following expression.

$$\begin{cases} C_{D0_{Base}} = \left(1 - \frac{A_e}{S_{ref}}\right)\frac{0.25}{Ma} & if \;\; Ma < 1 \\ C_{D0_{Base}} = \left(1 - \frac{A_e}{S_{ref}}\right)(0.12 + 0.13Ma^2) & if \;\; Ma > 1 \end{cases} \tag{5.2}$$

Where $S_{ref}$ is the reference surface, computed as the cross section of the rocket body. This contribution can become very high during un-powered coast (so when $A_e$ goes to zero).

Skin friction can be a primary contribution in subsonic flights, the following relation is based

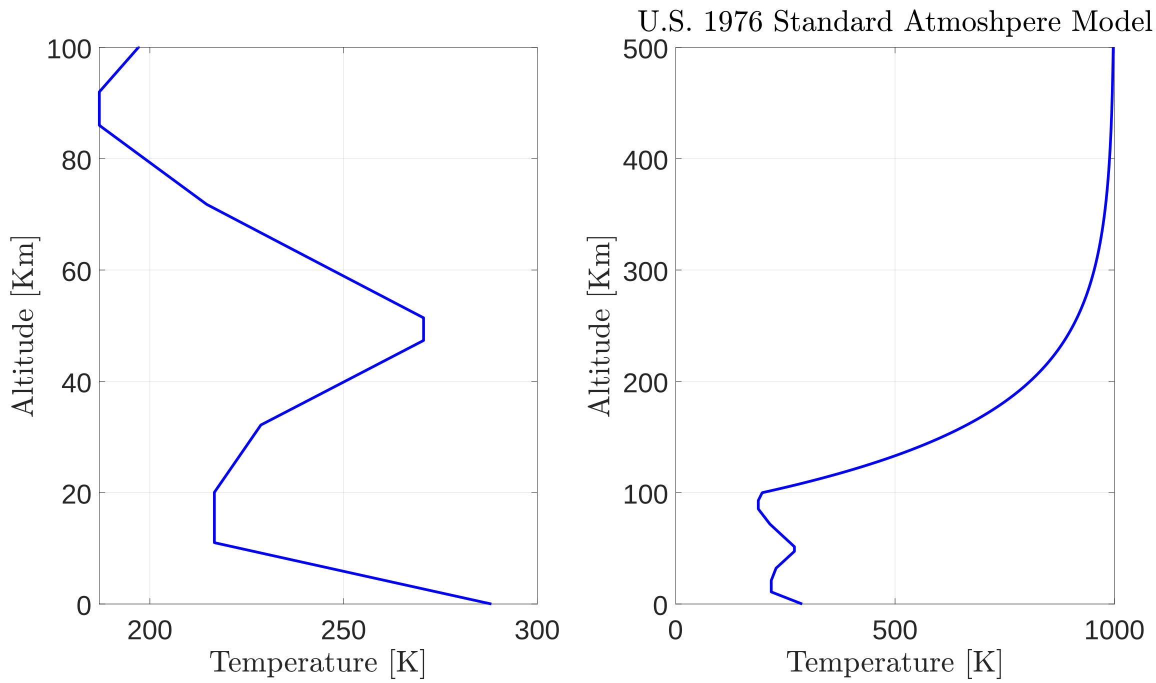


Figure 5.3: Atmospheric Temperature

on empiric correlations with the Reynolds number and it's valid within the hypothesis of turbulent boundary layer which can be an issue for low Mach numbers ($Ma < 0.2$) [1].

$$C_{D0_{friction}} = 0.031(L/D)\Big(\frac{Ma}{qL}\Big)^{0.2} \tag{5.3}$$

The last contribution is the wave drag, this is created by the effects of a shock wave at the nose.

$$C_{D0_{Wave,Sharp}} = \Big(1.586 + \frac{1.834}{Ma^2}\Big)\Big[\arctan\big(\frac{0.5}{L_N/D}\big)\Big]^{1.69} \qquad if \;\; Ma > 1 \tag{5.4}$$

Where $L_N$ is the length of the nose, which for a launcher is identified as the fairing.
The above equation is valid only on sharp noses, a method to account for the classical bluntness of launchers' fairings can be done in the following way. Using the previous equation the coefficient for a perfect hemispherical nose can be computed putting the ratio $L_N/D$ as 0.5, this is now identified as $C_{D0_{Wave,Hemi}}$. Finally scaling those two contributions is enough to get an accurate compromise for a blunt nose.

$$C_{D0_{Wave,Blunt}} = \frac{S_{ref} - S_{nose}}{S_{ref}} C_{D0_{Wave,Sharp}} + \frac{S_{nose}}{S_{ref}} C_{D0_{Wave,Hemi}} \tag{5.5}$$

[1] All the variables are in S.I units

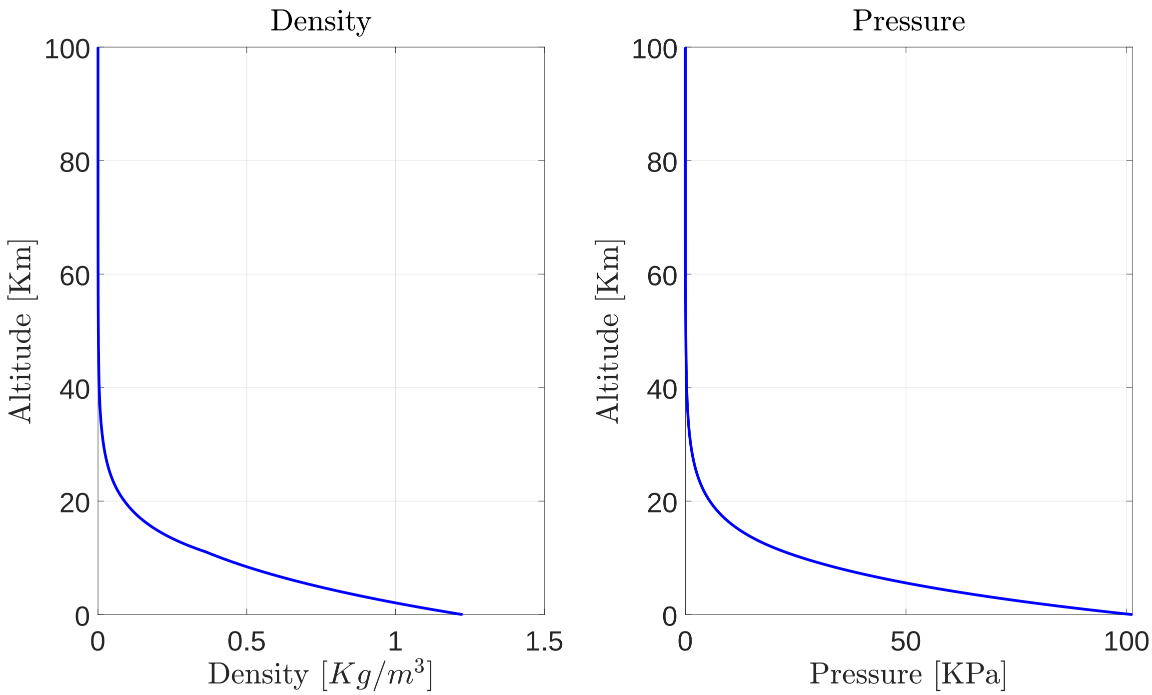


Figure 5.4: Atmospheric Pressure and Density

Where $S_{nose}$ is the area of the circle describing the bluntness.
All the above relations are only valid for supersonic flow, however shock waves can form also before the supersonic regime, in particular this coefficient start increasing at a certain Mach called "critical Mach number", this is usually found between Mach 0.6 and 0.8. The drag contribution in the transonic regime is very hard to compute and it's very shape-dependent, a simple way not to create any discontinuity is to increase this value from 0 (at critical Mach) to the maximum (at Mach 1) by means of a polynomial function.

The normal coefficient is by far easier than the drag one. This relation is based on the hypothesis of slender body theory (fineness ratio $> 5$) and cross flow theory.

$$C_N = \sin(2\alpha)\cos(\alpha/2) + 2L/D\sin(\alpha)^2 \tag{5.6}$$

Finally the drag and lift coefficient could be computed.

$$C_L = C_N\cos(\alpha) - C_{D0}\sin(\alpha) \tag{5.7}$$

$$C_D = C_N \sin(\alpha) + C_{D0} \cos(\alpha) \tag{5.8}$$

The lift and drag forces are immediately found.

$$Lift = \frac{1}{2}\rho V^2 S_{ref} C_L \tag{5.9}$$

$$Drag = \frac{1}{2}\rho V^2 S_{ref} C_D \tag{5.10}$$

Speaking of the application point, taking as hypothesis the cross flow theory and the slender body theory again an analytical solution can be found.

$$X_{AC} = 0.63 L_N (1 - \sin(\alpha)^2) + 0.5 L \sin(\alpha)^2 \tag{5.11}$$

$X_{AC}$ is considered from the tip of the nose.

Despite a normal launcher does not feel high angular velocities during launch, a rotation in the atmosphere generates an opposite torque on the body. Since this factor has a very minor contribution with respect to torques induced by the thrust or aerodynamic forces, the model is quite simple. Considering a rigid cylinder as the rocket body, the rotation around the roll axis does not generate dynamic pressure on the body, but just skin friction which is in general smaller compared to the normal skin friction, for those reasons a rotation around the roll axis does not generate an aerodynamic torque. For what concern pitch and yaw rotations, if the static pressure is assumed to be always constants, a rotation would creates a distribution of dynamic pressure on the body that can be seen as an opposed force couple on the rocket body.

$$M_{y,z} = -\frac{3}{4}\frac{L^4 \rho D \omega_{y,z}^2}{48} sign(\omega_{y,z}) \tag{5.12}$$

## 5.3 Aerodynamic Surfaces

The addition of aerodynamic surfaces can provide benefits in aerodynamic lift maneuverability and can also reduce the instability induced by the body normal force. However there are also disadvantages like the inevitable inert mass increment as well as the increase in drag. The choice of using wings or not is influenced by many factors, first among all the carrier aircraft interface that can limit the number and the dimensions of them. So the final design is not matter of this master thesis, this part only wants to give an overview on wings, show how are modeled and some elements that may drive the decision.
Looking at existing launchers, both Pegasus and LauncherOne has tail wings as can be seen in figure 5.5, furthermore Pegasus also have a bigger Delta wing on top of the first stage since the

trajectory control of this latter is done controlling those aerodynamic surfaces and not by TVC.

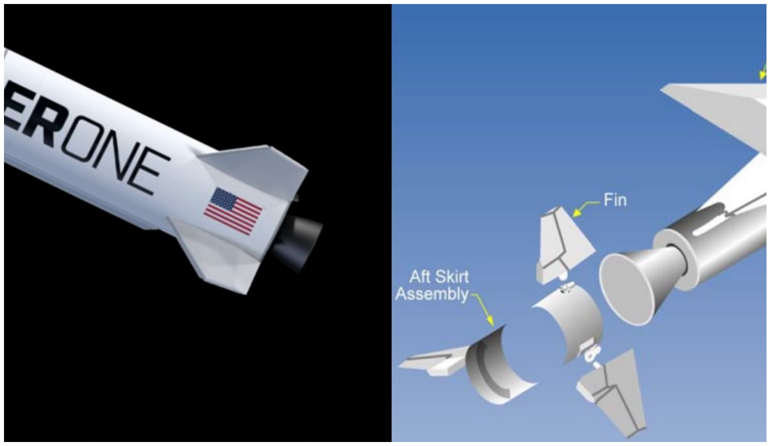


Figure 5.5: LauncherOne and PegasusXL Tail Fins [6] [7]

Again the work done by Sarigul-Klijn [22] comes in handy, since its study also considers the presence or not of aerodynamic wings on the rocket body. The result is a small increase of $\Delta V$ with wings if the initial flight path angle is quite small, however the final choice is again more complex and further analysis are required to get a definitive answer.
All the following models are again taken from Fleeman's book [3].
First of all the aspect ratio of the wing must be defined.

$$A_r = \frac{b_e^2}{S_e} \tag{5.13}$$

It's important to point out that the base of the wing $b_e$ is not the distance from the tip of the wing to the body, but twice as figure 5.6 shows.

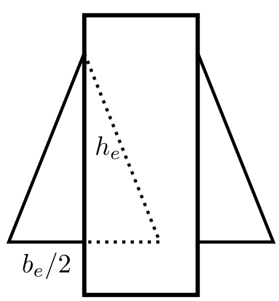


Figure 5.6: Triangular Wing Scheme

The normal coefficient of the wing is computed by means of the following equation. Those relation are based on the Newtonian impact theory, then if the Mach number is lower than a certain critical value that theory is augmented using the slender wing theory, if higher the linear wing theory is used.

$$\begin{cases} C_{n_{wing}} = \left(\frac{\pi A_r}{2}|\sin\alpha_w \cos\alpha_w| + 2\sin^2\alpha_w\right)\frac{S_{surf}}{S_{ref}} & if\ Ma < Ma_{cr,wing} \\ C_{n_{wing}} = \left(\frac{4|\sin\alpha_w \cos\alpha_w|}{(Ma^2-1)^{1/2}} + 2\sin^2\alpha_w\right)\frac{S_{surf}}{S_{ref}} & if\ Ma > Ma_{cr,wing} \end{cases} \tag{5.14}$$

Where the critical mach number for the wing is found as follows:

$$Ma_{cr,wing} = \sqrt{1 + \left(\frac{8}{\pi A_r}\right)^2} \tag{5.15}$$

In this case the angle $\alpha_w$ is different between the angle of attack of the body, angular velocities may cause different flow velocities even between wings themselves.
The drag coefficient in a similar fashion with equation (5.1) is made by some contributions, but in this case since wings are usually very thin, the base drag coefficient is negligible.
The friction drag and the wave drag coefficients are computed according to the following equations.

$$C_{D0_{wing,friction}} = 0.0078\left(\frac{Ma}{qc_{mac}}\right)^{0.2}\frac{2S_{surf}}{S_{ref}} \tag{5.16}$$

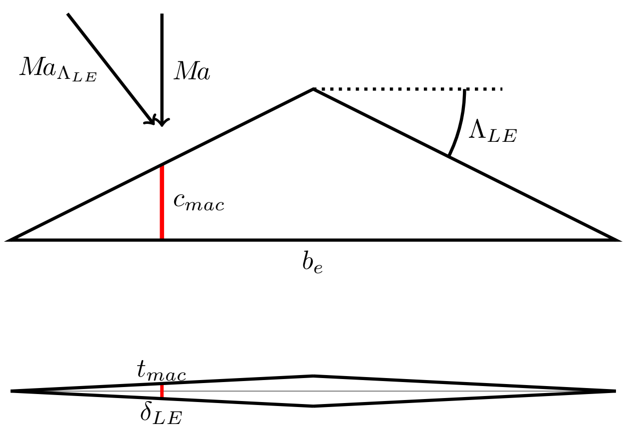


Figure 5.7: Delta Wing Scheme

$$C_{D0_{wing,wave}} = \frac{1.429}{Ma^2_{\Lambda LE}}\left((1.2Ma^2_{\Lambda LE})^{3.5}\left(\frac{2.4}{2.8Ma^2_{\Lambda LE} - 0.4}\right)^{2.5} - 1\right)\frac{(\sin^2\delta_{LE}\cos\Lambda_{LE}t_{mac}b_e)}{S_{ref}} \tag{5.17}$$

Where, $t_{mac}$ is the thickness of the wing in the mean chord position, $\delta_{LE}$ is the leading edge angle in the same position, and $Ma_{\Lambda_{LE}}$ is the Mach number component perpendicular to the leading edge; those contributions can be seen in figure 5.7.
This contribution has the same discontinuity issue discussed for equation (5.4), and it's solved again

using a polynomial function.
So the normal force and the zero-lift drag can be computed.

$$\begin{cases} N_{wing} = qS_{ref}C_{n_{wing}} \\ D_{0wing} = qS_{ref}C_{D0_{wing}} \end{cases} \tag{5.18}$$

Regarding the position of the center of pressure, the following procedure can derive it.

$$\begin{cases} \frac{X_{AC_{wing}}}{c_{mac}} = 0.25 & Ma < 0.7 \\ \frac{X_{AC_{wing}}}{c_{mac}} = \frac{A_r\sqrt{Ma^2-1}-0.67}{2A_r\sqrt{Ma^2-1}-1} & Ma > 2 \end{cases} \tag{5.19}$$

In this case $X_{AC_{wing}}$ is considered from the leading edge of the wing in the mean chord position. For values of Mach number between 0.7 and 2 a linear interpolation has been used.

Classical wing shapes are triangular or trapezoidal, however other shapes can be used with their respective advantages and disadvantages. As said at the beginning of this section, this work does not go into the details of such a choice, however a list of possible shapes and performances can be seen in figure 5.8.

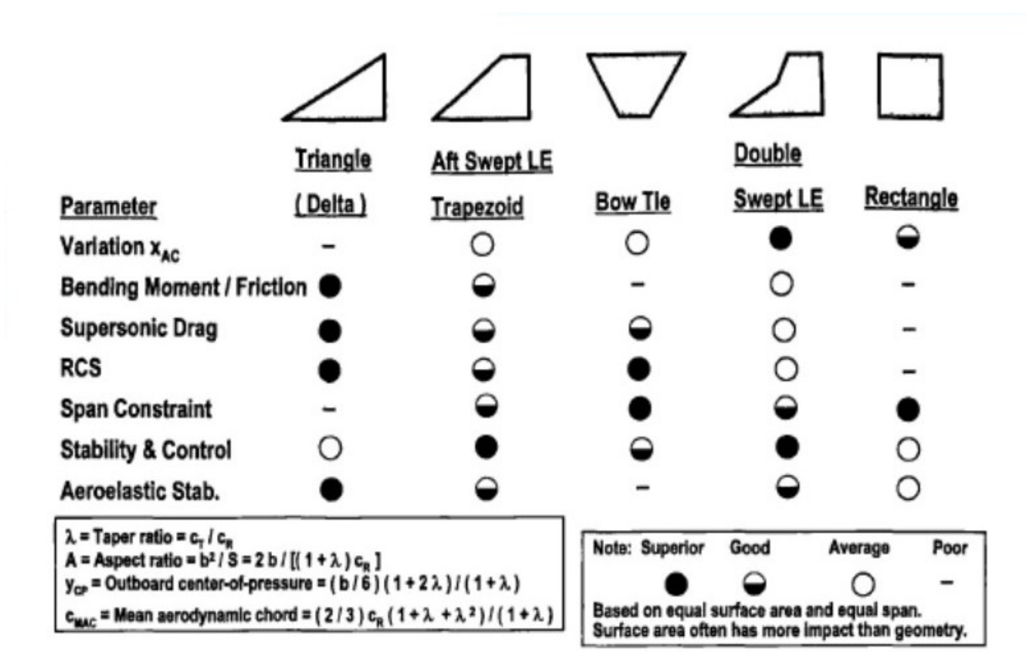


Figure 5.8: Fins Shape Parameters [3]

## 5.4 Thrust

Thrust is the main contribution among the forces acting on a rocket, the way to model it comes from the momentum balance across the vehicle and the result is quite simple.

$$T = \dot{m}V_e + (P_e - P_a)A_e \tag{5.20}$$

$V_e$ and $P_e$ are engines parameters and do not change during flight, $\dot{m}$ instead is function of the grain properties for a solid rocket motor and the throttling for a liquid/hybrid rocket engines so in general can change during the mission; $P_a$ is simply the ambient pressure and so it changes with the altitude becoming negligible from the second stage ignition on.
Since the static contribution does not play an important role during the flight, a constant thrust approach can be followed.

$$T = \dot{m}g_0 I_{sp-vac} \tag{5.21}$$

TVC, Thrust Vector Control is a control method that orient the force direction without changing its magnitude; it can be used to steer the vehicle even without atmospheric action like Pegasus uses for its first stage. There are several ways to orient the thrust vector so that the rocket follows the reference trajectory.
Classical SRMs move only the nozzle since the combustion chamber in this case is basically the entire rocket, LREs instead orient the whole engine using gimbals.
Considering the two deflection angles $\delta$ and $\beta$ respectively along Y and Z direction, the force vector in the body reference frame becomes:

$$\underline{F}_{thrust} = \begin{bmatrix} T\cos\beta\cos\delta \\ T\sin\delta \\ T\sin\beta\cos\delta \end{bmatrix} \tag{5.22}$$

Boundaries has been imposed to those two angles in order not to overcome technological limits, the maximum and minimum are set as $??deg$. Future works are required also to deal with the velocity at which the nozzle is tilted, this value as a technological maximum as well, and it must be designed not to incur in oscillations problems. This means that the natural frequencies of the rocket must be well known.

## 5.5 Inertia

Inertia is something that was not considered in the simplified model in chapter 4. The inertia matrix is required to compute the attitude of the launcher as well as the moments acting on the body introduced by thrust and lift.

A simple procedure is followed to compute that matrix. First of all, the rocket body is assumed to be a perfectly homogeneous cylinder. If the cylindrical symmetry is reasonable, the homogeneity of the body is usually not true, however it is used to simplify a lot the computations. Each stage is

treated as a independent cylinder, where only the thrusting one is changing its moment of inertia due to propellant burning, and the payload is modeled, again, as cylinder whose height is the fairing length.
A more refined work could separate better the contributions, including the TVC/Nozzle as independent parts, also the grain shape must be considered.

$$X_{cg} = \frac{\sum_{i=1}^{n} M_i X_{cgi}}{\sum_{i=1}^{n} M_i} \tag{5.23}$$

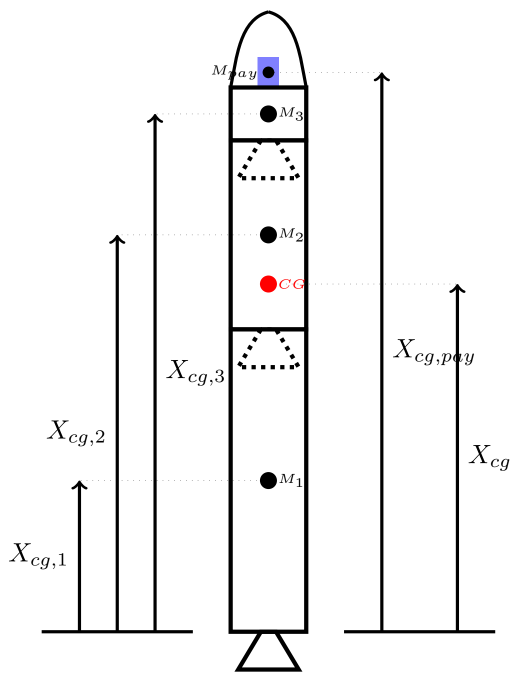


Figure 5.9: Rocket Center of Mass scheme

After computed the position of the center of mass, the 3 principal moment of inertia can be computed recalling that two of them are equal by means of the cylindrical symmetry hypothesis.

$$I_y = I_z = \sum_{i=1}^{n} \frac{M_i L_i^2}{12} + (X_{cgi} - X_{cg})^2 \tag{5.24}$$

$$I_x = \sum_{i=1}^{n} \frac{M_i D}{2} \tag{5.25}$$

## 5.6 Attitude

The attitude of the launcher plays a very critical role during the ascent phase, it determines the angle of attack which is the base of all aerodynamic force and torques and also the thrust direction. There are several ways to compute the attitude starting from the angular velocities:

- Direction Cosine Matrix (DCM)
- Quaternions
- Euler Angles (EA)

Euler angles are the fastest computationally speaking since they rely only on 3 variables, however there are singularities that may lead to several issues, this method may be useful in some parts of the launch where the attitude is far from those singularities. Moreover, under the hypothesis of small angles the attitude can be linearized.
DCM is a very robust solution, it is both unique and global but has 9 variables to integrate at each step, and should also be orthonormalized not to loose accuracy.
The attitude matrix $\mathbf{A}$ is defined as follows:

$$\mathbf{A}_{B/N} = \begin{bmatrix} \hat{x} \\ \hat{y} \\ \hat{z} \end{bmatrix} \tag{5.26}$$

Its integration and orthonormalization are done in the following ways:

$$\dot{\mathbf{A}}_{B/N} = -\begin{bmatrix} 0 & -\omega_z & \omega_y \\ \omega_z & 0 & -\omega_x \\ -\omega_y & \omega_x & 0 \end{bmatrix} \mathbf{A}_{B/N} \tag{5.27}$$

$$\mathbf{A}_{k+1} = \frac{3}{2}\mathbf{A}_k - \frac{\mathbf{A}_k \mathbf{A}_k^T \mathbf{A}_k}{2} \tag{5.28}$$

Quaternions instead have 4 variables, are global but not unique and must be normalized as well at each step; despite their computational velocity, are still comparable with DCM because they require a further passage to get the attitude matrix.

$$\dot{q} = \begin{bmatrix} \dot{q_1} \\ \dot{q_2} \\ \dot{q_3} \\ \dot{q_4} \end{bmatrix} = \frac{1}{2} \begin{bmatrix} 0 & \omega_z & -\omega_y & \omega_x \\ -\omega_z & 0 & \omega_x & \omega_y \\ \omega_y & -\omega_x & 0 & \omega_z \\ -\omega_x & -\omega_y & -\omega_z & 0 \end{bmatrix} \begin{bmatrix} q_1 \\ q_2 \\ q_3 \\ q_4 \end{bmatrix} \tag{5.29}$$

$$\mathbf{A}_{B/N} = \begin{bmatrix} q_1^2 - q_2^2 - q_3^2 + q_4^2 & 2(q_1 q_2 + q_3 q_4) & 2(q_1 q_3 - q_2 q_4) \\ 2(q_1 q_2 - q_3 q_4) & -q_1^2 + q_2^2 - q_3^2 + q_4^2 & 2(q_2 q_3 + q_1 q_4) \\ 2(q_1 q_3 + q_2 q_4) & 2(q_2 q_3 - q_1 q_4) & -q_1^2 - q_2^2 + q_3^2 + q_4^2 \end{bmatrix} \tag{5.30}$$

To sum up, DCM is the main model used for the attitude determination of the 6DOF model, however quaternions provides a good alternative in case of particularly heavy computational load therefore can be adopted for future simulations that would probably be computationally heavier. Euler Angles method is useful in the linear model.
All those models are taken from Markley's book [38].

## 5.7 Equation of Motion

Defining the launch location with respect to the center of the Earth:

$$\underline{X}_{launch} = \begin{bmatrix} 0 & 0 & R_E \end{bmatrix} \tag{5.31}$$

Then the position of the launcher can be computed again from the center of the Earth.

$$\underline{X}_{earth} = \underline{X}_{launch} + \begin{bmatrix} x & y & z \end{bmatrix} \tag{5.32}$$

With this the altitude can be derived which is used to compute atmospheric properties.

$$h = \|X_{earth}\| - R_E \tag{5.33}$$

Finally downrange and crossrange can be derived as follows:

$$\begin{cases} s = R_E \angle \left( \underline{X}_{launch}, \underline{X}^{\cancel{z}}_{earth} \right) \\ c = R_E \angle \left( \underline{X}_{launch}, \underline{X}^{\cancel{z}}_{earth} \right) \end{cases} \tag{5.34}$$

Where $\underline{X}^{\cancel{z}}_{earth}$ means that the $z$ component of that vector is zero. Those distances are crucial in the control chapter.

The force vector in the inertial frame is made up by contributions coming from aerodynamic forces, thrust and gravity.

$$\begin{bmatrix} F_x \\ F_y \\ F_z \end{bmatrix} = \mathbf{A}_{B/N} \underline{F}_{aero} + \mathbf{A}_{B/N} \underline{F}_{thrust} - \mu \frac{\underline{X}_{earth}}{\|\underline{X}_{earth}\|^3} \tag{5.35}$$

The derivatives of mass and velocities are immediately found.

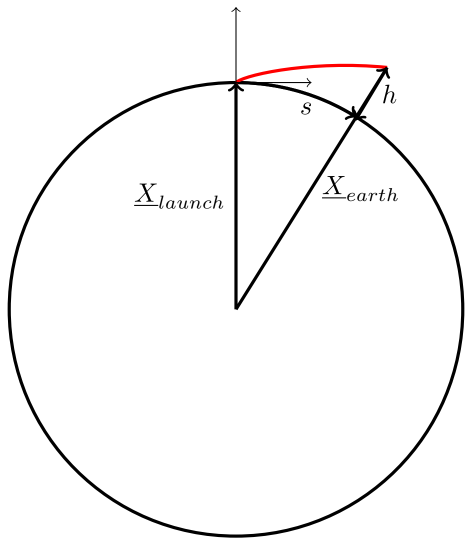

Figure 5.10: Equation of Motion Framework

$$\begin{cases} \ddot{x} = F_x/m \\ \ddot{y} = F_y/m \\ \ddot{z} = F_z/m \\ \dot{m} = \frac{T}{I_{sp}g_0} \end{cases} \tag{5.36}$$

While the angular velocities are integrated using the common Euler equations:

$$\begin{cases} \dot{\omega}_x = \frac{I_y - I_z}{I_x}\omega_y\omega_z + \frac{M_x}{I_x} \\ \dot{\omega}_y = \frac{I_z - I_x}{I_x}\omega_x\omega_z + \frac{M_y}{I_y} \\ \dot{\omega}_z = \frac{I_x - I_y}{I_x}\omega_x\omega_y + \frac{M_z}{I_z} \end{cases} \tag{5.37}$$

Both the integration algorithm and the tolerances are the same of the 3DOF model used in chapter 4.

## 5.8 Linearization

Once the full 6DOF is modeled, the next step is to linearize that model. The vast majority of MPC controllers makes use of a linear model in the form of a state space model. Moreover, the literature followed to design that kind of control is based on a discrete state space model, therefore the aim of this section is to pass from the complete 6DOF rocket model just explained to a discrete linear model. Each linearization is discussed in details and at the end a validation phase across every model used so far is made.
First of all, there are many non-linear elements in the complete model. Those can be seen in the

following list.

1. Mass and inertia
2. Atmosphere properties
3. Aerodynamic Forces
4. Attitude
5. Euler Equations
6. TVC angles

### 5.8.1 Mass and Inertia

Mass, inertia appear at the denominator in the equations of motion, therefore a linearization is basically impossible. The only solution left is to update those values, together with the center of mass position, at each time step and keep them constant across the MPC optimization phase, this could probably introduce the highest error in the linearization process.

### 5.8.2 Euler Equations

The non-linear part in this equations are the cross-term between each angular velocity, in order to get rid of them a few considerations must be done. Since the rocket is assumed to have cylindrical symmetry, two of the three principal moment of inertia are equal $I_y = I_z$. This assumption makes the roll angular velocity independent from the yaw and pitch ones, and since in this model no torques are applied along that axis, the roll angular velocity $\omega_x$ is assumed to be equal to 0 for the whole launch. This consideration leads to the fact that all the cross-terms of angular velocity are equal to 0 and the Euler equations shown in equation 5.37 become linear.

$$\begin{cases} \dot{\omega}_x = \frac{M_x}{I_x} \\ \dot{\omega}_y = \frac{M_y}{I_y} \\ \dot{\omega}_z = \frac{M_z}{I_z} \end{cases} \tag{5.38}$$

### 5.8.3 Attitude

The only way to linearize the rocket attitude system is by means of the Euler Angles and the hypothesis of small rotations, however the pitch angle varies far over the threshold of that hypothesis; for this reason the following procedure has been adopted.
A first rotation is performed using classical Euler angles that connect the inertia position to the so-called *"zero-angular position"*, which is the initial attitude of the launcher.
The rotation matrix is computed according to a $(X - Y - Z)$ rotation, and it's called *Eulerian*

*Attitude Matrix* $\mathbf{A}_{eul}$.

$$\mathbf{A}_{eul}(\phi,\theta,\psi) = \begin{bmatrix} \cos\psi\cos\theta & \cos\psi\sin\theta\sin\phi + \sin\psi\cos\phi & -\cos\psi\sin\theta\cos\phi + \sin\psi\sin\phi \\ -\sin\psi\cos\theta & -\sin\psi\sin\theta\sin\phi + \cos\psi\cos\phi & \sin\psi\sin\theta\cos\phi + \cos\psi\sin\phi \\ \sin\theta & -\cos\theta\sin\phi & \cos\theta\cos\phi \end{bmatrix} \tag{5.39}$$

Then, a second rotation is performed, this one brings a vector from the previous Eulerian frame, to the true attitude of the launcher by means of small angles approach. This rotation matrix is again a $(X-Y-Z)$ type, and it's called *Linearized Attitude Matrix* $\mathbf{A}_{lin}$.

$$\mathbf{A}_{lin}(\alpha_x,\alpha_y,\alpha_z) = \begin{bmatrix} 1 & \alpha_z & -\alpha_y \\ -\alpha_z & 1 & \alpha_x \\ \alpha_y & -\alpha_x & 1 \end{bmatrix} \tag{5.40}$$

The product of those two matrices gives a good link between the inertial and the body frame of reference, the small angles $\alpha_x, \alpha_y, \alpha_z$ are part of the state vector of the system while the Euler angles $\phi, \theta, \psi$ are updated at each time step using the final value of the small ones.

$$\underline{F}_n = \mathbf{A}_{eul}^T \mathbf{A}_{lin}^T \underline{F}_b \tag{5.41}$$

### 5.8.4 Atmosphere properties

As well as the mass, Temperature, density and pressure are computed using the altitude and kept constant for the current time step.

$$[\rho, Temp, P] = Atmosphere(Z_k) \tag{5.42}$$

### 5.8.5 Aerodynamic Forces

Aerodynamic forces are intrinsically non-linear.
The force vector in the body frame can be computed as follows:

$$F_{aero} = \begin{bmatrix} -D0 \\ N_y \\ N_x \end{bmatrix} \tag{5.43}$$

Where $D0$ is the zero-lift drag force, and $Ny, Nz$ are the normal forces acting respectively on the Y and Z axis.
$D0$ is computed using the pressure and velocity coming from the previous time step, and the drag

coefficient is equal to the complete one explained in section 5.2 using dynamic pressure and mach number again from the previous time step.
Regarding the normal forces derivation, this is more complex because the angle of attack must be referred to the Euler angles of the attitude; to do so an important approximation must be done.
In 3D a generic angle of attack $\alpha$ generates a normal force $N$ acting on the body which is function of that angle, this force can be simply decomposed into the Y and Z contributions $N_y$ and $N_z$.
Under the hypothesis of small angles (a spherical triangle approximates a planar one) the angle of attack $\alpha$ could be seen as the result of two angular contributions $\alpha_y$ and $\alpha_z$ which give rise to the two normal forces $N_y$ and $N_z$.

Taking into account the possibility that there could be an angle of attack even if the Euler angles are equal to 0, some initial angles $\alpha_{y0}, \alpha_{z0}$ must be used and computed at each time step.
The force vector can be re-written in this way:

$$F_{aero} = \begin{bmatrix} -D0 \\ N_{y0} + N_{y/\alpha}\alpha_z \\ N_{z0} + N_{z/\alpha}\alpha_y \end{bmatrix} \tag{5.44}$$

With:

$$\begin{cases} D0 = \frac{1}{2}\rho V^2 S C_{D0} \\ N_{y0} = \frac{1}{2}\rho V^2 S C_{N/\alpha}\alpha_{z0} \\ N_{z0} = \frac{1}{2}\rho V^2 S C_{N/\alpha}\alpha_{y0} \\ N_{y/\alpha} = N_{z/\alpha} = \frac{1}{2}\rho V^2 S C_{N/\alpha} \end{cases} \tag{5.45}$$

And $C_{N/\alpha} = 2$ that comes from equation (5.6).

### 5.8.6 TVC

Since the TVC deflection angles are usually below 10°, the small angle approximation can be used to get rid of the sinusoidal functions present in the complete case; so the body forces given by the thrust becomes:

$$F_{thrust} = \begin{bmatrix} T \\ T\delta \\ T\beta \end{bmatrix} \tag{5.46}$$

### 5.8.7 Linear System

The state vector is made of three spatial coordinates, three velocities, the three Euler angles and the angular velocities. The control vector $u$ represent the two TVC deflection angles, and the disturbance $d$ is simply put equal to 1.

$$X_c = \begin{bmatrix} x & y & z & \dot{x} & \dot{y} & \dot{z} & \alpha_x & \alpha_y & \alpha_z & \omega_x & \omega_y & \omega_z \end{bmatrix}^T \tag{5.47}$$

$$u = \begin{bmatrix} \delta \\ \beta \end{bmatrix} \tag{5.48}$$

While the overall force vector expressed in the body frame is the following:

$$\underline{F}_b = \begin{bmatrix} T - D0 \\ T\delta + N_{y0} + N_{y/\alpha}\alpha_z \\ T\beta + N_{z0} + N_{z/\alpha}\alpha_y \end{bmatrix} \tag{5.49}$$

Computing the inertial force vector from equation (5.41) and expressing it as a function of the state vector results in a state space system whose matrices are the following.

$$\mathbf{A}_c = \begin{bmatrix}
0 & 0 & 0 & 1 & 0 & 0 & 0 & 0 & 0 & 0 & 0 & 0 \\
0 & 0 & 0 & 0 & 1 & 0 & 0 & 0 & 0 & 0 & 0 & 0 \\
0 & 0 & 0 & 0 & 0 & 1 & 0 & 0 & 0 & 0 & 0 & 0 \\
0 & 0 & 0 & 0 & 0 & 0 & A_{\alpha x1}/m & A_{\alpha y1}/m & A_{\alpha z1}/m & 0 & 0 & 0 \\
0 & 0 & 0 & 0 & 0 & 0 & A_{\alpha x2}/m & A_{\alpha y2}/m & A_{\alpha z2}/m & 0 & 0 & 0 \\
0 & 0 & 0 & 0 & 0 & 0 & A_{\alpha x3}/m & A_{\alpha y3}/m & A_{\alpha z3}/m & 0 & 0 & 0 \\
0 & 0 & 0 & 0 & 0 & 0 & 0 & 0 & 0 & 1 & 0 & 0 \\
0 & 0 & 0 & 0 & 0 & 0 & 0 & 0 & 0 & 0 & 1 & 0 \\
0 & 0 & 0 & 0 & 0 & 0 & 0 & 0 & 0 & 0 & 0 & 1 \\
0 & 0 & 0 & 0 & 0 & 0 & 0 & 0 & 0 & 0 & 0 & 0 \\
0 & 0 & 0 & 0 & 0 & 0 & 0 & -N_{z/\alpha}L_{aero}/I_y & 0 & 0 & 0 & 0 \\
0 & 0 & 0 & 0 & 0 & 0 & 0 & 0 & N_{y/\alpha}L_{aero}/I_z & 0 & 0 & 0
\end{bmatrix} \tag{5.50}$$

$$\mathbf{B}_c = \begin{bmatrix}
0 & 0 \\
0 & 0 \\
0 & 0 \\
B_{\delta 1}/m & B_{\beta 1}/m \\
B_{\delta 2}/m & B_{\beta 2}/m \\
B_{\delta 3}/m & B_{\beta 3}/m \\
0 & 0 \\
0 & 0 \\
0 & 0 \\
0 & 0 \\
0 & TL_{tvc}/I_y \\
-TL_{tvc}/I_z & 0
\end{bmatrix} \tag{5.51}$$

$$
\mathbf{B}_{dist} = \begin{bmatrix} 0 \\ 0 \\ 0 \\ B_{c1}/m \\ B_{c2}/m \\ B_{c3}/m \\ 0 \\ 0 \\ 0 \\ 0 \\ -N_{z0}L_{aero}/I_y \\ N_{y0}L_{aero}/I_z \end{bmatrix} \tag{5.52}
$$

Where each contribution can be seen expanded in appendix A.
The resulting matrices are then placed in a continuous state space model.

$$
\begin{cases} \dot{X}_c = \mathbf{A}_c X_c + \mathbf{B}_c u + \mathbf{B}_{dist} d \\ y_c = \mathbf{C}_c X_c \end{cases} \tag{5.53}
$$

The subscript c means that the state vector and matrices are continuous. $y$ instead represents the position output, so simply the 3 spatial coordinates.

The discretization is done using a zero order hold method.
The results is the following.

$$
\begin{cases} X_d(k+1) = \mathbf{A}_d X_d(k) + \mathbf{B}_d u(k) + \mathbf{B}_{dist} d(k) \\ y_d(k) = \mathbf{C}_d X_d(k) \end{cases} \tag{5.54}
$$

Where the subscript d means the discreteness of the model.

## 5.9 Trajectory Validation

Across this work, 4 different dynamics have been used. At first the simple 3 degrees of freedom point mass explained in section 4.1, secondly, the full and complex six degrees of freedom derived in chapter 5, and last but not least, the linearized model together with its discretized just shown for MPC purposes. A nice way to check the validity of the trajectory that comes out from this work, is to compare them with something as similar as possible. Unfortunately the Pegasus launcher does not have any trajectory or precise mission profile available, just some rough number regarding the expected staging altitudes and velocities. Even the LauncherOne does not have any of those, maybe they can arrive later on when the launcher becomes fully operational.

One alternative to prove the validity of those trajectories, is to integrate those models with the

same initial conditions and look how they compare to each other. 3 different tests have been performed, the first using no tvc deflection and normal aerodynamic forces not considered, the second with a tvc control law applied and still no lift force, and last with tvc and all the aerodynamic forces considered.
Figure 5.11 shows trajectory and velocity for all four models. Despite being simulated for a long time (60 sec), the results are very nice. The trajectories are very close between each others, and the velocities are almost indistinguishable.

In figure 5.12 the same 4 models are integrated using a particular kind of control law. The $\beta$ tvc angle is deflected using triangular control law, having maximum value of 1 degree and period of 2 seconds. What can be noticed is that the 6dof, the linearized and the discrete models give almost the same results, the 3dof instead differ a lot from them The meaning of this deviation is due to the missing attitude of that model, therefore rotations have no effects on the trajectory. Moreover the $\chi$ angle is always considered from the velocity vector, while for the other models the $\beta$ angle is defined in body coordinates, therefore its inertial orientation depends on the attitude.

Finally, in figure 5.13, the models are integrated switching on the normal aerodynamic forces. In this case the 3dof model has not been used since it cannot account for normal aerodynamic forces, and its limits has already been exposed in the previous test. Also the discrete model has not been done, mainly for simplicity purposes. This test has been done to prove the linearization of the aerodynamic model explained in section 5.8.5. The control law in this case is still a triangular function, but the peak has been fixed to 0.5 degrees, and the period to 0.4 seconds. The two results are quite close up to 1 second, then the two attitudes start diverging This is mainly due to all the simplifications done to include a linear aerodynamic model, and also the hypothesis of small angle of attack. Far from that situation the two models are very different from each other.

From this validations two very important outcomes arise. The first is the validity of the models used so far, one of them has been taken from a book, while all the rest were being developed during this master thesis work. The other important result regards the precision of the linear system, if no normal aerodynamic force is applied (that is the case of second and third stage), this model should be updated every 10 seconds. Otherwise the instability effects of the lift constrains the update to be performed each second.

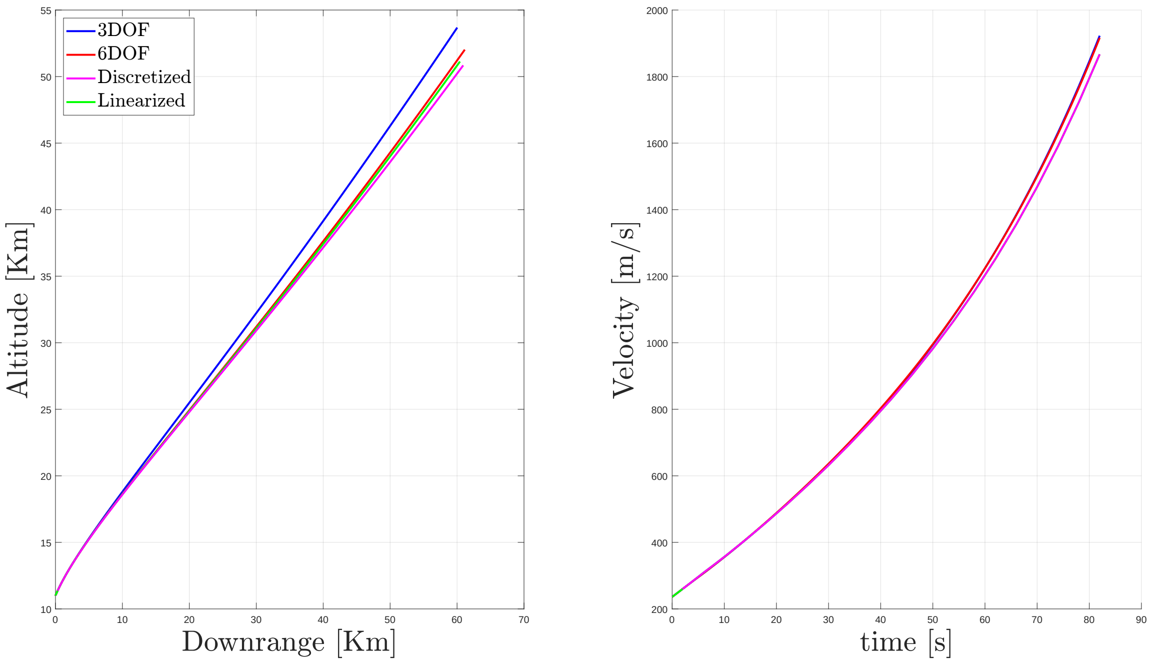


Figure 5.11: Static Trajectory Validation

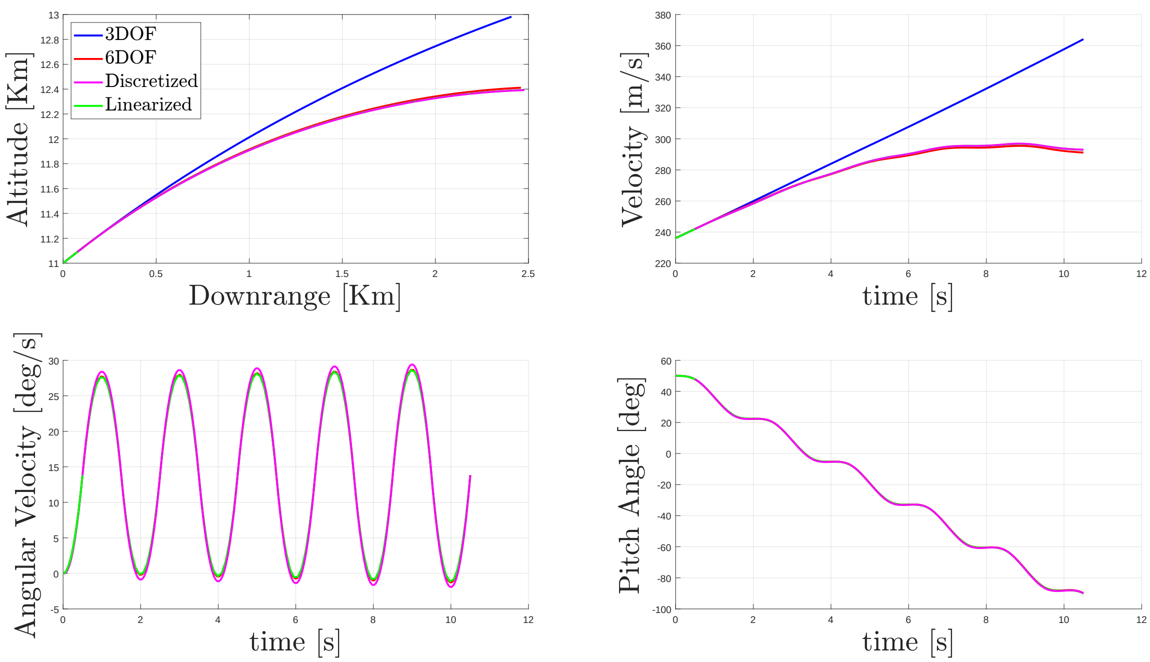


Figure 5.12: Dynamic Trajectory Validation

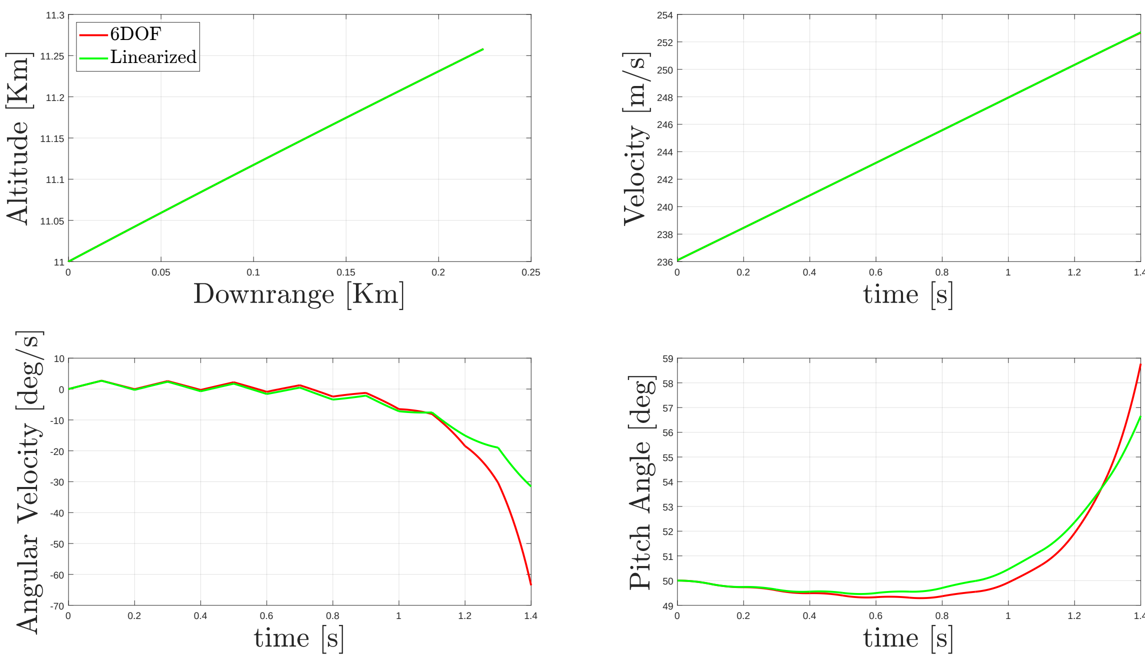


Figure 5.13: Dynamic Trajectory Validation with Aerodynamic Forces

# Chapter 6

# Ascent Control Law

As already said, a rocket launcher is intrinsically unstable during the atmospheric flight, so it requires a very precise control law, this control is introduced in the form of the TVC already modeled in section 5.4. A first very simple control law used in this master thesis is a Proportional-Derivative (PD), it gives quite good results despite the simplicity of the implementation so as a first guess is a good choice.
It is important to point out that this control is not intended to be the final control law of the launcher, instead this is something needed to prove and make use of the 6DOF derived in the last chapter that otherwise is unstable. Moreover this can provide more refined trajectory reference for further and more complex control laws. Therefore the simplicity in this case is a good and wise choice.
In the last section of this chapter is shown another kind of possible controller, the Model Predictive Control (MPC) which has been widely used in the oil and chemical industries since decades but is quite innovative in the space world. The aim of this last part is to derive the control law of the MPC showing the passages, and then test it using the linearized model just derived.

## 6.1 PD Controller

One of the most easy control law, nevertheless widely used, is the PD. Multiplying an error and its derivative with two scalar values results in a very easy and reliable control law for the ascent trajectory. More often PID controllers are used than PD, in this work the integral action has been discarded mainly for simplicity and computational speed purposes.

Given the fact that the reference trajectory has been computed using a 3 dof model with simplified atmospheric actions, the difference in velocity is expected do differ with respect to a model with a more complex aerodynamic model. For this reason it is a wise choice to follow a geometric trajectory compared to a motion law function of time.

The error is defined as the difference between the altitude for the $\beta$ angle, and the cross-range for the $\delta$ angle. The reference altitude and cross-range are interpolated using the downrange value.

Since the angle of attack provides the unstablizer lift force, a good choice is to add the tvc contribution that cancel out the moments introduced by the normal forces, those angle are defined $\beta_0$ and $\delta_0$.

$$\begin{cases} \beta = -K_p\left(\frac{Z-Z_{ref}}{Z_{ref}}\right) - K_d\left(\frac{\dot{Z}-\dot{Z}_ref}{\dot{Z}_ref}\right) + \beta_0 \\ \delta = -K_p\left(\frac{Y-Y_{ref}}{Y_{ref}}\right) - K_d\left(\frac{\dot{Y}-\dot{Y}_ref}{\dot{Y}_ref}\right) + \delta_0 \end{cases} \tag{6.1}$$

Where the two 0-angles are computed as:

$$\begin{cases} \beta_0 = \arcsin\left(\frac{N_z L_{aero}}{T L_{tvc}}\right) \\ \delta_0 = \arcsin\left(\frac{N_y L_{aero}}{T L_{tvc}}\right) \end{cases} \tag{6.2}$$

The next question is how to compute the parameters $K_p$ and $K_d$. First of all is worth mentioning that only one set of $K_p$ and $K_d$ is not enough to get a good tracking of the reference, for this reason the launch is divided into different temporal steps where each one has its own $K_p$ and $K_d$. Then a minimization is made up to compute a good set of those parameters without tuning them by hand.

This procedure is valid up to the second stage burnout, the third stage is discussed later on. The optimization works in the following way, the independent variables are the set of $K_p$ and $K_d$ for each time interval, while the cost function is selected to be the vector representing the errors between altitude and cross-range at the end of each interval and reference values computed at the same downrange, basically it must follow the geometric reference trajectory. The minimization is performed using a nonlinear least-square solver.

$$\underline{X}_{opt} = \begin{bmatrix} K_{p_1} & K_{d_1} & K_{p_2} & K_{d_2} & K_{p_3} & K_{d_3} & \dots & K_{p_n} & K_{d_n} \end{bmatrix} \tag{6.3}$$

$$\underline{J}_{opt} = \begin{bmatrix} (Z_{ref}(S_{end_1}) - Z_{end_1}) & (Z_{ref}(S_{end_2}) - Z_{end_2}) & \dots & (Z_{ref}(S_{end_n}) - Z_{end_n}) \end{bmatrix} \tag{6.4}$$

To account for the missing RCS of the third stage, the angular velocities has been forced to zero at the beginning of the burn, and the orientation of the rocket is imposed such that it is completely aligned with the velocity, therefore at 0 angle of attack.

After the second stage burnout there is a free coasting phase, during this part there is no control on the trajectory but only on the attitude. This means that a perfect tracking of this phase is possible only if the initial conditions on that phase are identically equal to the reference one. Since that condition is basically impossible, a full-tracking like the previous stages is not meaningful, therefore a new set of independent variables and errors is required.

As said, an altitude difference is unavoidable, but the only element that is worth following is the vertical velocity. Therefore only $K_d$ has a particular meaning. The best way to achieve such a control, is to target the orbit insertion as precise as possible. Again, the same solver is being used for this section.

This time, the cost function vector is made by the final constraints in terms of altitude, flight path angle and velocity. A penalty is imposed also if the angular velocities overcome a certain threshold (5 deg/s). In the angular velocities are small, the RCS of the third stage or the CubeSat can simply get rid of it using thrusters or other RCS hardware, but it is desirable to be as low as possible.

The vector to be minimized is the following:

$$\underline{J}_{3rd} = \left[(Z_{end} - Z_{orbit})/Z_{orbit} \quad (\gamma_{end})/\pi \quad (V_{end} - V_{orbit})/V_{orbit}\right] \tag{6.5}$$

## 6.2 MPC Controller

Model Predictive Control is an advanced method of process control that aims to compute a future manipulated control inputs to optimize the future behavior of the dynamic system. The optimization is performed over a finite time window called "horizon", furthermore its suitable for constrained systems since the optimization can be made thank to Quadratic Programming (QP) that can impose boundaries over inputs and outputs directly in the optimization process, this avoid finding nonphysical solutions.

What MPC practically does, is computing the predicted output of a dynamic system as a function of the initial plant conditions, and the manipulated variables for each time step. Then a cost function is defined that aims to the minimization of both the error between output and reference, and the control inputs themselves. If no constrained are impose the optimal solution can be found analytically like an Linear Quadratic Regulator (LQR) process, otherwise using QP the constrained solution can be computed.

In figure 6.1 the Model Predictive Control scheme used in this chapter can be seen. The rocket dynamic is integrated using the most complete model derived so far, the 6DOF. The state coming out from that integration is used in two different ways: first it is needed to update the linear model inside the controller, and most importantly, it is necessary to compute the error between the current state and the reference. Reference that comes from the simplified 3DOF model.
Inside the controller, the linear model provides the future predictions at each time step, those are needed by the optimization to compute the future control actions such that the error between predictions and reference is minimum.
One the optimized control actions are computed, its contribution at the first time step is extracted and used as TVC control in the 6DOF dynamic. After that the entire procedure is iterated again.

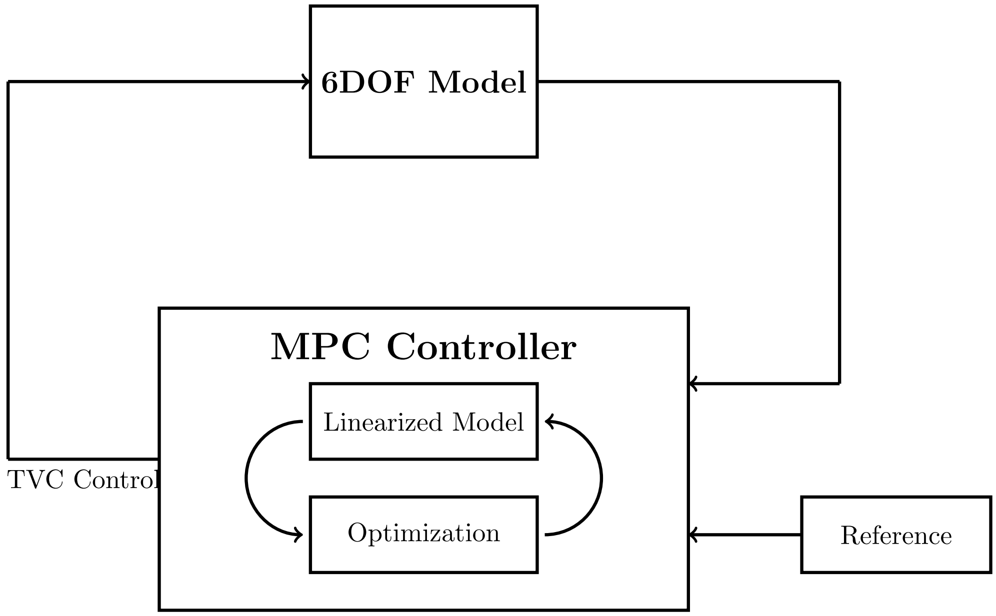


Figure 6.1: Model Predictive Control Scheme

The aim of this brief chapter is to show how the MPC controller is modeled and discuss about the results and possible future development. The procedure has been taken from the book [39].

The 6 degrees of freedom rocket dynamics has been linearized and discretized in section 5.8, this procedure starts with the discrete state space model shown in equation (5.54).

The first step is defining the difference between two intervals of the state and the input. Since the disturbance $d$ is basically constant it cancels out from the model and it is useful only to update the current state.

$$\begin{cases} \Delta X_d(k) = X_d(k) - X_d(k-1) \\ \Delta u(k) = u(k) - u(k-1) \end{cases} \tag{6.6}$$

Then, it is possible to create an augmented system.

$$X(k) = \begin{bmatrix} \Delta X_d(k) \\ y(k) \end{bmatrix} \tag{6.7}$$

And therefore its corresponding state space model.

$$\begin{cases} X(k+1) = \mathbf{A}X(k) + \mathbf{B}u(k) \\ y(k) = \mathbf{C}X(k) \end{cases} \tag{6.8}$$

Where the Matrices are found in the following way:

$$\mathbf{A} = \begin{bmatrix} \mathbf{A}_d & \mathbf{0} \\ \mathbf{C}_d\mathbf{A}_d & \mathbf{I} \end{bmatrix} \tag{6.9}$$

$$\mathbf{B} = \begin{bmatrix} \mathbf{B}_d \\ \mathbf{C}_d\mathbf{B}_d \end{bmatrix} \tag{6.10}$$

$$\mathbf{C} = \begin{bmatrix} \mathbf{0} & \mathbf{I} \end{bmatrix} \tag{6.11}$$

Now, let's define a couple of further matrices.

$$\Delta U = \begin{bmatrix} \Delta u(k_1)^T & \Delta u(k_1+1)^T & \dots & \Delta u(k_1+N_c-1)^T \end{bmatrix}^T \tag{6.12}$$

$$\mathbf{Y} = \begin{bmatrix} y(k_1+1 \mid k_1)^T & y(k_1+2 \mid k_1)^T & \dots & y(k_1+N_p \mid k_1)^T \end{bmatrix}^T \tag{6.13}$$

Where $N_c$ and $N_p$ are respectively the controlled horizon and the prediction horizon, and the latter is always grater or equal than the former. The vertical bar in the second matrix means that the output is computed using the information at the sample k1.

Without reporting all the passages is possible to get a link between those two matrices and the initial sample of the state vector.

$$\mathbf{Y} = \mathbf{F}X(k_1) + \mathbf{\Phi}\Delta U \tag{6.14}$$

Where the $\mathbf{F}$ and $\mathbf{\Phi}$ are defined as follows:

$$\mathbf{F} = \begin{bmatrix} \mathbf{CA} \\ \mathbf{CA^2} \\ \mathbf{CA^3} \\ \vdots \\ \mathbf{CA^{N_p}} \end{bmatrix} \tag{6.15}$$

$$\mathbf{\Phi} = \begin{bmatrix} \mathbf{CB} & \mathbf{0} & \mathbf{0} & \dots & \mathbf{0} \\ \mathbf{CAB} & \mathbf{CB} & \mathbf{0} & \dots & \mathbf{0} \\ \mathbf{CA}^2\mathbf{B} & \mathbf{CAB} & \mathbf{CB} & \dots & \mathbf{0} \\ \vdots & \vdots & \vdots & \vdots & \vdots \\ \mathbf{CA}^{N_p-1}\mathbf{B} & \mathbf{CA}^{N_p-2}\mathbf{B} & \mathbf{CA}^{N_p-3}\mathbf{B} & \dots & \mathbf{CA}^{N_p-N_c}\mathbf{B} \end{bmatrix} \tag{6.16}$$

The reference to be followed can be modeled as:

$$\mathbf{R}_s = \begin{bmatrix} 1 & 1 & 1 & \dots & 1 \end{bmatrix} r(k_1) = \bar{\mathbf{R}}_s r(k_1) \tag{6.17}$$

Where $r(k_1)$ is the reference vector at the sample $k_1$.

Finally the cost function can be set.

$$J = (\bar{\mathbf{R}}_s - \mathbf{Y})^T(\bar{\mathbf{R}}_s - \mathbf{Y}) + \Delta U^T \mathbf{R}_u \Delta U \tag{6.18}$$

$\mathbf{R}_u$ is simply an identity matrix multiplied by a certain factor where the greater is the more important is getting a small control values for the optimization process.
If no constraints over the control inputs are applied, the optimal control can be computed in the following way.

$$\Delta U = \left(\mathbf{\Phi}^T\mathbf{\Phi} + \mathbf{R}_u\right)^{-1}\left(\mathbf{\Phi}^T\bar{\mathbf{R}}_s r(k_1) - \mathbf{\Phi}^T\mathbf{F}X(k_1)\right) \tag{6.19}$$

The first 3 elements of that vector represent the difference in control to be applied at the sample $k_1$, then the linear system is integrated to get the state vector $X(k_1+1)$ and its corresponding reference $r(k_1+1)$, so the procedure can be iterated.
Alternatively, if maximum and minimum tvc are imposed, the control law can be derived using quadratic programming theory.

## 6.3 Results

First, let's take a look at the result coming out from PD controller. Figures 6.2,6.3,6.4 show the integration results of the first configuration, while figures 6.5,6.6,6.7 show the second. The dots represent the points at which the trajectory is divided as explained at the beginning of this chapter. The overall results are very good compared to the reference trajectory, this proves the feasibility of this kind of controller despite being very easy to implement. In the second configuration more than the first, the error due to a not perfect alignment during the coasting phase can be noticed as expressed before. Despite this error, the third stage aims at reaching the orbit in the best way possible, the error over the altitude is in the order of 20 Km, in line with the accuracy of an upper stage solid. Other simulations not reported here result in errors even below 4/5 Km for both configurations.
Again, is worth stressing the fact that this is not intended to be the perfect control of this launcher, this is a preliminary control law thought to test the 6DOF rocket model, and provide some initial references for a further test of the MPC controller or other control laws.

Regarding the MPC, a first test has been performed in order to ensure the validity of the controller. The test wants the rocket to follow a linear trajectory with constant altitude imposed at 11 Km. Maximum tvc has been imposed to 7 degrees, time step to 0.1 seconds, and prediction horizon and control horizon has been fixed respectively at 20 and 10.
The results can be seen in figures 6.8,6.9,6.10.
As can be noticed, the $\beta$ angle has some sort of random behavior and then it starts oscillating from the maximum to the minimum. Therefore the attitude of the rocket is uncontrolled making more and more rotations.

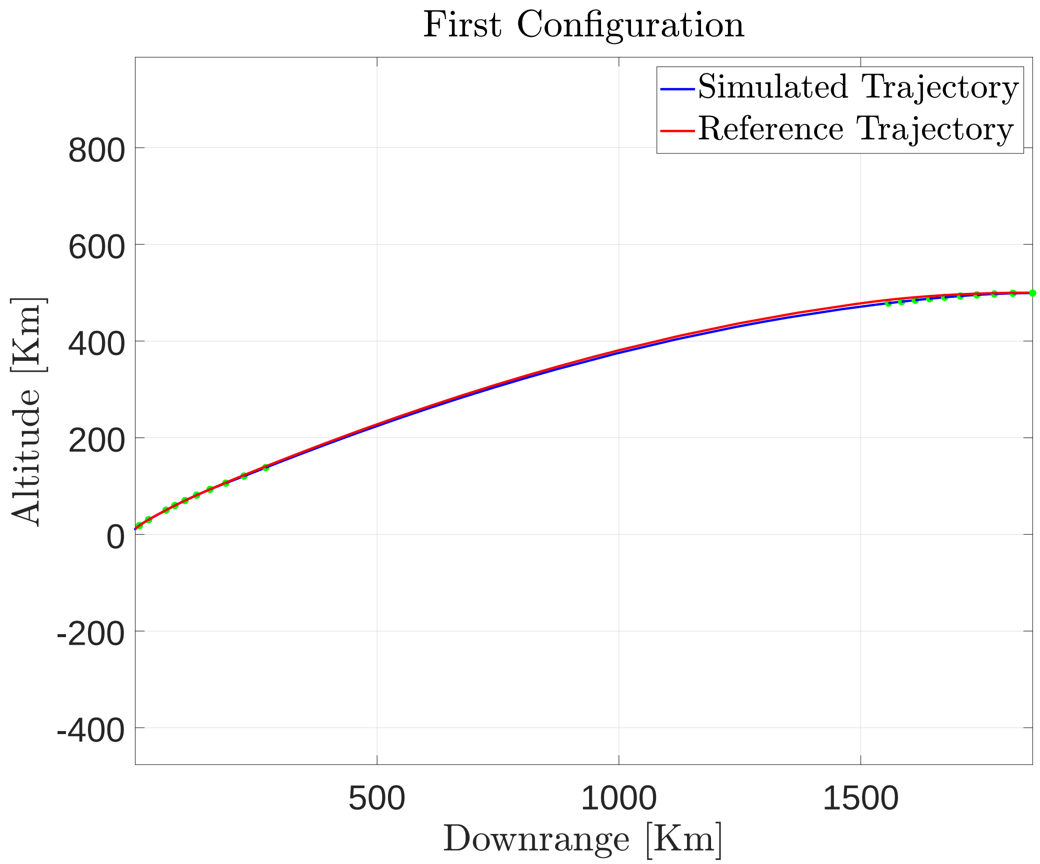

Figure 6.2: First Configuration Trajectory

A lot of more tests have been performed (yet not reported here) changing basically every variables, but no good result has been found yet.

### 6.3.1 Possible MPC Issues

As shown, the MPC did not result in a feasible control law. The possible reasons could be the following.

First, the continuous matrix $\mathbf{A}_c$ is singular, so there are problems in inverting the matrix during the solution and avoid the possibility of using other kind of laws such as LQR. The passage between continuous and discrete system makes the A matrix no more singular but it remains highly ill-conditioned.

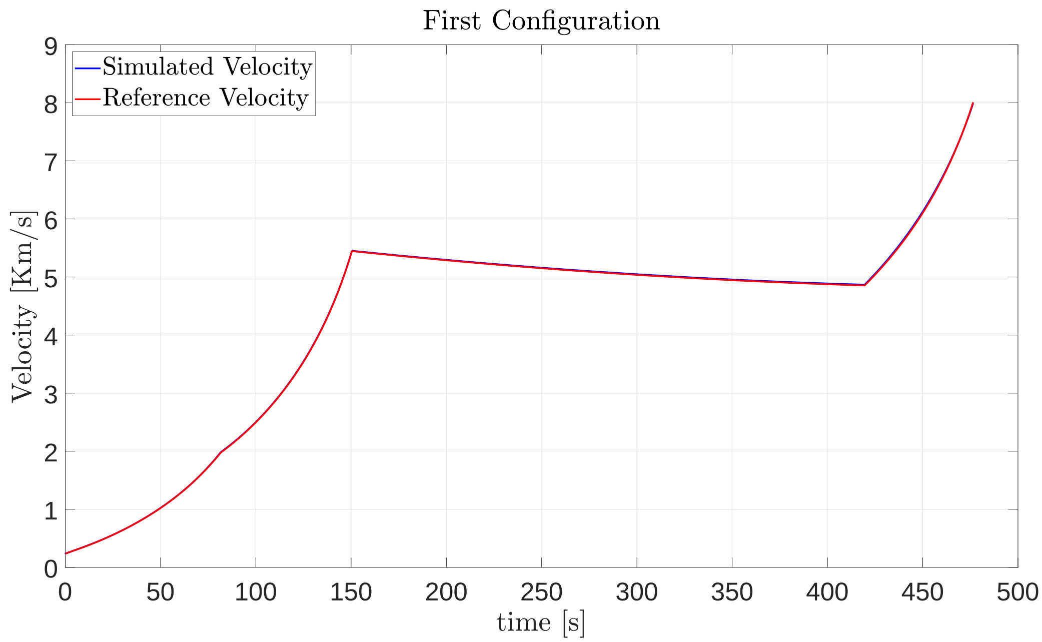


Figure 6.3: First Configuration Velocity

Another possible problem regards the non controllability (yet observable) of the continuous dynamic system, a possible solution is a change of coordinates from cartesian to another type, maybe even reducing the number of independent variables.

One final problem is the value of the Euler angles that must stay below certain threshold due to the hypothesis of small angles, the only way found so far is to put those angles as output values and control them. In this case not only the outputs are increasing, but moreover a reference value for those angles must be found that is not trivial since the standard reference comes from a simplified model without attitude. Furthermore in order to introduce boundaries of outputs a more complex procedure must be followed, and this lies beyond the purpose of this master thesis. Another possibility could be to give reference also from the attitude point of view and not only the trajectory, the reference could come from the usage of the PD controller just explained. In any case, there is plenty of work still to be done.

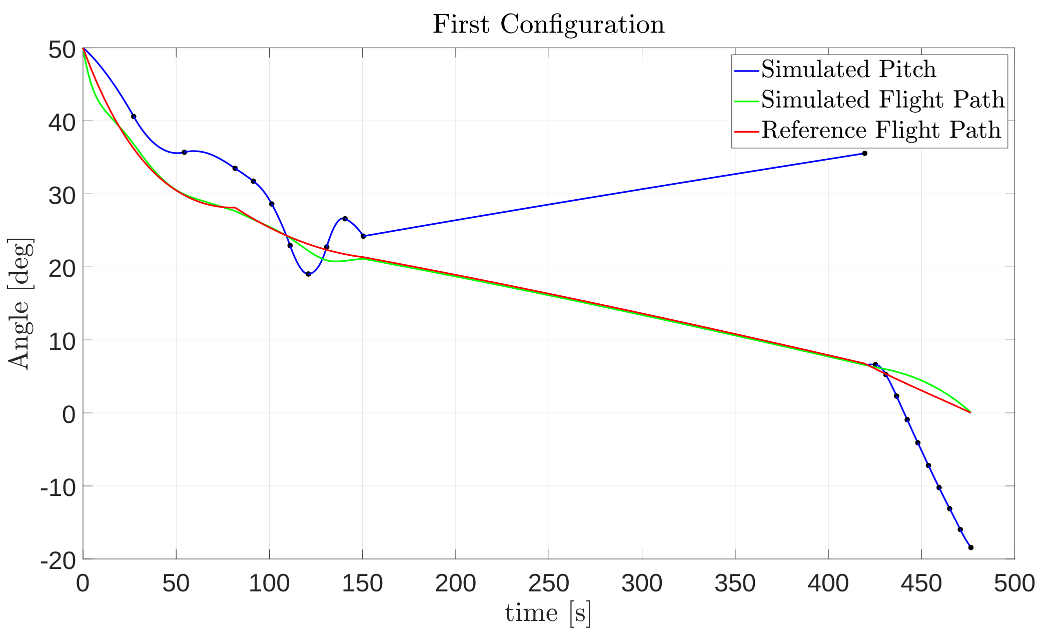


Figure 6.4: First Configuration Angles

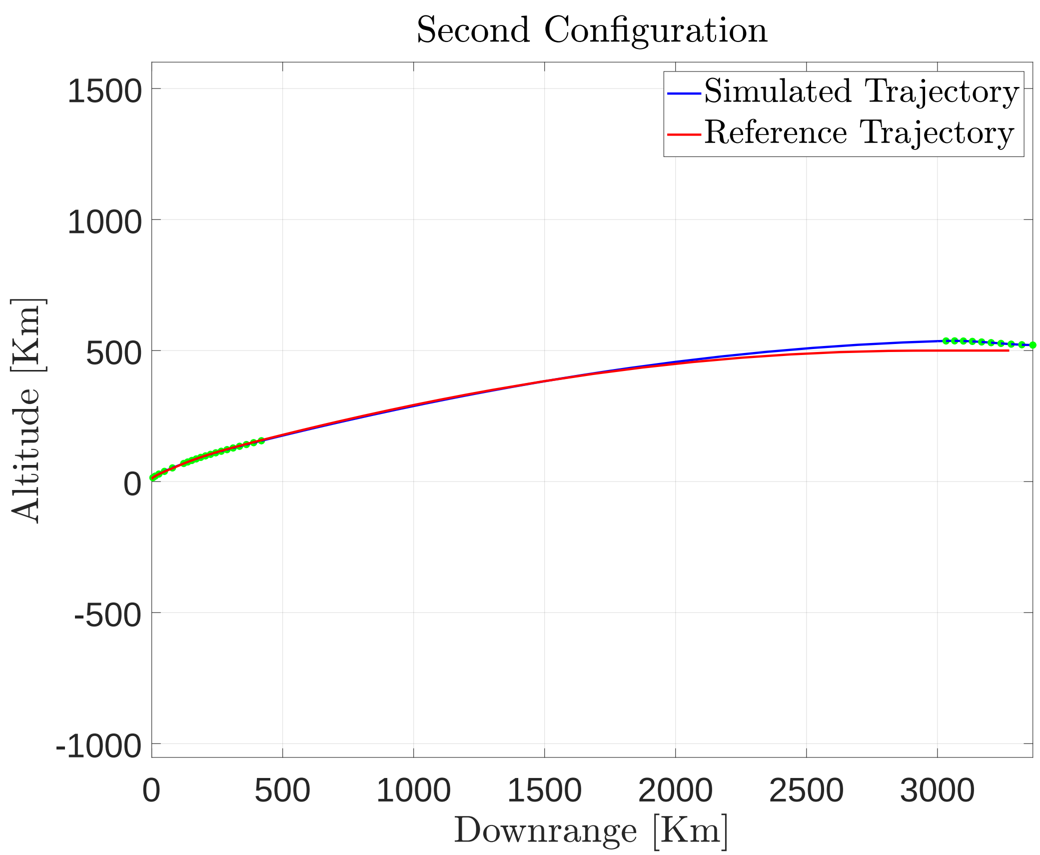


Figure 6.5: Second Configuration Trajectory

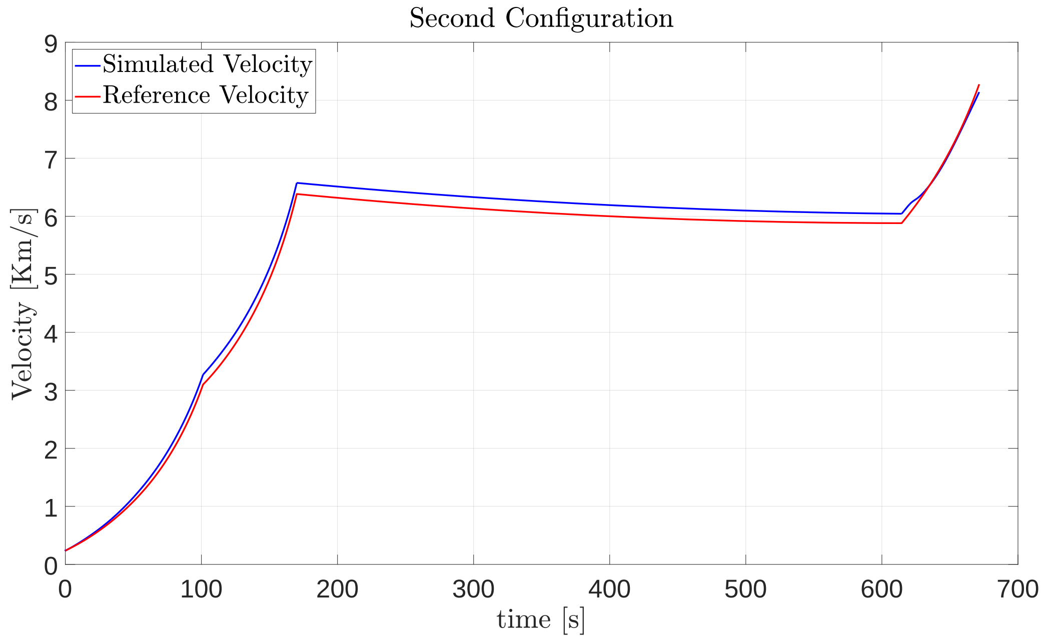


Figure 6.6: Second Configuration Velocity

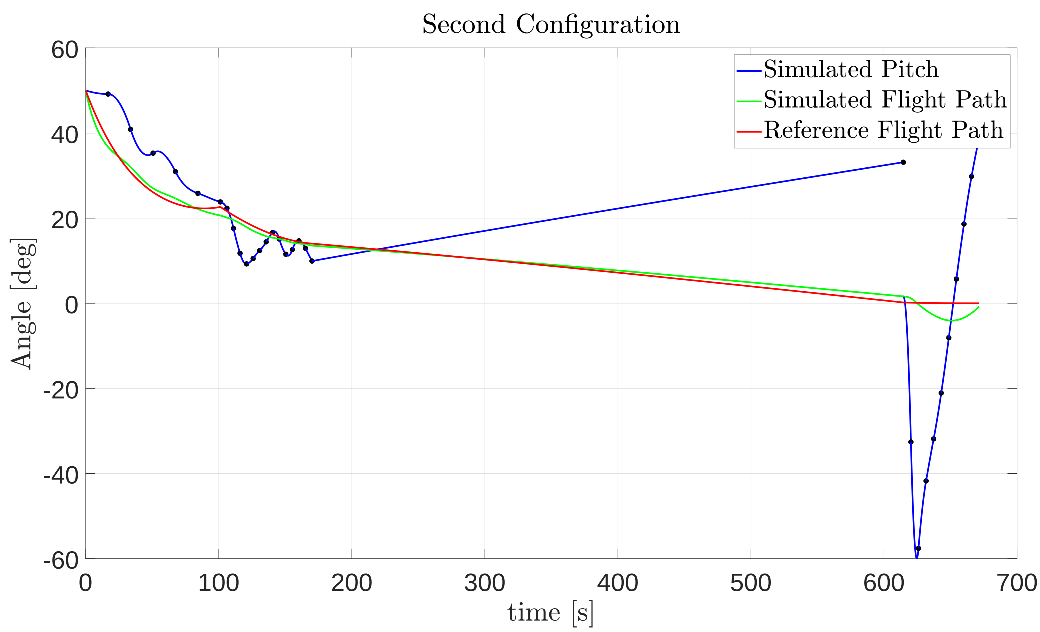


Figure 6.7: Second Configuration Angles

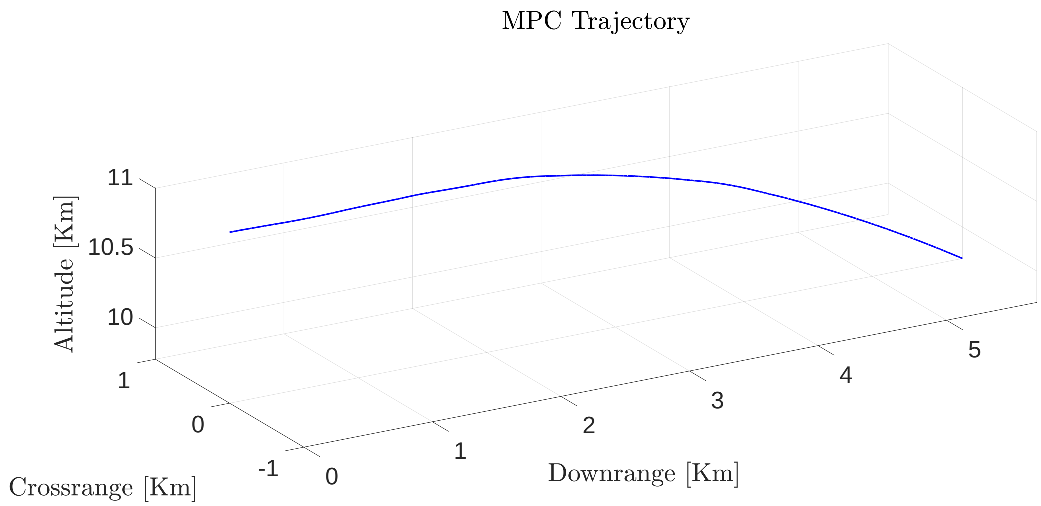


Figure 6.8: MPC Test Trajectory

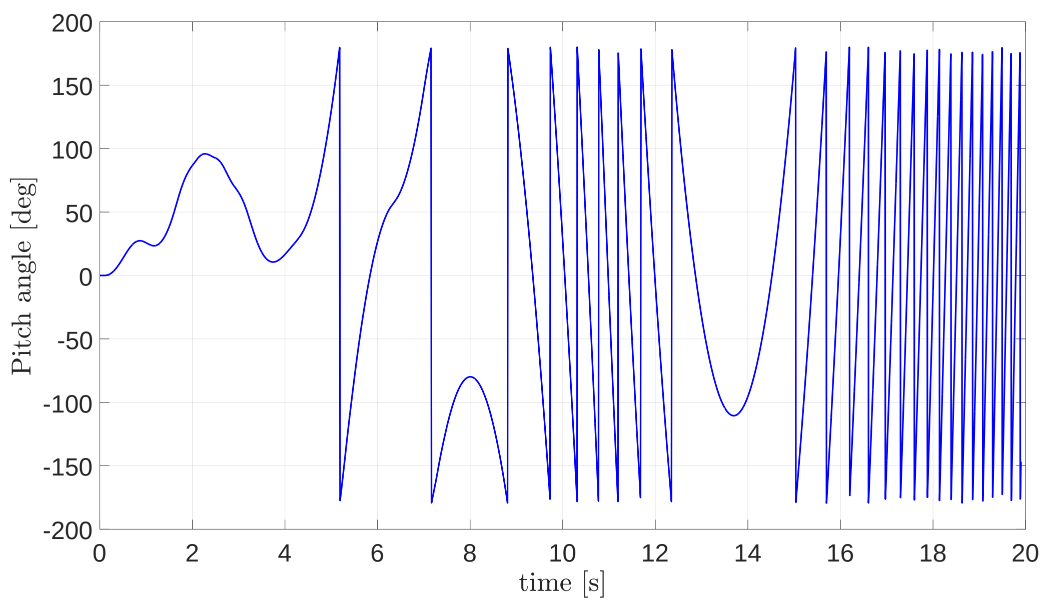


Figure 6.9: MPC Test Pitch

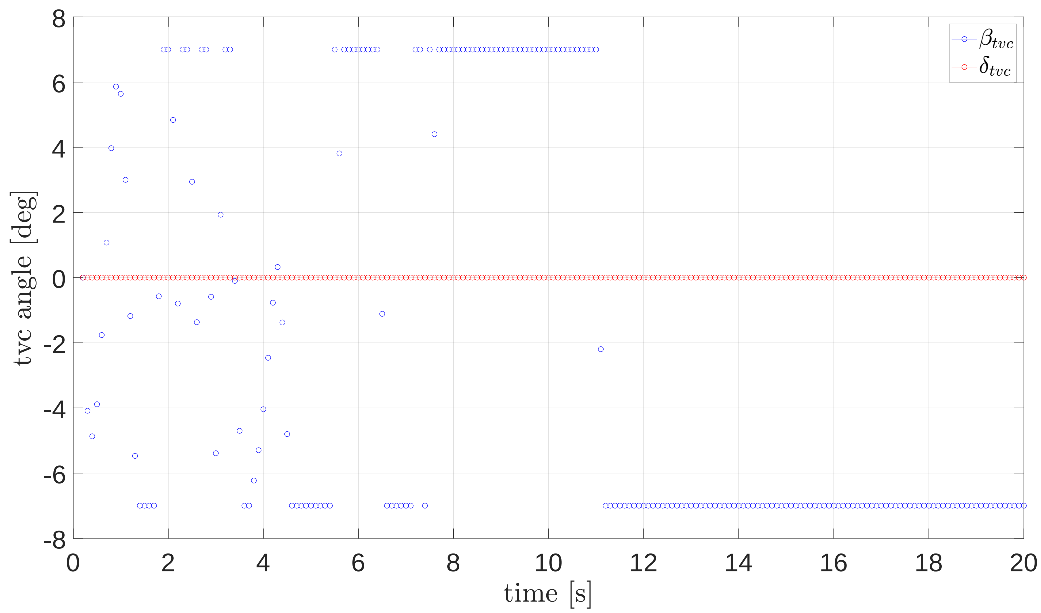


Figure 6.10: MPC Test TVC

# Chapter 7

# Conclusions

During this work, a first iteration of an air to orbit launch vehicle has been performed. This study has been done according to a Multidisciplinary approach that enhanced the design both from quality and time point of view. The outcome is a set of mass and dimension budget that prove the feasibility of this concept, and are required for a future concrete implementation from the industrial point of view.

Despite having used simple models, the launchers has been designed from every meaningful point of view, from the propulsion hardware to the guidance control law, passing by the launch location and the re-entry effects. Through this design process the help given by the multidisciplinary approach has been very effective in building the design breakdown shown in figure 1.5. That process was very useful
The multiconfiguration staging has been proven to be very effective in increasing the payload range without a correspondingly increase in the costs. The next step is to go on with the same approach but using models much more refined capable of considering losses and trajectory effects.

Regarding the propulsion architecture, solid rocket motors has proved their effectiveness in terms of both reliability, simplicity and costs, therefore they are the perfect candidate to start a more detailed implementation. The hybrid rocket engine of the third stage is very interesting, the only major drawbacks of this solution is probably the low TRL of the technology. Future works should assess the validity of this solution computing the advantages in a more quantitative way, and after that if the solution is proven to be

The work on the launch zones was very effective as well, it provided 5 candidates based on safety and proximity of Italian airports. Further work must be able to estimate better both the falling range, and the threat given by the dead rocket bodies. Moreover, political agreement must be made concerning the deployment and flight of rockets above foreign territories.

Regarding the last part, a complete 6DOF has been implemented to further demonstrate the validity of the previous design. Moreover, a very interesting linearization process has been performed and then tested with other models. The full model has been used together with a simple PD control law implemented just for this purpose.

Finally, a Model Predictive Control law has been derived from the linear state space system of the launcher just computed. Unfortunately this has not performed as expected, the probable causes can be found in paragraph 6.3.1.

To sum up what has been done in this master thesis.

## 7.1 Main Budgets

The final budgets in terms of mass can be seen in table 7.1. What can be noticed is that the second configuration has almost twice the mass of the first one. This is not surprising because also the payload is doubled. However, thanks to the multiconfiguration staging process, those two payloads very different from each other, are being launched by the same 4 solid rocket motors, just used in different configurations, thus reducing costs.

| **Masses**<br>Units | $\mathbf{M_{payload}}$<br>Kg | $\mathbf{M_p}$<br>Kg | $\mathbf{M_s}$<br>Kg | $\mathbf{M_0}$<br>Kg | $\mathbf{M_0 + 20\%margin}$<br>Kg |
|---|---|---|---|---|---|
| I Configuration | ??? | ??? | ??? | ??? | ??? |
| II Configuration | ??? | ??? | ??? | ??? | ??? |

Table 7.1: Final Launcher Budget

Another very interesting outcome, is shown in table 7.2. As said, the staging design does not account for any kind of losses, therefore a big margin over the $\Delta V$ must be imposed. The simple 3DOF rocket model accounts only for few losses, so the final velocities are lower. Finally the 6DOF is the most accurate one among the ones developed in this master thesis, this means that the final velocity is the closest to the real one.

| **Velocities**<br>Units | $\mathbf{V_{orbital}}$<br>Km/s | $\mathbf{\Delta VMargin}$<br>- | $\mathbf{V_{staging}}$<br>Km/s | $\mathbf{V_{3dof}}$<br>Km/s | $\mathbf{V_{6dof}}$<br>Km/s |
|---|---|---|---|---|---|
| I Configuration | 7.166 | 1.22 | 9.292 | 8.009 | 7.991 |
| II Configuration | 7.166 | 1.22 | 9.292 | 8.276 | 8.143 |

Table 7.2: Velocity Budget

## 7.2 Multidisciplinary Design Synthesis

bla bla bla

## 7.3 Further Work

There are many subsystems that were not designed in this master thesis. First of all, the avionics of the launcher and the RCS system of the third stage, during the coasting phase the engine is not working therefore the tvc is not able to control the attitude. Moreover launchers with a single engine can not control the roll axis, thrusters are then required.
Very important is the cost analysis, this is crucial to identify how much market the launcher could have, and get insights about how many motors should be built each year.
The control law in this work must be considered to be a sort tool needed to use the 6DOF rocket model (which is unstable otherwise), that is again a benchmark for the design done so far. However the PD control is quite poor and too much simplified with respect the other subsystems, the Model Predictive Control could be a very interesting alternative from both the quality and the innovation point of view.
Further works can certainly assess the feasibility of the MPC using a more detailed analysis, and if is proven to be unfeasible another type of control must be selected and designed for the ascent trajectory control.

# Bibliography


[1] Nanosat database https://www.nanosats.eu/.

[2] Janovsky R. Koelle D. E. *Development and transportation costs of space launch systems.* DGLR/CEAS European Air and Space Conference.

[3] Fleeman E. L. *Tactical Missile Design.* AIAA, 2006.

[4] Eurofighter https://www.eurofighter.com/the-aircraft.

[5] Sforza P. M. *Manned Spacecraft Design Principles.* University of Florida, 2016.

[6] Virgin Orbit. *LauncheOne Service Guide.* Launcher Manual.

[7] Orbital ATK. *Pegasus User's Guide Review.* Launcher Manual.

[8] Avio propulsion system https://www.avio.com/propulsion-system.

[9] ArianeSpace. *VEGA Payload User's Guide Version.* Launcher Manual.

[10] Nasa spaceflight https://www.nasaspaceflight.com/.

[11] Virgin orbit launcherone https://virginorbit.com/technology/.

[12] Nasa vcls https://www.nasa.gov/press-release/nasa-awards-venture-class-launch-services-contracts-for-cubesat-satellites.

[13] Firefly Aerospace. *Alpha Payload User's Guide Version 2.0.* Launcher Manual.

[14] RocketLab. *Electron Payload User's Guide Version 6.4.* Launcher Manual.

[15] Kroo I. M. Braun R. D., Moore A. A. *Collaborative Approach to Launch Vehicle Design.* Journal of Spacecraft and Rockets, 1997.

[16] Dépincé P. Chriette A. Balesdent M., Bérend N. *A survey of multidisciplinary design optimization methods in launch vehicle design.* Springer, 2011.

[17] Haftka R. T. Sobieszczanski-Sobieski J. *Multidisciplinary aerospace design optimization - Survey of recent developments.* AIAA 34th Aerospace Sciences Meeting and Exhibit, 1996.

[18] Castellini F. *Multidisciplinary Design Optimization for Expendable Launch Vehicles.* Ph.D. Thesis Politecnico di Milano, 2012.

[19] Vallado D. A. *Fundamentals of Astrodynamics and Applications*. Springer, 2007.

[20] ISIS Space. *CubeSats Deployer Brochure*. ISIS Space.

[21] Ruag https://www.ruag.com/en/products-services/space/launchers/launchers.

[22] Sarigul-Klijn M. Sarigul-Klijn N. *Air Launching Eart-to-Orbit Vehicles: Delta V gains from Launch Conditions and Vehicle Aerodynamics*. AIAA.

[23] Sutton P. G. *Rocket Propulsion Elements*. Wiley, 2010.

[24] Gordon S. McBride B. J. *Computer Program for Calculation of Complex Chemical Equilibrium Compositions and Applications*. NASA Lewis Research Center, 1996.

[25] Leary J. P. Landsbaum E. M., Salinas M. P. *Specific Impulse Prediction of Solid-Propellant Motors*. The Aerospace Corporation, El Segundo, Calif., 2012.

[26] Humble R. W. *Space Propulsion Analysis and Design*. McGraw-Hill, 1995.

[27] Lee J. Rhee I., Lee C. *Optimal design for hybrid rocket engine for air launch vehicle*. Journal of Mechanical Science and Technology 22, 2008.

[28] Vieira R. de Souza Costa F. *Preliminary Analysis of Hybrid Rockets for Launching Nanosats into LEO*. Journal of the Brazilian Society of Mechanics, Science and Engineering, 2010.

[29] Cantwell B. Stevens J. Karabeyoglu A., Falconer T. *Design of an Orbital Hybrid Rocket Vehicle Launched from Canberra Air Platform*. 41st AIAA/ASME/SAE/ASEE Joint Propulsion Conference and Exhibit, 2005.

[30] Byun Y. Lee J., Noh K. *Preliminary Design of the Hybrid Air-launching Rocket for Nanosat*. Fifth International Conference on Computational Science and Applications, 2007.

[31] Mullens P. Ventura M. *The use of hydrogen peroxide for propulsion and power*. 35th AIAA/ASME/SAE/ASEE Joint Propulsion Conference and Exhibit, 1999.

[32] Krishnan S. George P. *Fuel Regression rate enhancement studies in HTPB/GOx Hybrid Rocket Motors*. AIAA, 1998.

[33] Waite M. J. Hertzelle W. S. *Design of a small H2O2/HTPB hybrid sounding rocket motor*. AIAA, 1996.

[34] Massimo P. Bisin R. Galfetti L. Paravan C., Lisi F. *Burning Behavior Investigation of a Vortex Flow Pancake Hybrid Rocket Engine*. AIAA Propulsion and Energy 2019 Forum, 2019.

[35] NASA. *Aerothermodynamic Course*. JPL TFAWS, 2019.

[36] Bourbigot S. Tranchard P. *High Temperature-Dependent Thermal Properties of a Carbon-Fiber Epoxy Composite*. University of Lille, Unité Matériaux et Transformation, 2017.

[37] Jablonski A. M. *Deorbiting of microsatellites in Low Earth Orbit (LEO)*. Defence R and D Canada Ottawa, 2008.

[38] Crassidis J. L. Markley F. L. *Fundamentals of Spacecraft Attitude Determination and Control*. Springer, 2014.

[39] Wang L. *Model Predictive Control System Design and Implementation using Matlab*. Springer, 2008.

# Appendix A

# Appendix

$$
\begin{cases}
A_{\alpha x1} = N_{z0}\cos\theta\sin\psi + N_{y0}\sin\theta \\
A_{\alpha y1} = N_{z0}\cos\theta\cos\psi + N_{z/\alpha}\sin\theta - (T-D0)\sin\theta \\
A_{\alpha z1} = -N_{y0}\cos\theta\cos\psi - N_{y/\alpha}\cos\theta\sin\psi - (T-D0)\cos\theta\sin\psi \\
A_{\alpha x2} = -N_{z0}\cos\phi\cos\psi - N_{y0}\sin\phi\cos\theta + N_{z0}\sin\phi\sin\theta\sin\psi \\
A_{\alpha y2} = -N_{z/\alpha}\sin\phi\cos\theta + (T-D0)\sin\phi\cos\theta + N_{z0}\cos\phi\sin\psi + N_{z0}\sin\phi\sin\theta\cos\psi \\
A_{\alpha z2} = N_{y/\alpha}\cos\phi\cos\psi + (T-D0)\cos\phi\cos\psi - N_{y0}\cos\phi\sin\psi - N_{y0}\sin\phi\sin\theta\cos\psi + \\
-N_{y/\alpha}\sin\phi\sin\theta\sin\psi - (T-D0)\sin\phi\sin\theta\sin\psi \\
A_{\alpha x3} = N_{y0}\cos\phi\cos\psi - N_{z0}\sin\phi\cos\psi - N_{z0}\cos\phi\sin\theta\sin\psi \\
A_{\alpha y3} = N_{z/\alpha}\cos\phi\cos\psi - (T-D0)\cos\phi\cos\psi + Nz0\sin\phi\sin\psi - N_{z0}\cos\phi\sin\theta\cos\psi \\
A_{\alpha z3} = N_{y/\alpha}\sin\phi\cos\psi + (T-D0)\sin\phi\cos\psi - N_{y0}\sin\phi\sin\psi + N_{z0}\cos\phi\sin\theta\cos\psi + \\
+N_{y/\alpha}\cos\phi\sin\theta\sin\psi + (T-D0)\cos\phi\sin\theta\sin\psi \\
B_{\delta 1} = -T\cos\theta\cos\psi\alpha_z - T\cos\theta\sin\psi + T\sin\theta\alpha_x \\
B_{\beta 1} = T\cos\theta\cos\psi\alpha_y + T\cos\theta\sin\psi\alpha_x + T\sin\theta \\
B_{c1} = (T-D0)\cos\theta\cos\psi - N_{y0}\cos\theta\sin\psi + N_{z0}\sin\theta - mg_1 \\
B_{\delta 2} = T\cos\phi\cos\psi - T\sin\phi\cos\theta\alpha_x - T\cos\phi\sin\psi\alpha_z - T\sin\phi\sin\theta\cos\psi\alpha_z - T\sin\phi\sin\theta\sin\psi \\
B_{\beta 2} = -T\cos\phi\cos\psi\alpha_x - T\sin\phi\cos\theta + T\cos\phi\sin\psi\alpha_y + T\sin\phi\sin\theta\cos\psi\alpha_y + T\sin\phi\sin\theta\sin\psi\alpha_x \\
B_{c2} = N_{y0}\cos\phi\cos\psi - N_{z0}\sin\phi\cos\theta + (T-D0)\cos\phi\sin\psi + (T-D0)\sin\phi\sin\theta\cos\psi + \\
-N_{y0}\sin\phi\sin\theta\sin\psi - mg_2 \\
B_{\delta 3} = T\cos\phi\cos\psi\alpha_x + T\sin\phi\cos\psi - T\sin\phi\sin\psi\alpha_z + T\cos\phi\sin\theta\cos\psi\alpha_z + T\cos\phi\sin\theta\sin\psi \\
B_{\beta 3} = T\cos\phi\cos\psi - T\sin\phi\cos\psi\alpha_x + T\sin\phi\sin\psi\alpha_y - T\cos\phi\sin\theta\cos\psi\alpha_y - T\cos\phi\sin\theta\sin\psi\alpha_x \\
B_{c3} = N_{z0}\cos\phi\cos\psi + N_{y0}\sin\phi\cos\psi + (T-D0)\sin\phi\sin\psi - (T-D0)\cos\phi\sin\theta\cos\psi + \\
+N_{y0}\cos\phi\sin\theta\sin\psi - mg_3
\end{cases}
\tag{A.1}
$$